

—

Studies in Non-equilibrium Statistical Physics: Pattern Formation and Absorbing Phase Transitions

A Thesis

Submitted to
Tata Institute of Fundamental Research, Mumbai, India
for the degree of
Doctor of Philosophy
in
Physics

By

Rahul Dandekar
Department of Theoretical Physics
Tata Institute of Fundamental Research
Mumbai - 400 005, India

October 2014

Final version Submitted in July, 2015

Declaration

This thesis is a presentation of my original research work. Wherever contributions of others are involved, every effort is made to indicate this clearly, with due reference to the literature, and acknowledgement of collaborative research and discussions.

The work was done under the guidance of Professor Deepak Dhar, at the Tata Institute of Fundamental Research, Mumbai.

(Rahul Dandekar)

In my capacity as the supervisor of the candidate's thesis, I certify that the above statements are true to the best of my knowledge.

(Deepak Dhar)

Acknowledgements

I owe a huge debt to my supervisor, Prof. Deepak Dhar, for his guidance and unlimited wisdom, and also for his patience in dealing with my spells of losing and gaining interest in various topics, and his belief that someday I will learn the fine art of academic writing. I hope that he holds this belief even after reading this thesis.

Among my seniors, Kabir has provided me with both a role model and an outlet for frustration, although in the latter case the reverse is probably truer. I learnt a lot of worldly wisdom from Sasi. Tridib will always be associated with memories of my initial years and the malpuvas at Mohd. Ali Road. Other officemates, both past and present, are too numerous to name, but the DTP experience would have been utterly desolate without them.

Nikhil, Geet and Sambuddha made life in the office and outside far more bearable. Oh, yes, Geet wants a separate sentence all to himself. Nikhil (in a double role), Ravitej, Gourab, Aditi and Garima had the thankless job of being my closest friends, but they persisted through it for all six years. And all of the other batchmates shared with us not only classes and assignments but the whole winding wavering thread of PhD life.

And whether or not I needed someone to talk to, Anisha and Achal have been there, enriching my life through diverse yet lush conversation. Sonal, Parul and Surat have been able sparring partners, yet curiously supportive and understanding. I also thank Colaba girls for not bothering me too much and letting me concentrate on my research.

And all this and more would have been impossible without daily, hourly support of my parents, who never pushed me to pursue something I didn't find exciting. I can never repay the debts I owe them.

Collaborators

This thesis is based on work done under the supervision of Prof. Deepak Dhar.

Contents

Synopsis	iv
Publications	xx
Outline	1
1 Introduction to Surface and Proportionate Growth	3
1.1 Growth models: an overview	3
1.1.1 Growing aggregates	3
1.1.2 Growing surfaces	8
1.2 Proportionate Growth	11
1.2.1 Sandpiles	12
1.2.2 The Rotor-router Model	16
1.2.3 Almost-perfect circles in the rotor-router model	18
1.3 Growing Surfaces: The KPZ Universality Class	19
1.3.1 Universality classes for growing surfaces	19
1.3.2 Exact mappings in the KPZ class	21
Appendix: The Tracy-Widom distribution	25
2 Introduction to Active-Absorbing Phase Transitions	32
2.1 Absorbing phase transitions	32
2.1.1 Simple models showing absorbing phase transitions	34
2.2 Critical exponents	40
2.3 Universality classification	42
Appendix: A brief introduction to generating functions	46
3 Proportionate growth in patterns formed in the rotor-router model	51
3.1 Forming Patterns in the Rotor-router model	52
3.2 The Visit Function	54
3.3 Characterizing the Pattern as a Tiling	60
3.3.1 The Brooks-Smith-Stone-Tutte Mapping	60
3.3.2 The tiling as a resistor network on a square grid	62

3.3.3	Determining the visit function	64
3.4	Other starting backgrounds	65
3.4.1	Type II	65
3.4.2	Type III	66
3.4.3	Type IV	67
3.5	Bounded Fluctuations and Quasiperiodicity	69
3.6	Summary and concluding remarks	73
	Appendix: Derivation on eqn. (3.9) from matching of boundary conditions	74
4	Rotor-router Patterns on Noisy Backgrounds	76
4.1	Recurrent and Transient Backgrounds	77
4.1.1	Recurrence and Transience	77
4.1.2	Notation and Protocol	79
4.2	From Approximate to Exact Visit function	79
4.2.1	Point perturbations	82
4.3	Case I	85
4.3.1	The rules for drawing defect lines	85
4.3.2	The exact visit function and Tracy-Widom fluctuations	87
4.3.3	Lines of constant visit function	89
4.4	Case II	90
4.4.1	Rules for drawing defect lines	91
4.4.2	Lines of constant visit function	93
4.4.3	Transition from recurrence to transience	94
4.5	Conclusions	97
5	A Class of Active-Absorbing Phase Transitions	100
5.1	Definition of the model	101
5.2	Phase Space Picture	102
5.3	Counting steady-state configurations using generating functions	105
5.4	Activity and Transience fields	108
5.4.1	Activity field	109
5.4.2	Transience field	109
5.5	A Mapping to a Gas of Defects	111
5.6	Non-equilibrium exponents of the Conserved Lattice Gas	112
5.6.1	Steady-state exponents	112
5.6.2	Random initial conditions	114
5.7	Summary and Concluding Remarks	117
	Appendix I: Counting the Absorbing Configurations	118
	Appendix II: Counting the isolated active 1s	120
6	Summary and Concluding Remarks	124

Synopsis

1. Introduction

In recent years, non-equilibrium phenomena have been the focus of studies in statistical mechanics. The discovery of nontrivial exactly soluble models has been important in developing a deeper understanding of several nonequilibrium phenomena. Properties such as universality of critical exponents have been found to hold true even for nonequilibrium phase transitions. In this synopsis, I describe my studies on two model systems that benefit from the simplicity of the models which makes them amenable to exact analysis, and yet display behaviour shared by more complicated models.

Growing patterns in which the internal structure grows proportionately with the pattern are said to exhibit proportionate growth. Such growth is seen in young animals, for instance, where the internal organs grow as the body grows. A simple far-from-equilibrium model which has been found to show proportionate growth is the sandpile model, where the patterns were created by dropping sand on the origin of a 2D lattice and letting the configuration stabilise [1] [2]. These studies are reviewed in [3]. The structure of some such patterns was characterized and was found to be described by discrete analytic functions on graphs, where the graph depends on the pattern being studied.

The first topic we describe is proportionately growing patterns in another model, called the rotor-router model. The rotor-router model shows self-organised criticality in its steady state, like the sandpile model. It has also been of interest to computer scientists as a derandomised version of the random walk. The rotor-router model on the square lattice is defined as follows [4] [5]: There is an arrow attached to every lattice site, which points to one of its four neighbours. When a walker reaches a site, it rotates the arrow attached to that site by 90° counterclockwise and takes a step in the new direction of the arrow (fig. 1). Since the update procedure is deterministic, the configuration of arrows and the position of the walker after n steps is fully determined by the initial configuration. The rotor-router model being a de-randomized version of the random walk on a lattice, has also been studied in the context of derandomization of a general deterministic algorithm using random numbers

[6] [7]. We drop rotor-router walkers one by one on the origin of a 2D square lattice, allow them to walk until they hit the boundary of the lattice, and study the region affected by the first N ($< L$) walkers. This region (the ‘pattern’) shows interesting and complicated internal structure (fig 2), which grows proportionately with the pattern itself. We show in a simple way, using a relation between resistor networks and tilings of squares by rectangles, a connection between the structure of these patterns and discrete analytic functions on the square lattice. We have also studied the structure of patterns formed starting from some other periodic backgrounds and have been able to characterize their structure as well.

The structures described above were observed starting from regular, periodic initial conditions. An important question for proportionate growth in such deterministic models is whether, starting from noisy initial conditions, the property of proportionate growth still holds. This has been studied in the sandpile model [8] [9], for example, where for small noise strengths the structure of the individual pattern is only slightly modified, but for larger noise strength, after averaging over noise, the structure is characterized by a non-trivial structures in density profile, and this remains true even for large noise.

We studied the structure of the rotor-router patterns formed starting with random perturbations of a given periodic background. In certain cases, we found that we could exactly determine the aspect ratio of the pattern and its fluctuations, through an exact mapping to a solvable and well-studied model of anisotropic directed percolation[10][11]. The fluctuations in this special case follow the Tracy-Widom distribution. We find a phase transition in the shape of the region explored by the first walker, where the number of sites visited by the first walker before reaching the boundary of an $L \times L$ lattice grows, for large L as $O(L^3)$ below the transition, while it grows as $O(L)$ above the transition. We find that this transition falls in the KPZ universality class, for which the exponents are known exactly.

The second problem we study concerns active-absorbing phase transitions, which are an important class of non-equilibrium systems [12][13]. For some values of parameters, the system eventually reaches a unique steady-state, whereas for other values it eventually falls into one of many possible absorbing states, after which it gets stuck in that state. In sys-

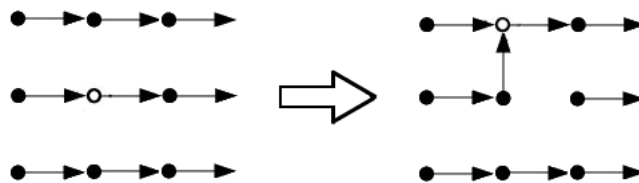


Figure 1: A single rotor-router move: The position of the walker is marked by an unfilled circle.

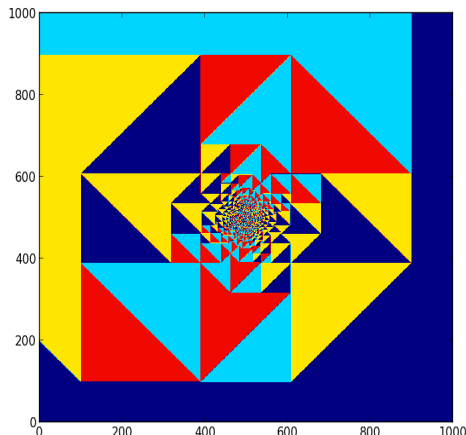


Figure 2: Pattern formed by depositing rotor-router walkers at the origin of a square lattice, starting from an initial configuration of all arrows pointing East, after 1600 walkers. Note that the second picture is scaled by a factor 4 compared to the first. Colour code: dark blue - \rightarrow , light blue - \uparrow , yellow - \leftarrow , red - \downarrow

tems characterized by stochastic rules which allow for growth or dissipation of activity in a region depending on the local neighbourhood, and for diffusion to surrounding regions, such transitions are expected to fall in the universality class of Directed Percolation, as conjectured by Grassberger and Janssen in the early 1980s [14].

We were interested in systems where the number of particles is conserved. In such cases, due to the additional conservation law, the Grassberger-Janssen conjecture is not expected to hold. However, the numerical analysis of the transition in such models has resulted in conflicting results [27], and it would be helpful to have nontrivial exactly solvable models as a testing ground for such analyses. There have been few exactly solvable models with a complex phase space structure which show active-absorbing transitions with a conserved number of particles. Aside from two models created by de Oliveira and da Silva in [15], solvable conserved-particle-number models which show an absorbing phase transition generally have the same exponents as the simplest such example, which is the Conserved Lattice Gas [16].

We constructed, following [15], a class of exactly solvable models, all of which display an active-absorbing transition in one dimension. We found that the steady-state can be exactly determined, and we calculated the (static) critical exponents of the transition, using the generating function technique. Our analysis showed that the order parameter exponent $\beta = n$ for the n^{th} model in the class. This shows emphatically that these models do not belong to the Directed Percolation universality class, and in fact each model in the class, for $n > 1$, defines a separate universality class for active-absorbing phase transitions in 1D.

2. Pattern Formation in the Rotor-Router Model

In this section we describe the study of proportionately growing patterns for the rotor-router model starting from periodic backgrounds. The characterization here turns out to be simpler than in the case of the sandpile model, related to the fact that here one only deals with piece-wise linear functions instead of piece-wise quadratic functions.

We form patterns in the rotor-router model by putting walkers one by one at the origin and letting them walk till they leave from the edge of the lattice. A new walker is introduced at the origin when the previous walker has left. We study the configuration of arrows when the N -th walker has just left the system. In this section, we mainly consider the case where the initial configuration is such that all arrows are parallel, pointing due East (\rightarrow). Clearly, the first walker put at the origin would move along the positive y -axis, rotating the arrows it encounters to point North. The second walker rotates the arrow at the origin to point West, and then walks North along the vertical line $x = -1$. After a large number of walkers have left the lattice, the pattern of arrows left behind is a complex one made of triangular and dart-like patches (fig 2).

To characterize the structure of the pattern, we determined the sizes of the different patches in the pattern, using as input the observed arrangement of these elements in the pattern. For this, we use the Brooks-Smith-Stone-Tutte (BSST) mapping ([17]) which allows one to find the sizes of all the squares in a square tiling using only information about their geometric arrangement in the tiling. Each tiling corresponds to a resistor network with horizontal lines in the tiling as the nodes in the network. The function V where $V(X)$ is the height in the tiling of the node X measured from the base can be shown to be harmonic on this graph, $\nabla^2 V = 0$, where ∇^2 is the discrete Laplacian on the square grid.

We consider the pattern in fig. 2. Rescaling the pattern formed when the number of walkers $N \rightarrow \infty$, to have diameter $D' = 1$ and centred at the origin, the rescaled pattern has features at arbitrarily small scales. We then look at the pattern as a tiling of a square by smaller squares (fig. 3 (a)), and construct the corresponding resistor network (figs. 3 (b) and (c)). The resistor-network forms a square grid, with only one missing bond between nodes A and K (Fig. 3 (c)).

Label nodes on the resistor network by their integer coordinates (m, n) . We will choose the coordinates so that the node A has the Euclidean coordinate $(0, 0)$ and the node K has the coordinate $(0, -1)$. Since the pattern has been rescaled to be of unit diameter centred at the origin, this gives $V(0, 0) = 1/2$, and $V(0, -1) = -1/2$. The solution of the resistor network problem for this graph is well known, $V(m, n)$ being given by the following superposition of Green's functions for an infinite square lattice $G_{sq}(m, n)$:

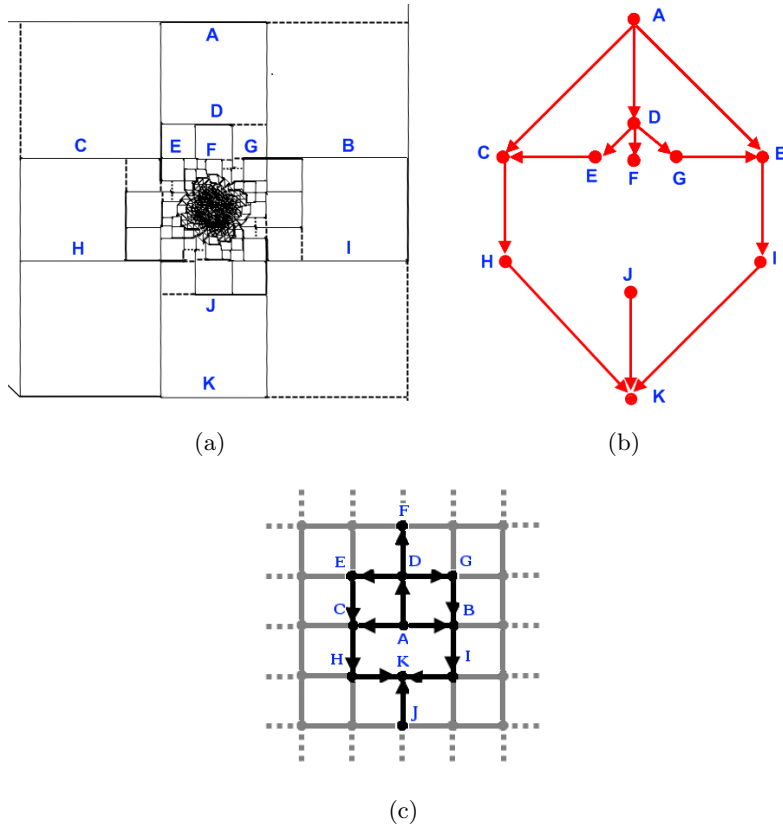


Figure 3: (a) The pattern as a square tiling. The first few levels of the corresponding network are shown. (b) Part of the resistor network corresponding to the tiling above. The edges illustrated part (a) are in black with arrows indicating the direction of the current. Note that some nodes (for example (1,0) and (1,1)) correspond to horizontal segments which lie at the same height, but have not been grouped together as a single segment. (c) The graph in part (b) shown as a part of the complete resistor network for the tiling in (a). The complete resistor network has the form of a square lattice.

$$V(m, n) = 2(G_{sq}(m, n + 1) - G_{sq}(m, n)) \quad (1)$$

where [18]

$$G_{sq}(m, n) = \int_{-\pi}^{\pi} \frac{dk_1}{2\pi} \int_{-\pi}^{\pi} \frac{dk_2}{2\pi} \frac{1 - \cos(k_1 m + k_2 n)}{2 - \cos k_1 - \cos k_2} \quad (2)$$

From this solution we get the sizes of various elements in the pattern. For example, the size of the big squares at the four corners of Fig. 3 (a) is given by the difference in the vertical co-ordinates of lines A and B. From Fig. 3 (c) this is equal to $V(A) - V(B) = V(0, 0) - V(1, 0)$. Using the values $V(1, 0) = \frac{2}{\pi} - 1/2$ and $V(0, 0) = 1/2$, the size of these largest squares in the pattern relative to the size of the pattern is $1 - \frac{2}{\pi}$.

The visit function $V_N(x, y)$ on the original square lattice is defined as the number of times the site (x, y) visited by N walkers before they exit the lattice. In each of the tri-

angular or dart-shaped regions in fig 2, $V_N(x, y)$ can be proved to be a piecewise linear function $mx + ny + c_{m,n}$, with m and n integers. An important construction is a one-to-one correspondence between regions across which the form of $V_N(x, y)$ does not change, and squares in the tiling picture of the pattern. This allows one to use eqn. 1 to determine the visit function everywhere in the pattern.

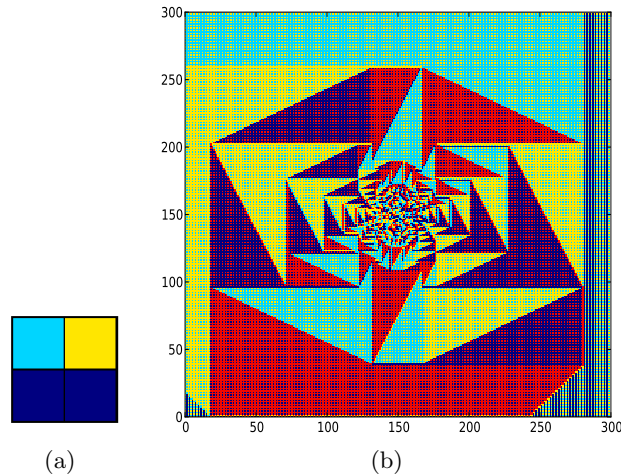


Figure 4: Pattern formed the initial backgrounds generated by tiling the lattice with the 2x2 unit cell given in (a) is shown in (b) after 700 walkers put at the origin have left the lattice. Colour code: dark blue - \rightarrow , light blue - \uparrow , yellow - \leftarrow , red - \downarrow .

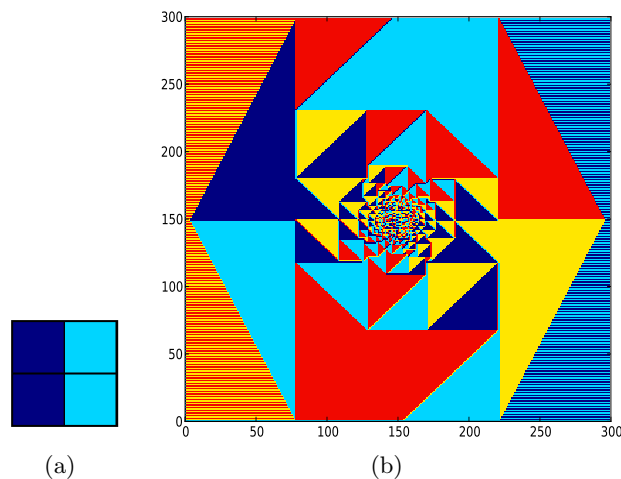
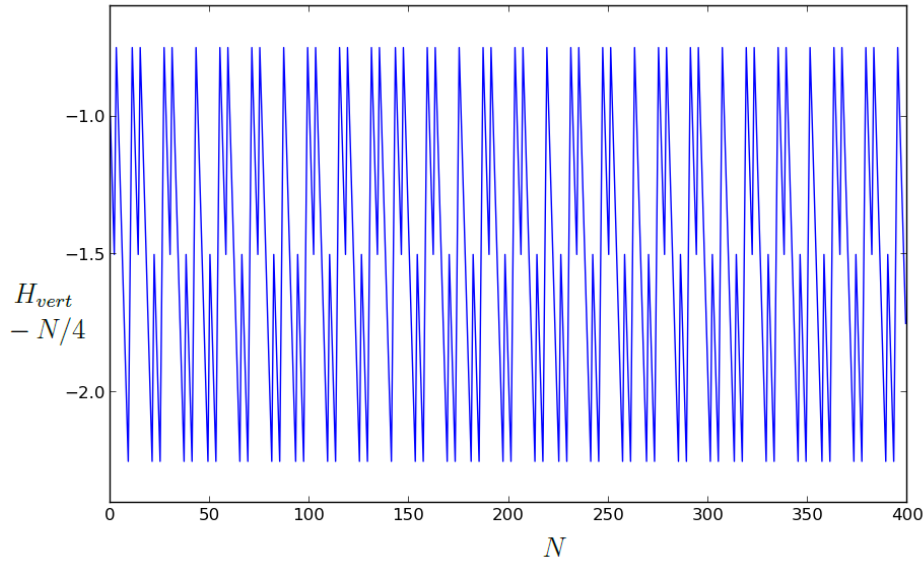


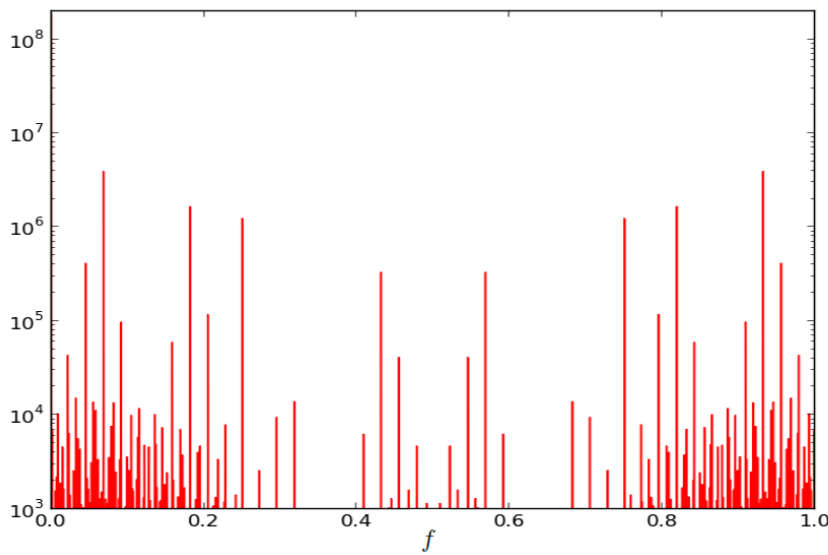
Figure 5: Pattern formed the initial backgrounds generated by 2x2 unit cell given in (a) is shown in (b) after 900 walkers put at the origin have left the lattice. Colour code: dark blue - \rightarrow , light blue - \uparrow , yellow - \leftarrow , red - \downarrow .

The analysis above was also extended to other patterns formed by starting from backgrounds generated by 2x2 unit cells, of which two examples are shown in figs 4 and 5. In case of the pattern in fig 4, where the bounding shape is a rectangular rather than a square,

the aspect ratio of the pattern can also be calculated from the above analysis.



(a)



(b)

Figure 6: (a) Fluctuations of the vertical boundary along the positive y -axis, $H_{vert} - N/4$, vs. the number of rotor-router walkers put on the lattice so far, N , and (b) its power spectrum against rescaled frequency f (on a semi-log plot, arbitrary units)

Eqn. 1 predicts the asymptotic growth rates of all the patches in the pattern (ie, the sizes of the patches after N walkers have left the lattice, for finite N). We also examined the fluctuations, for finite N , about the asymptotically expected rates of growth. Surprisingly, these are bounded and quasiperiodic functions of N (fig 6). Our numerical studies suggest that this behaviour is a general property of the sizes of various elements in the pattern.

3. Rotor-router patterns on Noisy Backgrounds

In this section, we will study patterns formed in the rotor-router model starting from noisy backgrounds.

We will be constructing background arrow configurations out of 2×2 unit cells, and it is convenient to establish a notation for such backgrounds. We will use the numbers 0, 1, 2 and 3 to refer to arrows pointing in the directions \rightarrow , \uparrow , \leftarrow and \downarrow respectively. Unit cells, and the backgrounds made by periodic repetition of them, will both be denoted by an inline 2×2 matrix. In a background denoted by $\begin{pmatrix} 3 & 2 \\ 0 & 1 \end{pmatrix}$, the element (i, j) ($i, j = 1, 2$) denotes the direction of the arrow at site (i, j) points, and the background is constructed by periodically repeating this unit cell in both directions. A randomly background where a fraction p of the cells are randomly assigned to be of type A and a fraction $(1 - p)$ are of type B will be denoted by $\{A, B|p, 1 - p\}$. (This denotes an ensemble of starting backgrounds rather than a single one.)

For the pattern described in the previous section, the first walker follows a straight-line path to infinity without visiting any site more than once. A background arrow configuration where the first walker dropped at the origin visits each site only finitely many times before reaching infinity is called a transient background. The first walker on a ‘recurrent’ background, on the other hand, visits each site infinitely many times before it reaches infinity. Every starting background is either recurrent or transient [19].

We study the path of the first walker on the recurrent background formed starting from the unit cell $\begin{pmatrix} 3 & 2 \\ 0 & 1 \end{pmatrix}$ and on perturbations of this background.

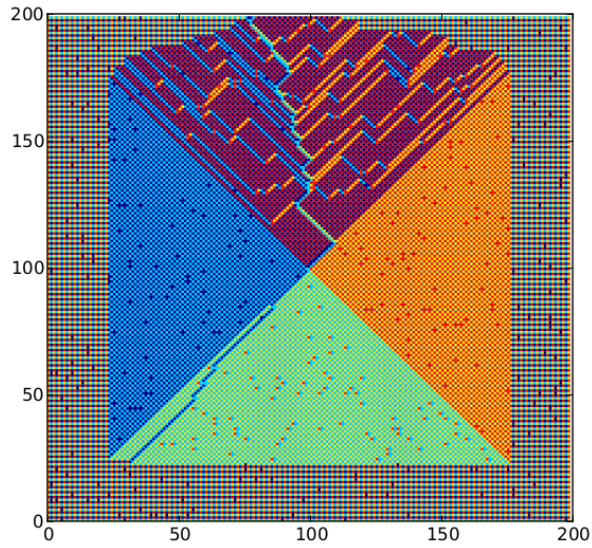
The first walker on the unperturbed background comes back to the origin infinitely many times, and the pattern it forms consists of just four growing triangular patches. The walker visits all interior sites four times for every increase of 4 in the width of the pattern. Defining the radius of the pattern as half its width, the visit function when the diameter of the pattern is R is (up to an $O(1)$ constant) $V_R^0(x, y) = 2R - 2|x|$ or $V_R^0(x, y) = 2R - 2|y|$ depending on the patch. We now study how this visit function changes when one perturbs the starting background.

We study two perturbations of this background:

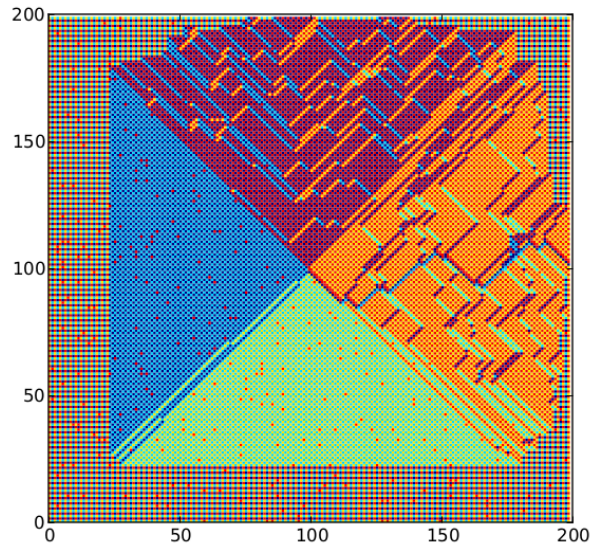
1. (See fig 7 (a)) The new background is $\{(\begin{pmatrix} 3 & 2 \\ 0 & 1 \end{pmatrix}), (\begin{pmatrix} 3 & 2 \\ 0 & 0 \end{pmatrix}), (\begin{pmatrix} 3 & 3 \\ 0 & 1 \end{pmatrix}), (\begin{pmatrix} 3 & 3 \\ 0 & 0 \end{pmatrix})|(1-p)^2, p(1-p), p(1-p), p^2\}$. For $p = 1$ the background is transient while for all $p < 1$ it is recurrent. We show that only one patch out of the four is affected by the perturbation.
2. (See fig 7 (b)) The new background is $\{(\begin{pmatrix} 3 & 2 \\ 0 & 1 \end{pmatrix}), (\begin{pmatrix} 3 & 2 \\ 0 & 2 \end{pmatrix})|(1-p), p\}$. Here, two patches are

affected by the perturbation, and the transition from recurrence to transience happens for $0 < p_c < 1$.

First we elaborate on our findings in case (1). The noise generates terrace-like structures in one of the patches that affect the visit function. We show that the noise does not affect the visit function in the other three patches. The rules for generating terraces from the noise realization can be exactly determined, and are illustrated in fig 8. Define the height



(a)



(b)

Figure 7: Patterns created starting from the backgrounds (a) $\{(\begin{smallmatrix} 3 & 2 \\ 0 & 1 \end{smallmatrix}), (\begin{smallmatrix} 3 & 2 \\ 0 & 0 \end{smallmatrix}), (\begin{smallmatrix} 3 & 3 \\ 0 & 1 \end{smallmatrix}), (\begin{smallmatrix} 3 & 3 \\ 0 & 0 \end{smallmatrix}) | (1-p)^2, p(1-p), p(1-p), p^2\}$ and (b) $\{(\begin{smallmatrix} 3 & 2 \\ 0 & 1 \end{smallmatrix}), (\begin{smallmatrix} 3 & 2 \\ 0 & 2 \end{smallmatrix}) | (1-p), p\}$. The pattern created by the unperturbed ($p = 0$) background consists of four triangular patches. Colour code: dark blue - \rightarrow , light blue - \uparrow , yellow - \leftarrow , red - \downarrow

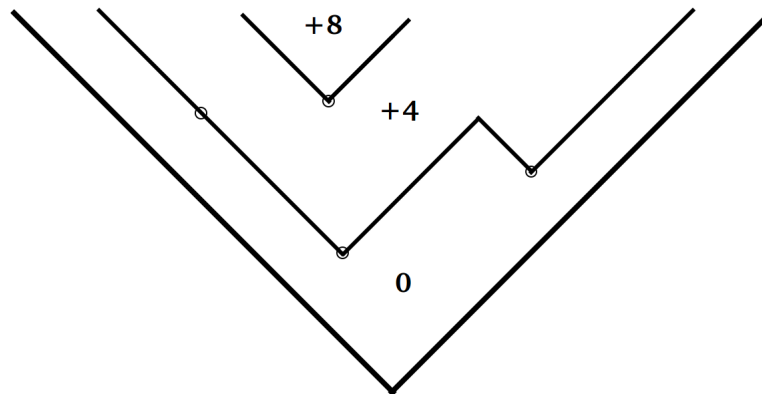


Figure 8: An example illustrating the construction of terraces. The unfilled circles denote noise points (perturbed unit cells). Each noise point creates a 45° wedge, and if two wedges meet they are part of a single step of the staircase. Noise points on an existing staircase have no effect. The height at a point is 4 times the number of steps you have to cross to reach the point.

function $h(x, y)$ at the lattice point (x, y) as the number of terrace-steps crossed to get to the point from the boundary of the patch. The visit function in the patch is then given by $V(x, y) = V_R^0(x, y) + 4h(x, y)$. The boundaries of the pattern are determined by putting $V(x, y) = 0$, and hence the terraces extend the boundary of the patch. Similar patterns have earlier been observed in the study of Anisotropic Directed Percolation (ADP) by Rajesh and Dhar [10], and in the study of Bernoulli matchings by Majumdar and Nechaev [20] [21]. There exists an exact correspondence between the patterns formed in case (1) and these two models. This allows the calculation of the average height profile $h(x, y)$, which along the line of longest extent ($x = 0$) is given by:

$$h(0, y) = 2 \frac{\sqrt{p} - p}{1 - p} y + y^{1/3} a(p) X \quad (3)$$

where X is a random variable which is Tracy-Widom distributed [22], and $a(p)$ is the amplitude of the fluctuations, which can also be calculated. If at some noise strength p_c there is a transition such that the boundary of the patch reaches infinity, that corresponds to a wetting transition in the corresponding percolation problem, which in this case is the ADP model studied in [10].

Consider simulating the model on a finite lattice. If there is a transition from recurrence of the backgrounds to transience, at p_c , for $p \geq p_c$ the walker reaches the boundary of the lattice after visiting the origin only finitely many times, even for $L \rightarrow \infty$. The order parameter for the transition is the ratio of the average number of visits to the origin for

a given noise strength, to the lattice size L : $v(p) = \lim_{L \rightarrow \infty} v(p, L)/L$. $v(p) = 0$ in the transient phase. From the result for $h(x, y)$ we derive the exact formula

$$v(p) = 1 - 2 \frac{\sqrt{p} - p}{1 - p} \quad (4)$$

The background is thus recurrent for all $p < 1$, while the $p = 1$ case is transient. From eqn. (3), the fluctuations in the order parameter would scale as $L^{1/3}$, obeying KPZ scaling [23], and the numerics are consistent with this prediction.

For the second background, shown in fig 7 (b), two patches are affected by the noise, and we cannot determine the height function $h(x, y)$ exactly. In this case it is observed from simulations that the transition happens at $p_c \approx 0.6$, and for $p > p_c$ the background is transient. As p is increased to p_c , the shape of the visited region becomes increasingly anisotropic, and its longest elongation is along the line $x = y$.

In this case the terraces in both patches invade each other, and a region around the 45° line $x = y$ reaches a state where they have equal density. It can be proved that the rules for generating staircases of both types, call them types A and B , are exactly symmetrical. The height function falls when crossing staircases of type A and rises when crossing those of type B . Hence there is an $h \rightarrow -h$ symmetry for the fluctuations of the height along the line $x = y$, superimposed on a uniform decrease as one gets farther from the origin. Fluctuations in $h(x, x)$ are hence expected to fall into the Edwards-Wilkinson [24] rather than into the KPZ class, and scale as $x^{1/4}$ rather than the $x^{1/3}$ in eqn 3. Since this is the direction of greatest extent of the pattern, the fluctuations in $v(p)$ also go as $L^{1/4}$, a prediction verified by numerical simulations.

4. An exactly solved class of active-absorbing phase transitions

There has recently been a lot of interest in models showing an active-absorbing phase transition, especially in systems with a conserved number of particles [27][16][25][26]. The simplest example of such a transition occurs in the so-called Conserved Lattice Gas (CLG), which is defined by the transitions $110 \rightarrow 101$, $011 \rightarrow 101$, where both occurring at rate unity, and 1 denotes an occupied site and 0 denotes an empty site. Active (or moveable) particles are ones with one vacant neighbour and one occupied neighbour. In this model [28], if one starts with density $< 1/2$, all particles eventually move away from each other and all activity ceases. The system is said to have entered an absorbing state. There are infinitely many absorbing states at a given density $< 1/2$, in the thermodynamic limit. For a density $> 1/2$, the system eventually enters a steady-state, where the density of active particles $\rho_a \sim (\rho - 1/2)$ near the transition point. The activity density near the transition density ρ_c defines the exponent β through the relation $\rho_a \sim (\rho - \rho_c)^\beta$. For the CLG, $\beta = 1$.

We develop a class of such models related to the Conserved Lattice Gas for which, in addition to having a steady-state that can be exactly determined, have the interesting property that the order parameter exponent β for the transition is > 1 . In most equilibrium and non-equilibrium systems, including Directed Percolation, one finds that $\beta < 1$, in all dimensions where the transition exists. This shows that these models are not in the same universality class as Directed Percolation. In fact, the models for each n fall into a different universality class.

Our models are generalizations of a model proposed by da Silva and de Oliveira [15], which has $\beta = 2$, to construct a class of lattice-gas models with assisted hopping and finite-range interactions, for which the steady-state, and the value of β can be determined exactly to be n , where n can be made to take any integral value, depending on the model. The models are defined on a line of L sites with N particles, and at most one particle can occupy one site. A configuration is denoted by a binary string $0^{m_1}1^{n_1}0^{m_2}\dots$, where 1^m denotes a cluster of m particles and 0^n denotes cluster of n empty sites. The model with range n is defined by the following set of transition rules:

$$1^{m+1}0^k \xrightarrow{\Gamma_1(i,k)} 1^m0^i10^{k-i}, \quad (5)$$

$$0^k1^{m+1} \xrightarrow{\Gamma_1(i,k)} 0^{k-i}10^i1^m, \quad (6)$$

$$1^m0^i10^{i'}1^{m'} \xrightarrow{\Gamma_2(i,i')} 1^{m+1}0^{i+i'}1^{m'}, \quad (7)$$

$$1^m0^i10^{i'}1^{m'} \xrightarrow{\Gamma_2(i',i+i')} 1^m0^{i+i'}1^{m'+1}, \quad (8)$$

where $\Gamma_1(i, k) = 0$ for $i > n$, and we assume that $\Gamma(1, k) \neq 0$ for all k . $\Gamma_2(i, k) = 0$ if $k > n$. The transitions are illustrated in fig. 9.

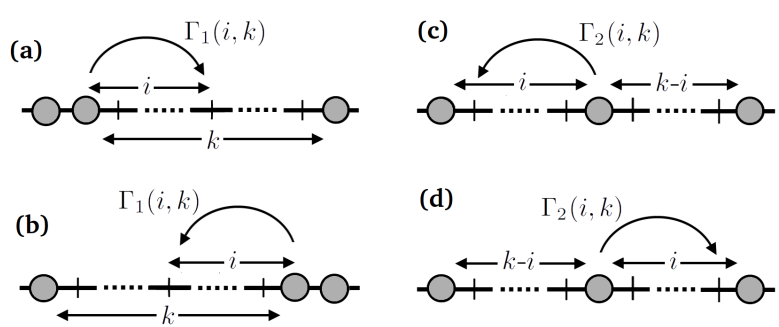


Figure 9: The hopping rates for the model with range n . In (a) and (b), a particle activated by an occupied nearest neighbour site jumps a distance i at most $\min(n, k)$ into a neighbouring cluster of empty sites which has length k . The reverse transitions are shown in (c) and (d) respectively and have non-vanishing rates only for $k \leq n$.

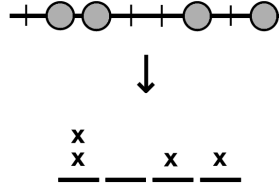


Figure 10: A configuration in the $n = 2$ model on a ring of $L = 8$ sites with $N = 4$ particles, and corresponding defect gas configuration with $N_d = 4$ defects on N sites

In the processes given in eqns (5) and (6), a particle hops by a distance at most n into a 0-cluster. For the processes in eqns (7) and (8), a particle surrounded by $\leq n$ zeroes hops left or right with equal probability to the nearest 1 on that side. Since $\Gamma_2(i, k) = 0$ for $k > n$, 0-clusters of length $> n$ break-up due to the first two processes and are not created by the dynamics, and eventually only surviving configurations have all 0-clusters of length $\leq n$. Now, we assume that $\Gamma_1(i, k) = \Gamma_2(i, k) \neq 0$ for $1 \leq i \leq k \leq n$, which means that detailed balance is satisfied in this subspace of configurations, and hence at a given density all such configurations are present with equal probability. Since below a density $\rho = 1/(n+1)$ there cannot be any such configurations, whereas above this density a unique, connected active sector exists, for the model with range n , the phase transition happens as $\rho_c = 1/(n+1)$. However, if the initial conditions belong to the transient sector, the transition density might depend on the protocol followed to prepare the initial condition. A simple protocol which can be shown to reach the active steady state for $\rho > \rho_c$ with probability 1 is to start with a fully occupied lattice and delete particles, letting the system relax after each deletion, until one gets to the required density.

Within the steady-state sector, we constructed a useful mapping to a gas of ‘defects’, illustrated for a simple case in fig. 10. The particles in the original configuration become sites in the defect configuration. If a 0-cluster in the configuration has a length $r (\leq n)$, it corresponds to $n-r$ defects at the site corresponding to the particle preceding the 0-cluster. The mapping to defects allows us to easily calculate the activity density of the model in the steady-state. A particle in the original configuration is active if two neighbouring sites in the corresponding defect configuration have a total of $> n$ defects. Near ρ_c , the defect gas is a dilute gas, and hence the probability of finding n defects together goes as ρ_d^n , which implies that the activity near ρ_c for the model with range n goes as $(\rho - \rho_c)^n$, and hence $\beta = n$.

The properties of the models were exactly determined by counting the number of allowed configurations. Define $C_n(x, y) = \sum_{L=1}^{\infty} \sum_{N=1}^L C(N, L) x^N y^L$ as the generating function of the model with range n , where $C(N, L)$ is the number of steady-state configurations with N particles on a ring with L sites. Since the steady-state contains only configurations without 0-clusters of length $> n$, $C_n(x, y)$ can be written as a generating function for configurations generated by the elementary strings $1, 10, \dots, 10^n$:

$$C_n(x, y) = \left(1 - xy \frac{1 - y^{n+1}}{1 - y}\right)^{-1} - 1 \quad (9)$$

The activity density ρ_a can be determined, by a similar counting procedure, as a parametric function of the density ρ throughout the active phase. Near $\rho = \rho_c$, one can then show that $\beta = n$ for the model n .

These models have a ‘ladder’ of transient configurations, which do not form part of the steady-state sector, and once left are never visited again. These are, for the model with hopping range n , all configurations with at least one 0-cluster of length $> n$. The number of these 0-clusters decreases monotonically in time. However, we introduce a field h which takes the evolution back up the transient ‘ladder’, by adding the following transitions to definition of the model:

$$1^{m+1}0^k \xleftarrow{h} 1^m 010^{k-1} \text{ for } k > n \text{ and } m \geq 1 \quad (10)$$

This field h is closely related to the concept of a field which couples to the activity, which for the CLG (the $n = 1$ model) has been studied earlier using a mean-field analysis [13]. We find that with our construction of the field, the steady-state properties can be determined, and the corresponding generating function $C(x, y, h)$ is a simple function. The exponent δ , defined by $\rho_a|_{\rho=\rho_c} \sim h^{1/\delta}$, can be calculated to be $\delta = 2/n$ for the model with range n . Thus, we were able to calculate the three independent stationary exponents of the models β , ν and δ exactly.

Bibliography

- [1] D. Dhar, T. Sadhu and S. Chandra, EPL, **85** 48002
- [2] T. Sadhu and D. Dhar, Physical Review E, **85** 021107 (2012)
- [3] D. Dhar and T. Sadhu, J. Stat. Mech. P11006 (2013); arXiv:1310.1359.
- [4] V. B. Priezzhev, D. Dhar, A. Dhar and S. Krishnamurthy, Physical Review Letters, **77** 5079 (1996)
- [5] A. M. Povolotsky, V. B. Priezzhev, and R. R. Scherbakov, Physical Review E, **58** 5449 (1998)
- [6] J. Propp, Chaos, **20** 037110 (2010)
- [7] A. E. Holroyd, L. Levine, K. Meszaros, Y. Peres, J. Propp and D. B. Wilson, Progress in Probability, **60** 331 (2008); arXiv:0801.330
- [8] T. Sadhu and D. Dhar, Journal of Statistical Physics, **138** 815 (2010)
- [9] T. Sadhu and D. Dhar, Journal of Statistical Mechanics: Theory and Experiment, P03001 (2011)
- [10] R. Rajesh and D. Dhar, Phys. Rev. Lett. **81** 1646 (1998).
- [11] S. N. Majumdar, arXiv: 0701193.
- [12] G. Grinstein and M. A. Munoz, in *Fourth Granada Lectures in Computational Physics*, edited by P. L. Garrido and J. Marro, Lecture Notes in Physics Vol. 493 (Springer, Berlin, 1997), p. 223.
- [13] S. Lubeck, Int. J. Mod. Phys. B **18**, 3977 (2004).
- [14] H. K. Janssen, Z. Phys. B **42** 151 (1981);
P. Grassberger, Z. Phys. B, **47**, 365 (1982).
- [15] E. F. da Silva, and M. J. de Oliveira, J. Phys. A: Math. Gen. **41**, 385004 (2008).
- [16] M. Rossi, R. Pastor-Satorras, and A. Vespignani, Phys. Rev. Lett. **85**, 1803 (2000).

-
- [17] R. L. Brooks, C. A. B. Smith, A. H. Stone and W. T. Tutte, *Duke Mathematical Journal* **7** 312.
- [18] F. Spitzer, *Principles of Random Walk*, pp. 124, 148-51, (Van Nostrand, Princeton, 1964);
- [19] A. E. Holroyd and J. Propp, *Contemporary Mathematics*, **520** 105 (2010); arXiv:0904.4507
- [20] S. N. Majumdar, and S. Nechaev, *Phys. Rev. E*, **72**, 020901 (2005).
- [21] S. N. Majumdar, K. Mallick, and S. Nechaev, *Phys. Rev. E*, **77**, 011110 (2008).
- [22] C. A. Tracy, and H. Widom (1994), *Comm. Math. Phys.*, **159**, 151 (1994)
- [23] M. Kardar, G. Parisi, and Y.C. Zhang, *Phys. Rev. Lett.*, **56**, 889 (1986).
- [24] S. F. Edwards and D. R. Wilkinson, *Proceedings of the Royal Society of London. A. Mathematical and Physical Sciences* **381**, 17 (1982).
- [25] A. Vespignani, R. Dickman, M. A. Munoz, S. Zapperi, *Phys. Rev. E* **62**, 4564 (2000).
- [26] R. Dickman, M. A. Munoz, A. Vespignani, S. Zapperi, *Braz. J. Phys.* **30**, 27 (2000).
- [27] M. Basu, U. Basu, S. Bondyopadhyay, P. K. Mohanty, and H. Hinrichsen, *Phys. Rev. Lett.* **109**, 015702 (2012).
- [28] M. J. de Oliveira, *Phys. Rev. E* **71**, 016112 (2005).

Publications

- R. Dandekar and D. Dhar,
Proportionate growth in patterns formed in the rotor-router model, *Journal of Statistical Mechanics: Theory and Experiment*, P11030 (2014)
arxiv:1312.6888
- R. Dandekar,
Proportionately growing patterns on noisy backgrounds and KPZ scaling,
in preparation
- R. Dandekar and D. Dhar,
A class of exactly solved assisted-hopping models of active-inactive state transition on a line,
EPL (Europhysics Letters), **104** 26003 (2013)

Other Publications

- R. Dandekar,
Comment on ‘Self-organized cooperative criticality in coupled complex systems’, *EPL (Europhysics Letters)*, **107** 10001 (2014).

Outline

This thesis is organised as follows:

Chapters 1 and 2 form the introductory part of the thesis. In Chapter 1, we will review previous studies of the growth of surfaces and aggregates of particles, with an emphasis on Kardar-Parisi-Zhang (KPZ) and Edwards-Wilkinson (EW) surfaces, and on aggregates formed by starting from a seed in deterministic particle models. We place these particular models in the context of general growth models, then describe proportionate growth in the rotor-router aggregation and sandpile models. We also describe in detail growth models in the KPZ universality class and recently discovered exact mappings between these models, which allow one to determine the full distribution of the fluctuations in the growing surfaces.

In chapter 2, we review the phenomenon of absorbing phase transitions, in systems with and without a conserved number of particles. Absorbing states are states which the dynamics can lead to but cannot escape from. Absorbing (or active-absorbing) phase transitions are transitions in which, as an external parameter is tuned, the long-time limit of the system changes from an active fluctuating steady-state to an absorbing state where no further change occurs. These transitions are governed by static and dynamical critical exponents which obey well-known scaling relations. We will also discuss the phenomena of universality, wherein transitions in many diverse systems nevertheless show the same critical exponents near the transition. The classification of universality classes of absorbing phase transitions, especially those in systems with a conserved number of particles, has been a topic of particular interest in the recent literature.

In chapter 3, we study the growing patterns formed in the rotor-router model by adding N walkers at the center of an $L \times L$ two-dimensional square lattice, starting with a periodic background of arrows, and relaxing to a stable configuration. The pattern is made of a large number of triangular and quadrilateral regions, where in each region all arrows point in the same direction. We show that the pattern formed by arrows which have been rotated at least one full circle, may be described in terms of a tiling of the plane by squares of different sizes. The sizes of these squares, and the size of the pattern, grow linearly with N , for $1 \ll N < 2L$. We use the Brooks-Smith-Stone-Tutte theorem relating tilings of squares

by smaller squares to resistor networks, to determine the exact relative sizes of these tiles. The scaling limit of the number of visits $\phi(\xi, \eta)$ as a function of the scaled position (ξ, η) is also determined. We also present numerical evidence that the deviations of the sizes of different squares in the tiling from the asymptotic linear growth law are always $O(1)$, and are quasiperiodic functions of N .

In chapter 4, we will consider the patterns formed by rotor-router walkers on backgrounds which are not perfectly periodic, but are perturbations of periodic backgrounds with the arrow directions changed at some randomly chosen sites. We see that this noise creates ‘defect lines’ in some of the patches, which also affect the shapes of the patch boundaries. We study perturbations on particular starting backgrounds, and how the presence of the noise affects the shapes of the patches in the pattern and how these properties vary as the noise strength p is varied.

In chapter 5, we present the construction and analysis of a class of assisted-hopping models which show an active-absorbing phase transitions in one dimension. The models are a generalization of the Conserved Lattice Gas (CLG) model defined in Chapter 1. The steady state for all the models in the class can be exactly determined and various quantities calculated easily with the help of generating functions. We show that, for the model where the particles have a hopping range n , for $n = 1, 2, 3, \dots$, the critical exponent $\beta = n$. The model with $n = 2$ was first defined by da Silva and de Oliveira. The models with $n > 2$ are new universality classes for active-absorbing phase transitions.

Chapter 1

Introduction to Surface and Proportionate Growth

In this chapter, we will review previous studies of the growth of surfaces and aggregates of particles, with an emphasis on Kardar-Parisi-Zhang (KPZ) and Edwards-Wilkinson (EW) surfaces, and on aggregates formed by starting from a seed in deterministic particle models. However, we first place these particular models in the context of general growth models in section I. In section II, we describe the rotor-router aggregation and sandpile models for proportionate growth. In section III, we describe growth models in the KPZ universality class and recently discovered exact mappings between these models, and describe how these allow us to determine the full distribution of the fluctuations in the growing surfaces.

1.1 Growth models: an overview

In this section we describe known models of stochastically growing aggregates and their surfaces. This allows us to introduce a formalism for analysing growing aggregates, and their surfaces, formed in a deterministic cellular automaton model in Chapters 3 and 4.

We first describe various models for growth of an aggregate from a seed. Then we will move on to studying the surfaces of these growing aggregates, which gives us an opportunity to introduce models of growth starting from flat surface as well. Good reviews are in Viscek's book [1] and the review by Herrmann [2]. Note that we do not consider reaction-diffusion or hydrodynamic pattern formation models here, see [3] for a review.

1.1.1 Growing aggregates

The Eden Model

One of the simplest models of the growth of a random aggregate, starting from a single seed, was proposed by Eden in 1961 [4]. In this model, a cluster grows starting from an

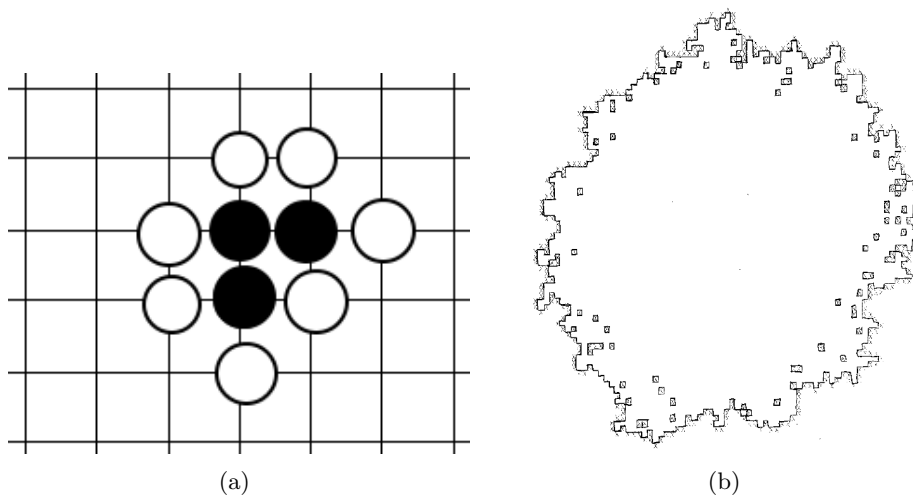


Figure 1.1: (a) A small Eden Cluster with the growth sites shown as unfilled circles. (b) An Eden cluster of 1500 sites. The sites denoted by X represent growth sites for the next time-step. Reprinted with permission, from [2].

initial seed at the origin, according to the following rules: The process begins with the origin as the nucleation site, and all other sites unoccupied. The sites which, at a given time-step, are the neighbours of the sites at the edge of the cluster are called growth sites. A new site is drawn at random from the growth sites at each time-step, and this site becomes part of the connected set of sites, called a cluster. The cluster thus grows in size by 1 at each time-step.

The clusters grown by this method are found to be compact structures, that is, the radius of an Eden cluster in d dimensions grows with time as $R \sim t^{1/d}$. However, the surface of the Eden cluster shows interesting fluctuation properties. The asymptotic shape of an Eden cluster depends on the lattice on which it is grown, and does not tend to a circular shape as one might naively expect [6, 7].

One simple extension of the Eden model is the model by Williams and Bjercknes [8], which allows occupied sites to become unoccupied at a later time: a randomly chosen growth site becomes part of the cluster with probability α , or a randomly chosen edge site of the cluster becomes unoccupied with probability β . As long as the ratio $\alpha/\beta > 1$, the cluster grows with time, and is expected to show the same scaling laws as the Eden model.

Growth of Percolation Clusters

The Eden model can be modified in the following two ways to produce growing percolation clusters:

In the first one [9], sites can exist in three states: occupied, unoccupied or immunized.

One modifies the Eden rule to the rule that an unoccupied non-immunized neighbouring site of the cluster might become occupied with probability p , or become ‘immunized’ with probability $(1 - p)$. Immunized sites can not be occupied at any later time. For $p < p_c$, where p_c is the percolation threshold on the particular lattice, the cluster grows until it reaches a finite size for which there are no more growth sites on the boundary. For $p > p_c$, with a non-zero probability the growth produces an infinite cluster. The fully grown clusters are created with the same probabilities as site percolation clusters; however, while growing they do not have the same surface structure as percolation clusters.

The second extension, Invasion Percolation [10], was defined by Wilkinson as a growth model that generates critical percolation clusters without the need for fine-tuning of a parameter. One assigns a random number w_e to each edge e on the lattice, called its weight. w_e is chosen from a uniform distribution $[0, 1]$. At each new time-step, instead of choosing a random site on the boundary to add to the cluster, one chooses the boundary edge of the lowest weight. One then adds the neighbour along the edge to the cluster. (Sometimes the lowest weight boundary edge already has both its end sites in the cluster, in which case it is simply removed from the list of boundary edges.)

From bond percolation, we know that if edges on a lattice are randomly occupied with probability $p > p_c$, then an infinite cluster results. Thus it is reasonable that even at large times, the invasion cluster will not get to a stage where edges with weights $p > p_c$ are being added to the cluster (not considering initial transients). In fact, a theorem due to Haggstrom, Peres and Schonmann [11] says that if η_i is the weight of the edge added at the i -th time-step, the maximum of the sequence η_i tends to p_c as $i \rightarrow \infty$. The bulk properties of the growing cluster, for example the fractal dimension, are the same as those of the spanning cluster in the percolation problem at p_c . Thus invasion percolation finds the critical value on its own, and generates a critical cluster. Thus it can be considered an example of self-organized criticality.

Diffusion-Limited Aggregation

Diffusion-Limited Aggregation was introduced by Witten and Sander in 1981 [12] to model the formation of soot particles in air by aggregation. Since then the model has been applied to various other phenomena, such as viscous fingering, spinodal decomposition, and several other applications.

The model is defined as follows: we start with a seed at the origin. A particle starts diffusing from a point in an arbitrary direction far away from the origin, and diffuses until it either escapes to infinity (in computer simulations a cutoff is imposed) or reaches a site next to the seed, at which point it sticks there. Then a new particle is released from an

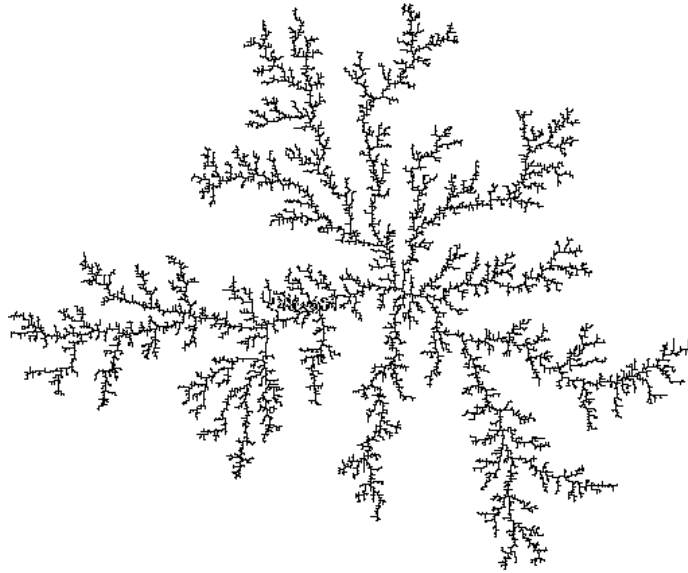


Figure 1.2: A Diffusion-Limited Aggregation cluster in the continuum. Picture taken from magnin.plil.net/spip.php?article102

arbitrary direction far away from the origin and starts diffusing, again either diffusing to infinity or sticking to the growing cluster. This process can be performed in the continuum, or on a lattice (in which case the particles perform random walks). The cluster has a tree-like shape, as shown in fig 1.2, and the properties of the cluster depend on the type of lattice used. The DLA clusters are fractals, unlike the Eden clusters: in the continuum, the mass of a cluster varies with its radius as R^a , with $a \approx 1.715 < 2$ which implies that the cluster is not space-filling. While on a square lattice in 2d, the exponent is $a_{sq} \approx 1.5$ [13].

The tree-like shape of the cluster may be viewed as the result of the instability of a circularly growing cluster to perturbations of its surface: bumps on the surface expose more surface area and hence grow faster than the surroundings, while growth in the valleys is slower. Since the particles are finite-sized, they themselves provide the perturbations necessary to destabilize circular growth. The outer ‘branches’ of the tree-like structures formed due to this instability grow faster than the inner branches, as few particles reach the inner branches without getting stuck on the way [14].

The basic DLA model can be modified by introducing a probability for sticking: at every encounter with the cluster, a particle sticks with probability $p \leq 1$. For $p \ll 1$ and for small sizes of the cluster, a particle has a chance to explore the entire boundary of the cluster before settling at some site on the boundary. Thus, all sites on the boundary are equiprobable sites for growth, and the cluster is approximately an Eden cluster of that size. However, once the cluster becomes large enough, for any finite p , the particle can only explore a finite neighbourhood of the site of its initial attempt at sticking, before getting

stuck. Thus the asymptotic cluster is still a DLA cluster. In the limit $p \rightarrow 0$, the aggregation becomes truly reaction-Limited, and one recovers the Eden model.

Cluster-cluster aggregation

Instead of aggregating models where particles attach to a single growing cluster, one can define models where two diffusing clusters of sizes m and n stick to each other and form a cluster of size $m + n$ when they meet, with rates $k(m, n)$ depending on the sizes of the two clusters [22]. Simulations, and exact solutions of a few integrable kernels show the existence of a gelation transition, such that after a given time an infinite cluster forms, although all particles might not be part of the cluster. The order and the exponents of the cluster depend on the exact form of $k(m, n)$. For more details on cluster-cluster aggregation see [23] and Viscek's book [1].

Internal Diffusion-Limit Aggregation

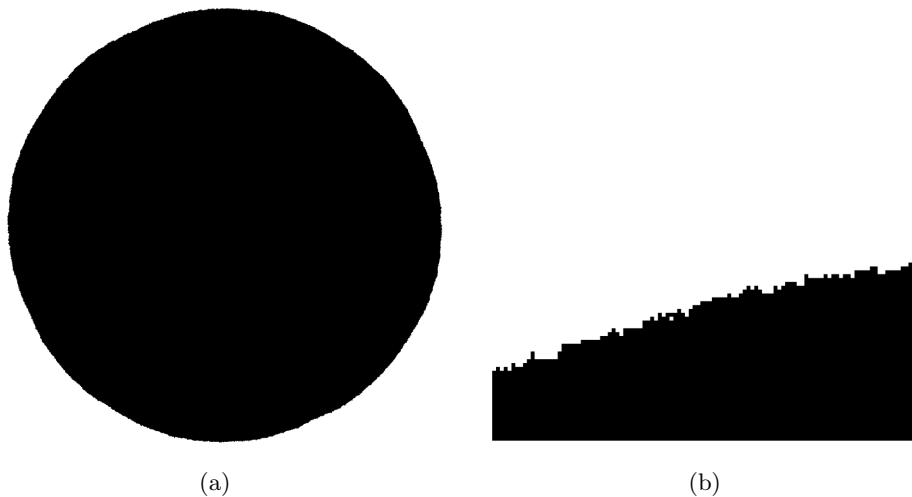


Figure 1.3: (a) An Internal DLA cluster on the square lattice, with 10^6 particles. (b) Detail of the boundary of the cluster. Both pictures courtesy of Lionel Levine.

Internal DLA was proposed by Lawler, Bramson and Griffeath [34] as a model of growing clusters on the lattice which are seeded from the inside rather than the outside. The process starts with a seed at the origin. A new particle is added at the origin, and performs a random walk on the lattice until it reaches a site outside the cluster. It stops at the first such site it visits, and this site becomes part of the cluster, after which the process is repeated by putting another walker at the origin. Internal DLA, even on a lattice, is not susceptible to the DLA instability to bumps on the surfaces. In fact, the converse is true - valleys in the surface are more likely to be filled. It has been proved that the asymptotic shape is a circle, and the fluctuations about circularity when the average radius is R , are bounded at most

by $\log(R)$ [35].

1.1.2 Growing surfaces

In this subsection we describe the growth of surfaces of growing aggregates. As explained later, growing surfaces usually fall into one of two universality classes. Here, using various models, we motivate the important quantities to be studied and show that they have universal properties.

Eden Surfaces



Figure 1.4: An Eden cluster growing on a flat surface. Courtesy of Jean-Francois Gouyet [36].

The average radius of an Eden cluster in d -dimensions grows with time as $\langle R \rangle \sim t^{1/d}$ as given earlier. (The angular brackets denote averages over the different realisations of the process.) Another important quantity is the magnitude of fluctuations about this expected radius, $\sigma^2 = \langle R^2 \rangle - \langle R \rangle^2$. The scaling of the fluctuations with the radius of the cluster defines an exponent, β , as

$$\sigma \sim \langle R \rangle^\beta \tag{1.1}$$

These exponents can also be defined for other growing surfaces [15], and it is found that many different models have the same values of the exponents. This universality of the exponents, and the relation to other models of growing surfaces, is best understood by starting from a line of initial sites on the lattice rather than a seed. More precisely, we work on a square lattice with periodicity L in the x -direction, made of sites (x, y) where the site $(x + L, y)$ is identified with the site (x, y) . The sites in the segment at $y = 0$ are all occupied, and function as seeds for the growth. The growth proceeds in the y direction according to the Eden rules: at each time-step, a site randomly selected from the set of sites which are empty neighbours of the cluster sites gets added to the cluster. Simulations show that this cluster is again compact, and defining the height in a layer x as $h(x)$ = the maximum height of an occupied site in the layer, we find the average height of the cluster

$\langle h \rangle \sim t/L$. Similarly to radial cluster growth, we can define the variance $\sigma^2 = \langle h^2 \rangle - \langle h \rangle^2$. There exists a crossover time scale,

$$\tau \sim L^z \quad (1.2)$$

such that σ grows as

$$\sigma \sim \langle h \rangle^\beta \text{ for } t \ll L^z \quad (1.3)$$

while for $t \gg L^z$ it saturates at the value

$$\sigma \sim L^\alpha \quad (1.4)$$

These equations define three exponents, β , α and z . One writes an asymptotic scaling form for σ as

$$\sigma \sim L^\alpha f\left(\frac{\langle h \rangle}{L^z}\right) \quad (1.5)$$

where $f(x)$ is called a scaling function. To agree with eqns. (1.3) and (1.4), we need that $f(x) \sim x^\beta$ as $x \rightarrow 0$ and $f(x) \rightarrow 1$ as $x \rightarrow \infty$. This gives a scaling relation between the exponents

$$\beta = \alpha/z \quad (1.6)$$

In $d = 2$, numerical simulations show that for Eden growth on a flat surface, $\alpha \approx 0.5$ and $\beta \approx 0.33$ [5].

Since the growth of the surface is translation-invariant in the direction x , and since the only macroscopic length scale in the problem is L , we expect that the correlation function

$$C(x) = \langle (h(x' + x) - h(x'))^2 \rangle \quad (1.7)$$

varies as a power-law, $C(x) \sim x^{2\alpha}$. The exponent α is called the Hurst exponent, and in this case it is the same as the exponent α defined from the average height fluctuations.

The exponents of the Eden growth from a line in 1+1 dimensions can be predicted from the analysis of the KPZ equation, see section III. For now, we describe two other models of surface growth - one which falls in the same universality class (has the same values for the exponents α and z) as Eden growth from a line, and another which does not.

Ballistic Deposition

This and the next model fall under the category of deposition-evaporation models, where particles are deposited onto a growing surface, or evaporated from it. For both the models, we discuss only the cases where there is no evaporation from the surface.



Figure 1.5: A ballistic deposition cluster growing on a flat surface. Courtesy of Jean-Francois Gouyet [36].

In ballistic deposition [19], particles are dropped normally onto a surface, and travel ballistically downwards until they reach a cell adjacent to a cell already in the cluster, and stick there. The position of the dropping particles over the direction along the surface is chosen uniformly randomly. Thus the new growth occurs uniformly over the exposed neighbours of the growing cluster. (The empty sites in the bulk cannot be occupied later.)

An Eden cluster, on the other hand, chooses a new site over the unoccupied neighbours of the cluster, whether in the bulk or on the surface. However, since both Eden and ballistic deposition clusters are compact (observed in simulations), for large cluster sizes if we rescale time, the growth of both surfaces should proceed in approximately the same way. This expectation is confirmed by simulations, the exponents β and z for the ballistic deposition models are the same as those for the Eden model. Both models fall in the KPZ universality class.

Random Deposition with surface diffusion

If particles are dropped uniformly over a substrate and stick to the topmost particle in the layer they are dropped in, we have the random deposition model. The cluster is then simply a collection of independently growing stacks, and the height of each stack and the variance of h over the sample grow as t and $t^{1/2}$ respectively.

In random deposition with surface diffusion, a particle which drops onto the topmost particle in a layer does not stick there - instead, it diffuses to a neighbouring site if the height at the neighbouring site is lower than that at the current site, continuing this process for a fixed number of time-steps, at the end of which it sticks to the site it has ended up on. Thus the different stacks do not grow independently, and although the average height still grows as t , the variance is much reduced from the random deposition case. Edwards and Wilkinson in 1982 [17] derived an evolution equation for the coarse-grained $h(x)$ for this

model, (see section III for details) which gives

$$\sigma \sim L^{1/2} f\left(\frac{\langle h \rangle}{L^2}\right) \quad (1.8)$$

The scaling relation $\beta = \alpha/z$ gives $\beta = 1/4$.

The Polynuclear Growth model

Another interesting model of a growing surface is the Polynuclear growth, or PNG, model [20, 21]. The polynuclear growth model is defined in one-dimension and continuous time. It concerns the growth of a one-dimensional interface, growing without overhangs - thus one that can be characterised by a function $h(x, t)$, which is the height of the interface at position x and time t . The function $h(x)$ in the PNG model is an integer valued function with discontinuous jumps of ± 1 (see fig 1.6). We call these jumps as kinks (when the increase going in the $+x$ direction is $+1$) or antikinks (when it is -1). The dynamics of the interface is best described in terms of these kinks and antikinks in $h(x)$. Kink-antikink pairs are nucleated at rate unity per unit length. (The blue part of $h(x)$ in the figure. Once nucleated, the kinks move towards the right and the antikinks move towards the left, both at unit velocity. Kinks and antikinks annihilate upon meeting. (See fig. 1.6). The fluctuations of the height in this model scale in with the same exponents as the Eden and Ballistic Deposition models discussed above.

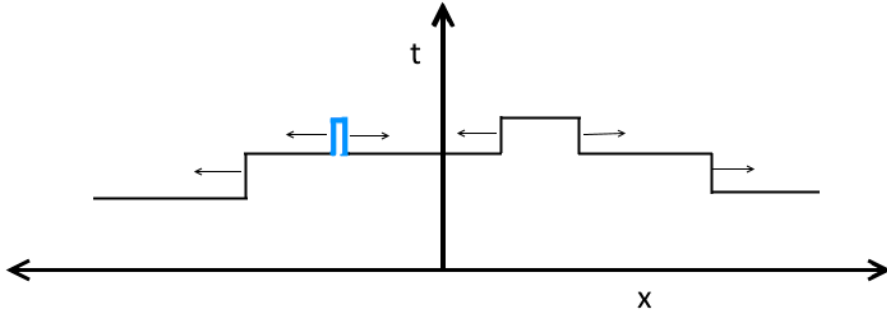


Figure 1.6: The evolution of $h(x)$ in the PNG model. The pair of discontinuities in blue have just been generated, and will move in opposite directions.

1.2 Proportionate Growth

In section I, we observed that the aggregation models defined there did not show any internal structure, showing growth and change only at the boundaries. In this section, we study deterministic aggregation models, with particle input at the origin, which show internal structure which grows at the same rate as the pattern itself. Such growth is termed ‘proportionate growth’.

Approximately proportionately growing patterns are found in biology: as baby animals grow from birth to adulthood, the different parts of the body grow roughly proportionately to each other. While proportionate growth is quite typical in the animal kingdom, examples of proportionate growth outside biology are hard to find. In this section, we discuss growing patterns formed in the abelian sandpile model (ASM) which show proportionate growth. Here, the patterns are formed by depositing particles one by one at the origin of a finite square lattice and letting the configuration relax using the ASM relaxation rules, until it becomes stable. We then define the rotor-router model, a model of a derandomized random walker on a lattice, and use the model to define a derandomized version of the IDLA, which shows interesting internal structure, and proportionate growth.

1.2.1 Sandpiles

The abelian sandpile model [25, 26] is defined on a 2D $L \times L$ square lattice as follows: particles are dropped randomly on the sites of the lattice. If, after a particle has been dropped on a site, the height of the site (ie, the number of particles on the site) exceeds 3, one particle from the site is sent to each of its nearest neighbours, thus reducing the height of the site by 4 and increasing the height at each neighbour by 1. This is known as a ‘toppling’. In the process, some other heights might exceed 3, and those sites are toppled, and so on. When a boundary site of the lattice is toppled, the number of particles on the lattice decreases by one. (When a corner site topples, it decreases by two.) This is known as an avalanche, and it stops once all heights are less than 4. Then the next particle is dropped on the lattice. This model is thus a model with deterministic toppling rules, but random drive, and boundary dissipation. In the steady-state, it shows no intrinsic length scale, except the lattice size L . This means that the height-height correlation function decays as a power law, and the probability distributions for avalanche size and duration also decay as power laws. The sandpile system is said to exhibit self-organized criticality. For more details on the sandpile model see [27].

We now discuss earlier work on patterns formed in the sandpile model. The patterns are formed by starting with a periodic height configuration on the lattice, and dropping particles only at the origin of the lattice and relaxing until all heights are < 3 [28]. Fig 1.7 shows the pattern formed after dropping N particles on an originally empty lattice. The radius of the pattern grows with the number of particles N as $R \sim \sqrt{N}$, and the internal structure of the pattern also grows proportionally. A simpler pattern is formed on the F-lattice. As shown in fig 1.8, on the F-lattice each site has two incoming bonds and two outgoing bonds. During a toppling the particles exit from each site along the outgoing bonds. Thus, the threshold height is 2, and in a relaxed configuration all sites have heights 0 or 1. One starts with a checkerboard initial pattern, with heights 0 and 1 on alternate sites, and drops particles on the origin. The resulting pattern (fig. 1.8 (b)) exhibits proportionate growth

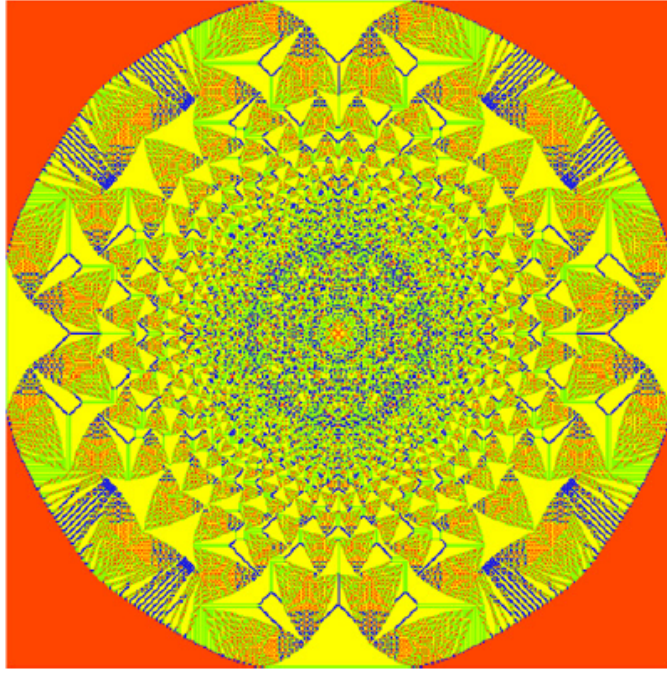


Figure 1.7: A growing pattern in the sandpile model on the square lattice, starting with all heights zero. As more particles are added, the size of the pattern grows and the internal structure grows along with it (except for the finite-width lines inside the patches), and hence the pattern looks like a bigger version of this one. Color code: R,G,B,Y = 0,1,2,3. Reprinted with permission, from [24].

[29]. This pattern is made of macroscopic patches where, inside each patch, the height is a given periodic function. An important quantity is the number of topplings as a function of the site co-ordinate, $\Phi(x, y)$. On the lattice, due to mass conservation, this quantity obeys the equation

$$\nabla^2 \Phi(x, y) = \Delta \rho(x, y) \quad (1.9)$$

where ∇^2 is the lattice Laplacian, and $\Delta \rho$ is the difference between the initial and the final heights at the site (x, y) . To study the properties of the asymptotic pattern ($N \rightarrow \infty$), when all the internal structures are well-resolved, one defines the scaled toppling function:

$$\phi(\xi, \eta) = \lim_{N \rightarrow \infty} N^{-a} \Phi(\lfloor \xi N^b \rfloor, \lfloor \eta N^b \rfloor) \quad (1.10)$$

where a and b are chosen so that one gets a finite ϕ in a bounded finite region of the plane. For compact patterns, we have $a = 2$ and $b = 1/2$. For compact patterns, it was shown that ϕ within each patch is a quadratic function of the co-ordinates, $\phi_P = a\xi^2 + b\eta^2 + c\xi\eta + d_P\xi + e_P\eta + f_P$. For the F-lattice pattern starting from a checkerboard background, it turns out that the adjacency graph of the patches forms a square grid on a two-sheeted Riemann surface, with the origin having eight edges. If we label the position of patch P on this adjacency graph as (m, n) , it turns out that a_P , b_P and c_P are simple

functions of m and n (for details see [29]). Now, using the fact that ϕ is continuous across patch boundaries, it was shown that the matching condition can be put in the form

$$\nabla^2 d_{m,n} = 0 \quad (1.11)$$

$$\nabla^2 e_{m,n} = 0 \quad (1.12)$$

where the Laplacian ∇^2 is taken on either the odd sublattice or the even sublattice of the square grid. These equations were solved in [29] to derive the form of the asymptotic toppling function for all the patches, which allowed them to evaluate the relative sizes of the various patches in the pattern. The structure of the patterns has an intriguing connection with discrete analytic functions on the graph [39].

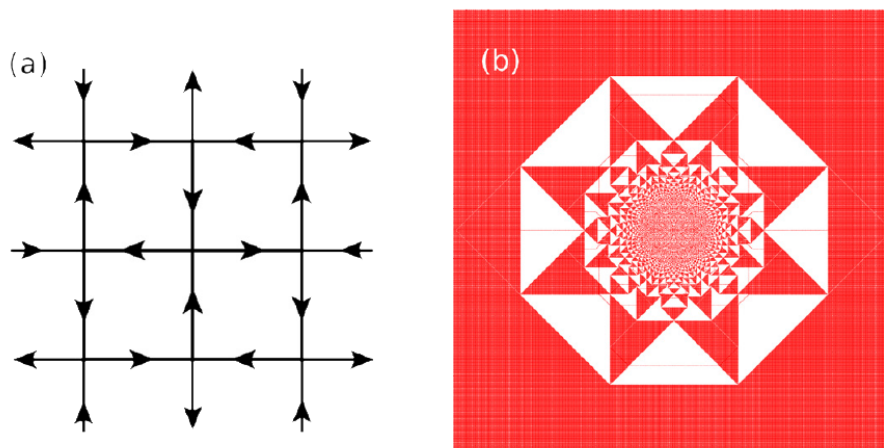


Figure 1.8: (a) The structure of the F-lattice. (b) A growing pattern in the sandpile model on the F-lattice lattice, starting with a checkerboard pattern of 0s and 1s. Color code: Red = 0, White = 1. Reprinted with permission, from [29].

Thus, the toppling function for the pattern was calculated by solving the Laplace equation on the adjacency graph of the patches. For several other patterns studied, including linearly growing ones, it turns out that one part of the toppling function inside each patch encodes the co-ordinates of the patch on the adjacency graph, and the coefficients of the other part obey a Laplace equation on the adjacency graph [30, 37]. For many patterns, we show in Chapter 3 that this relationship follows naturally, and most easily, from the fact that the patterns can be seen as tilings of squares by smaller squares.

There is also an interesting connection between some sandpile patterns and Apollonian circle packing, which was discovered by Levine, Pedgen and Smart [40]. Another object in the sandpile model known to exhibit interesting structure is the identity configuration. For details, see [32] and [33].

Note that the sandpile model is a deterministic model, but natural systems almost certainly have some element of noise. Sadhu and Dhar also studied the effects of various kinds of noise on the growth of the patterns [31]. They found, firstly, that adding a slight non-deterministic element to the dynamics of the model, such that in a small fraction of topplings particles are not transferred equally to the nearest neighbours, destroys the internal structure of the pattern after a short while. It has also been found that adding dissipation, in the form that in a small fraction of topplings all the particles at the site are lost, not only destroys the pattern but slows down the growth to a logarithmic rate [38].

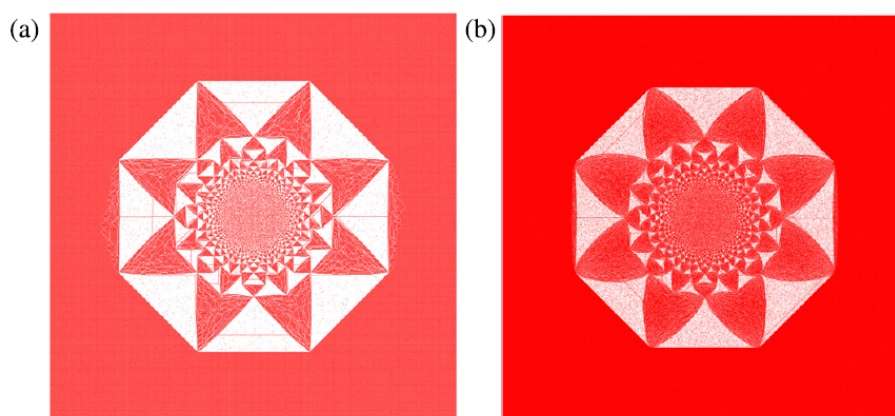


Figure 1.9: The sandpile pattern on an F-lattice starting with a checkerboard configuration, where a fraction p of 1s are changed to 0s. (a) $p = 0.01$, (b) $p = 0.1$. Color code: Red = 0, White = 1. Reprinted with permission, from [24].

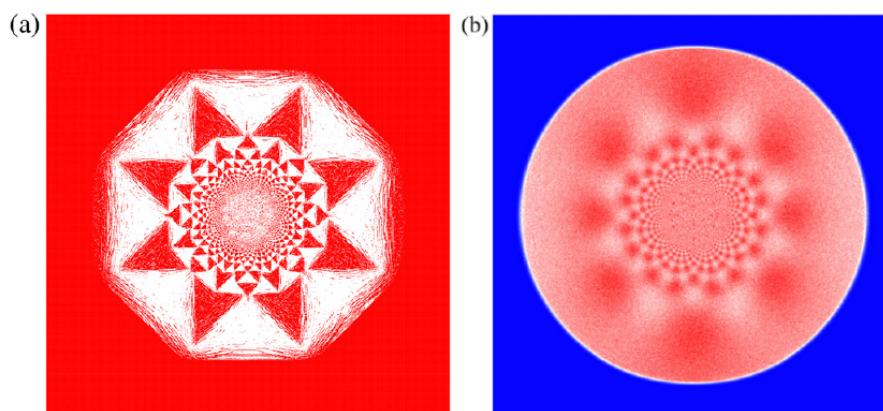


Figure 1.10: The sandpile pattern on an F-lattice starting with a checkerboard configuration, where a fraction p of 1s are changed to 0s and a fraction p of 0s are changed to 1s. (a) $p = 0.01$, Color code: Red = 0, White = 1. (b) $p = 0.2$, averaged over many realizations of noise. The figure shows the deviation from a uniform density 0.5. White denotes moderately excess density ($\delta h = 0.14$) and red denotes large excess density (the reddest areas have $\delta h = 0.25$). Picture reprinted with permission from [24].

The most interesting results for sandpile patterns with noise are obtained when the initial sand configuration on the lattice is made non-periodic, but keeping the toppling rules deterministic. On the F-lattice, instead of starting with a checkerboard pattern of 1s and 0s, one can randomly change a fraction p of the 1s to 0s. One then gets the pattern shown in fig 1.9 (a), where, interestingly, although internal noisy structures develop inside the patches, the patches are still well-resolved for small noise, and the boundaries between them are still sharply defined. On the other hand, if one changes a fraction p of the 0s to 1s as well, the boundaries between the patches turn fuzzy even for small noise (fig 1.10 (a)), and for large p it is hard to see any remaining structure in the pattern. However, averaging over several realizations of the disorder, one gets a picture like fig 1.10 (b), which shows a very weak density inhomogeneity for all p , corresponding roughly to the positions of the patches in the original pattern.

1.2.2 The Rotor-router Model

The rotor-router model is a simple model of a deterministic walk, in which the walker locally modifies the medium it moves in, affecting its subsequent motion when it returns to the same site. The model was originally introduced in the context of self-organized criticality, and called the Eulerian Walker model [41, 42, 43]. The name comes from the fact that on a finite undirected graph, the walk eventually settles into an Euler cycle, in which each edge of the graph is visited exactly once in each direction.

The topic of deterministic walks on a lattice has a long history within physics and mathematics, being first proposed by Chris Langton as ‘Langton’s ants’ as a particular cellular automaton [44]. The kinetic theory properties of such walks and the relation to random walks on a lattice became an object of study in the following decades [45, 46, 47]. Within the mathematics community, Jim Propp independently proposed the same model as the Eulerian Walker, as a derandomized version of the random walk, naming it the rotor-router model [48]. Reviews of earlier work on the rotor-router model may be found in [50] and [51]. An introductory discussion of derandomization techniques in computer science may be found in [54].

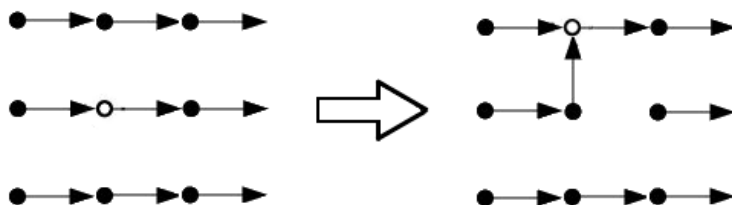


Figure 1.11: A single rotor-router model.

Now we define the rotor-router model more precisely, on a two-dimensional square lattice. The rules of the model are as follows: There is an arrow attached to every lattice site, which points in the direction of one of its four neighbours. When a walker reaches a site, it rotates the arrow attached to that site by 90° counterclockwise and takes a step in the new direction of the arrow (fig. 1.11). For sites which have been visited by the walker at least once, the current direction of the arrow shows the direction of last exit of the walker from that site. Since the update procedure is deterministic, the configuration of arrows and the position of the walker after n steps is fully determined by the initial configuration.

The rotor-router as defined above can be generalized to an arbitrary graph by introducing the notion of a ‘stack’ on each site: a stack is a infinite sequence of instructions of the type ‘go to X ’, where X is one of the neighbours of the site. On arrival at any site, the walker follows the instruction of the topmost entry of the stack at that site. Once it is obeyed, this instruction is deleted (or ‘popped’) from the list, so that the next time the walker arrives at the site, it finds a new instruction. If stack is an infinite repetition of ‘North-West-South-East’, we get the model we study in this paper. If the entries are chosen randomly, we get a random stack. A random stack on every site leads to a random walk on the graph.

The rotor-router model has an abelian property, in the following sense: starting with a given arrow configuration, and positions of n walkers on the lattice, the final arrow configuration on the lattice, once all the walkers have ended up at the sink, is independent of the order in which the walkers are moved. Also, in the final configuration, the arrows in the region visited by the walkers do not form any loops. This follows from a theorem by Broder [52] which says that the last-exit edges of the sites visited by a walker always form a spanning tree.

Consider starting with a number of walkers on a given background, and consider the state of the arrow configuration when the walkers might not have yet reached the sink. $\rho(x, y)$ denotes for the direction of the arrow at site (x, y) . $\sigma(x, y)$, called the walker configuration, denotes the number of walkers on site (x, y) . Call the starting arrow and walker configurations as ρ_i and σ_i respectively. Let $u(x, y)$ denote the total number of times the site (x, y) is visited - the visit function (or ‘odometer function’) at the point (x, y) . Then ρ and σ at any time obey the equation

$$\mathcal{L}u(\rho_i)(x, y) = \sigma(x, y) - \sigma_i(x, y) \quad (1.13)$$

where the ‘stack Laplacian’ \mathcal{L} is defined as difference between the total number of times the arrows at neighbouring sites have pointed towards site (x, y) in $u(\rho_i)$ rotations, and the value of $u(\rho_i)$ at the site (x, y) [53]. Thus once all the walkers have reached the sink, $\mathcal{L}(\rho, \rho_i)(x, y) = 0$. The value of \mathcal{L} being non-zero at a site indicates that some walkers have

not yet reached the sink.

1.2.3 Almost-perfect circles in the rotor-router model

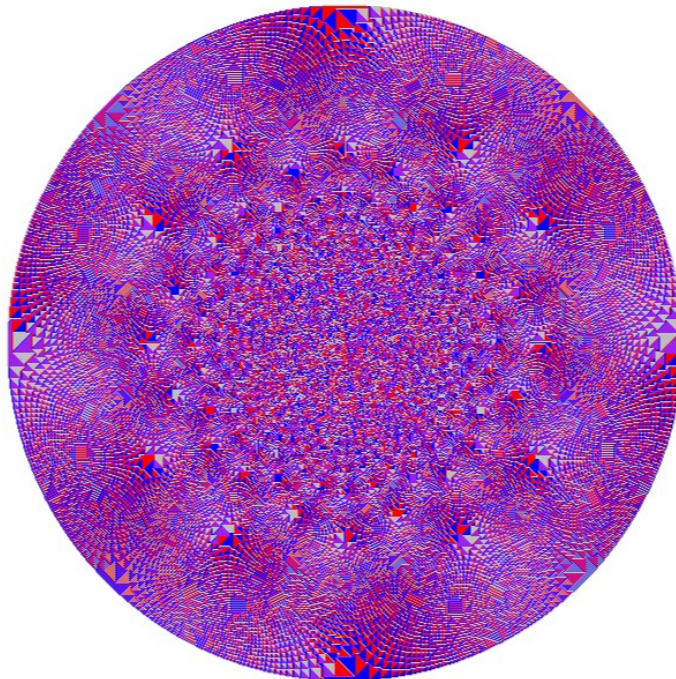


Figure 1.12: A rotor-router aggregation cluster on the square lattice after 270,000 particles, starting with all arrows pointing right. Color code: Red = North, Blue = South, Purple = West, White = East. Courtesy of Yuval Peres.

Levine and Peres [57, 58] have studied the behaviour of a pattern formed by putting walkers at the origin in an aggregating version of the rotor-router model, as the natural derandomized extension of the Internal DLA clusters. In this version of the model, the first walker to visit a site sticks to the site. Hence, the first walker sticks to the origin, but the second walker rotates the arrow attached to the origin and walks to one of the neighbours and sticks there, and so on. One gets a compact aggregate growing around the origin, in a roughly circular shape, with the radius growing as $N^{1/2}$, where N is the number of walkers. The surprising thing Levine and Peres found was that the shape of the aggregate is almost a perfect circle, with simulations indicating that the difference between the inner and outer radii is $O(1)$ and does not grow with N . However, so far the best analytical upper bounds on this quantity are logarithmic in N .

When starting with a regular initial arrow configuration on the lattice (e.g. all arrows pointing in the same direction), the aggregate formed shows quite interesting internal structure, with large triangular patches in some regions. The structure of these patches seems quite similar to the ones studied in Chapter 3 in the non-aggregating version of the rotor-router model, but it has not yet been characterized. An interesting suggestion made by

Matt Cook is that this pattern is extremely similar to a Moire patterns created on the unit circle in the complex plane [59].

1.3 Growing Surfaces: The KPZ Universality Class

In section 1.1 we discussed many different growing surfaces. Remarkably, in many of these models, the exponents α and β have similar values. In this section we discuss the two main universality classes of growing rough surfaces. Then we discuss a more remarkable form of universality that has been discovered in the past thirty years in various superficially unconnected models in statistical physics. It is a universality manifest not just in the scaling properties of certain variables, but in their probability distributions as well. We present a few exact mappings between such models which are relevant to this thesis, first from a model of subsequence matching to the asymmetric exclusion process, and then from the ASEP to growing surfaces.

1.3.1 Universality classes for growing surfaces

To study the dynamics of non-equilibrium systems, one often integrates out the microscopic degrees of freedom to get a Langevin equation for a coarse-grained field, which represents the mesoscopic degrees of freedom. In fact, one can usually write down the Langevin equation using only the symmetries of the microscopic dynamics, and keeping all terms allowed by these symmetries. One then determines which terms are relevant or irrelevant in a renormalization sense. The values of the parameters in the coarse-grained description depend, of course, on the parameters in the microscopic dynamics.

To study growing surfaces, the relevant mesoscopic field is a coarse-grained height function $h(x, t)$, without overhangs, defined on continuous space and time. (Note that if the model has overhangs, it has to be shown that their existence is irrelevant after the coarse-graining.) For many models, such as the Eden model, one can argue that overhangs are irrelevant for the mesoscopic dynamics. We restrict the Langevin equation for $h(x, t)$ to obey the following constraints ([61]):

- (i) There is translation invariance along the growth direction, that is, the dynamics of growth does not depend on the heights.
- (ii) In the plane perpendicular to the growth direction, we have translation, inversion and rotation symmetries.
- (iii) The equation is first order in time.
- (iv) The randomness in the growth dynamics is local in space and time.

These symmetries dictate that the only surviving terms in the Langevin equation are of the form $(\nabla^a h)^c$ where the product ac is even, or products of such terms. The most general

such Langevin equation looks like

$$\frac{\partial h}{\partial t} = c + D_1 \nabla^2 h + D_2 \nabla^4 h + \lambda_1 (\nabla h)^2 + \lambda_2 (\nabla^2 h)^2 + \dots + \eta \quad (1.14)$$

where η is a delta-correlated noise in space and time. Note that the first term can be removed by transforming to the frame moving with velocity c . In 1+1 dimensions, it can be shown by power-counting arguments that the terms with coefficients D_2 , λ_2 and all λ_n for $n > 2$ are irrelevant under renormalization flow, if $D_1 \neq 0$. Thus, we concentrate on the following Langevin equation:

$$\frac{\partial h}{\partial t} = D \nabla^2 h + \lambda (\nabla h)^2 + \eta \quad (1.15)$$

This is known as the Kardar-Parisi-Zhang equation [18]. Note that this equation is not invariant under the transform $h \rightarrow -h$, that is, if $h(x, t)$ is a solution to this equation, $-h(x, t)$ is not, unless $h = 0$ everywhere. However, sometimes the microscopic dynamics is symmetric under $h \rightarrow -h$ (note that we are talking about the dynamics in the Galilean-transformed frame moving with average height). In the Galilean-transformed frame, this can also be taken to mean that the dynamics is invariant under time-reversal. This would set $\lambda = 0$ by symmetry, and we get the Edwards-Wilkinson equation [17]

$$\frac{\partial h}{\partial t} = D \nabla^2 h + \eta \quad (1.16)$$

Since this is a linear equation, it is easily solved for $h(x, t)$ in terms of $\eta(x, t)$, as

$$h(x, t) = \int_0^t dt' \int_{-\infty}^{\infty} dx' \frac{e^{-(x-x')^2/4D(t-t')}}{\sqrt{4\pi D(t-t')}} \eta(x', t') \quad (1.17)$$

which leads to the result $\langle h(x, t)^2 \rangle = \Gamma \sqrt{2t/\pi D}$. This gives us the value of the exponent $\beta = 1/4$. Also, inhomogenities in the surface spread out diffusively, and hence we have the exponent $z = 2$, which gives $\alpha = 1/2$.

We now turn to the KPZ equation, which describes processes when there is no up-down symmetry in the dynamics (in the frame moving with the average growth velocity). Ballistic deposition and Eden growth from a line are both examples of this. Although this equation cannot be exactly solved as simply as the EW equation, the exponents for 1+1 dimensions are long known from dimensional analysis. If one considers the probability distribution for height fluctuations, $\Pi[h(x)]$, it satisfies a Fokker-Planck equation:

$$\frac{\partial \Pi}{\partial t} = - \int dx \frac{\delta}{\delta h} [(D \nabla^2 h + \lambda (\nabla h)^2) \Pi] + \Gamma \int dx \frac{\delta^2 \Pi}{\delta h^2} \quad (1.18)$$

which has the implicit stationary solution in 1D:

$$\Pi = \exp \left[- \int dx \frac{D}{2\Gamma} \left(\frac{\partial h}{\partial x} \right)^2 \right] \quad (1.19)$$

We use dimensional analysis to find the exponents, taking into account that D and Γ only appear in the combination D/Γ . We assume that the lateral (across the surface) directions and the vertical (growth) directions have independent scaling dimensions, $L = [x]$ and $H = [h]$. From eqn. (1.15), we have $[\lambda] = L^2 H^{-1} [t]^{-1}$. Matching dimensions, we get

$$w \sim (\lambda t)^{1/3} (\Gamma/D)^{2/3}, \quad l \sim (\lambda t)^{2/3} (\Gamma/D)^{1/3} \quad (1.20)$$

where w denotes that fluctuations in height, and l denotes the length scale along the surface (the correlation length). Thus we find that $\beta = 1/3$ and $\alpha = 2/3$, and hence $z = 2$.

For more models of growing surfaces in the KPZ class, see the review by Halpin-Healy and Zhang [16].

1.3.2 Exact mappings in the KPZ class

In this subsection, we discuss the Bernoulli matching model and its mapping to the Asymmetric Exclusion Process (ASEP), which can be solved exactly using the Bethe Ansatz. For more details on the mapping, see Priezzhev and Schutz [64].

The Bernoulli matching problem [65] is a special case of the problem of finding the longest common subsequence (LCS) given two sequences of characters. (A subsequence of a sequence is a sequence of characters that appear in the same order as in the main sequence.) For example, the sequences ABCABBABABC and BABBCBA have the common subsequence ‘ABCBA’, as given by the underlined letters, and this is also the longest common subsequence for these two sequences. In the Bernoulli matching problem, we ask the probability distribution of the length of the LCS $l_{m,n}$, for two random sequences, one of length m and the other of length n , picked from an alphabet of c letters. (Thus, two randomly picked characters have a probability $p = 1/c$ of matching. Then, $l_{i,j}$, the LCS for the first i characters of sequence 1 and first j characters of sequence 2, obeys the recursion relation

$$l_{i,j} = \max[l_{i-1,j}, l_{i-1,j-1} + \eta_{i,j}, l_{i,j-1}] \quad (1.21)$$

where $\eta_{i,j}$ is a Bernoulli random variable which is 1 with probability p and 0 with probability $(1-p)$. Fig 1.13 shows the values of $l_{i,j}$ and the values of (i,j) for which $\eta_{i,j} = 1$. Regions with different values of $l_{i,j}$ are separated by terraces constructed in the following way: Draw vertical and horizontal lines at right angles from the cells $\{m,n\}$ where the characters at positions m and n match, and stop them when the lines meet. The resulting function $l_{m,n}$

is related to the wetted surface in 3-dimensional anisotropic directed percolation studied by Rajesh and Dhar [69], and also to a five-vertex model [68]. However, here we use a mapping to the Asymmetric Exclusion Process, since the ASEP can be directly mapped to a height model.

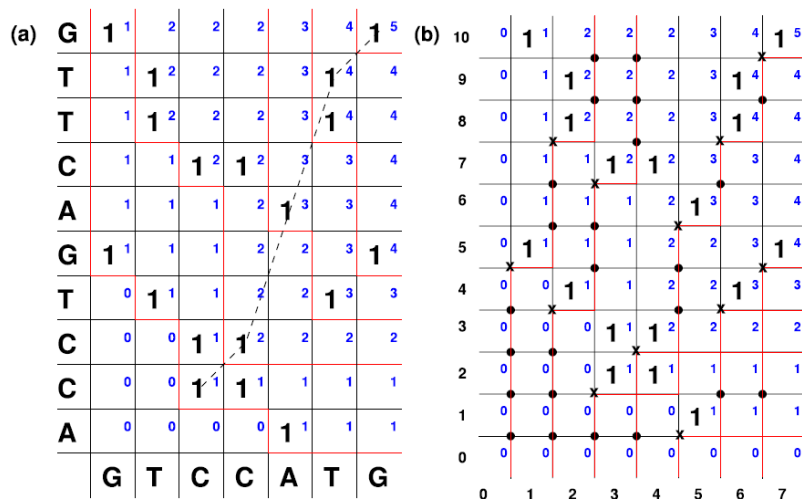


Figure 1.13: (a) Figure showing the terraces (red lines) and the values of $l_{i,j}$ for two sequences of lengths 7 and 10. Cells marked with a '1' denote values of i and j where the characters match. (b) The 'hole' trajectories constructed by erasing the vertical red lines from the figure on the left and drawing vertical red lines where there were none. Rightward jumps of the trajectories happen with probability p . Figures reproduced with permission from [64].

Looking at the vertical axis as time and the horizontal axis as space, the terraces in the model can be seen as the space-time trajectories of individual particles in an exclusion model on a 1D lattice (note that the terraces do not overlap). The 'particles' in this exclusion model can move several horizontal steps before a vertical step. This does not correspond to the behaviour of particles in the exactly solvable discrete-time Asymmetric Exclusion Process, where, particles can only be moved one step per unit time. Priezzhev and Schutz constructed a mapping to the ASEP by looking at the movement of 'holes' on the lattice. The holes, in fact move only a distance of one or zero to the right per time-step. The terraces and the hole trajectories are shown in fig 1.13. In the hole trajectories picture, $l_{m,n}$ changes by 1 whenever, moving horizontally, there is *no* vertical hole world-line between two sites, and does not change when one crosses a hole world-line.

We then make a further mapping $(i, j) \rightarrow (1 - i, j)$ (a reflection about the vertical line $x = 1$), and then interchange hole moves \leftrightarrow hole non-moves. That is, on the reflected trajectories, one draws new trajectories by moving the holes one step to the right when in the original trajectory they did *not* move, and keeping the holes at the same site when in the original trajectory they *did* move. Fig. 1.14 shows this transformation.

Priezzhev and Schutz find that the resulting trajectories correspond to a discrete-time ASEP of the holes with backward sequential updates. A backward sequential update is when, at each time-step, one examines the holes on the lattice sequentially, moving from right to left along the lattice. A hole is moved a step to the right with probability $(1 - p)$ or not moved with probability p .

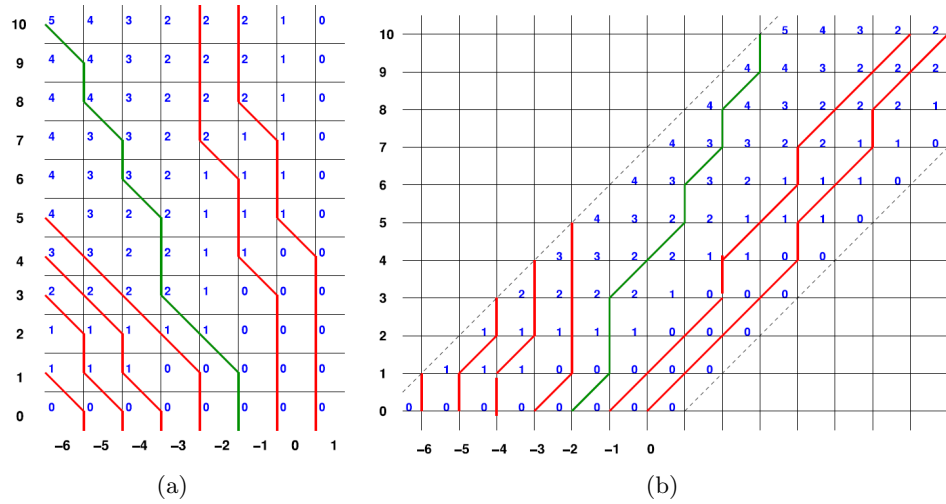


Figure 1.14: (a) The hole trajectories after reflection about the line $x = 1$. Note that rightward moves are indicated by an 45° segment in order to avoid apparent intersections of trajectories. (b) The trajectories in part (a) after interchanging moves and non-moves. Also shown is a diagonal line starting from $(-7, 0)$ upto a time $t = 10$. Counting the trajectories crossing this line, we get $l_{7,10} = 4$. Figures reproduced with permission from [64].

The interpretation of $l_{m,n}$ in the new model, as can be seen from the figure, is the following: if X is the number of hole trajectories crossing the diagonal line from $(-m, 0)$ to $(n - m, n)$, $l_{m,n} = m - X$. The boundary condition that $l_{m,n} = 0$ for $m = 0$ and $n = 0$ (so that the counting of the LIS starts from the $m, n = 1$) is implemented by starting with the step initial condition that all sites for $x \leq 0$ are occupied by holes, and all sites for $x > 0$ occupied by particles, at $t = 0$.

The expression for $l_{m,n}$ was first derived by Seppalainen [66], and by Rajesh and Dhar [69] for a model which can be exactly mapped onto the Bernoulli Matching model, as shown by Majumdar and Nechaev [67, 68]. The number of trajectories crossing this line was calculated by Priezzhev and Schutz using the Bethe Ansatz solution of the ASEP, and

for large m and n this gives for the Bernoulli matching problem

$$l_{m,n} = \begin{cases} m & \text{if } x < py \\ \frac{1}{1-p}(2\sqrt{pnm} - p(m+n)) + A(p, m, n)\xi_{GUE} & \text{if } py \leq x \leq p^{-1}y \\ n & \text{if } p^{-1}y < x \end{cases} \quad (1.22)$$

for $m \gg 1$ or $n \gg 1$. ξ_{GUE} is a random variable distributed according to the Tracy-Widom distribution corresponding to the Gaussian Unitary Ensemble, and $A(p, x, y) = (pxy)^{1/6}/(1-p) \left[(1+p) - \sqrt{p/xy}(x+y) \right]^{2/3}$. For more on the Tracy-Widom distribution see the Appendix.

We now present a mapping of the ASEP to a growing surface in the KPZ universality class. In fact, using the Bethe Ansatz solution one can show that for this growing surface, the fluctuations of h also follow the Tracy-Widom distribution.

We start with an initial condition of the ASEP in which all sites with $x \leq 0$ are occupied by particles and unoccupied for $x > 0$. At every time step, we apply some method of update (random sequential, backward sequential, parallel) to move moveable particles one step to the right, with probability $p \leq 1$. The corresponding dynamics for the height model will differ slightly in all the cases mentioned. Denoting the occupation variables for the ASEP with $\eta_i = 0, 1$, we define height variables on the dual lattice with $h_{i+1/2} - h_{i-1/2} = (1 - 2\eta_i)$. Thus, we get a height surface $h_{j+1/2}$ with downward-sloping parts (going left to right) when there is a particle on the lattice, and upward-sloping parts when there is a hole. A moveable particle in the ASEP, namely a configuration 10, consists of a local minimum in the surface. The changes in height at a particular time thus happen only at the local minima in the surface at that time.

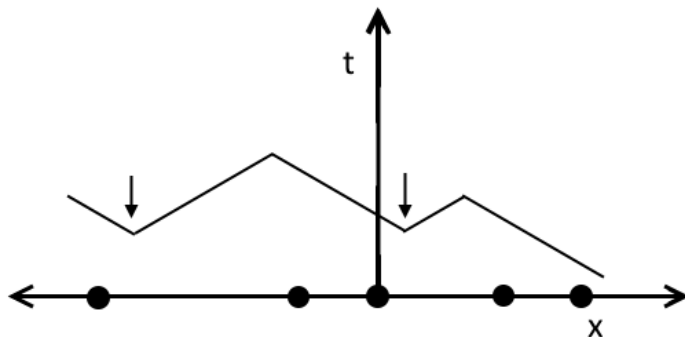


Figure 1.15: A tasep configuration and the corresponding growing surface. The arrows indicate the possible moves available at this stage.

A move $10 \rightarrow 01$ at sites $i, i+1$ corresponds to the height at the site $i+1/2$ increasing

by 2. Thus the site is no longer a local minimum, but its adjacent sites might become new local minima. Backward sequential updates for the height surface correspond to scanning the height surface from left to right and raising the height at every local minimum encountered by 2 with probability $(1 - p)$, and keeping it unchanged with probability p .

It is evident that the dynamics is not symmetric under time-reversal, as the dynamics destroys the local minima of the surface present at a given time and but does nothing to the maxima. Thus we expect that the fluctuations of the height belong to the KPZ class, and thus expect its variance to scale as $t^{1/3}$. $l_{m,n}$ for the Bernoulli Matching problem is related to the number of hole trajectories crossing the diagonal line from $(-m, 0)$ to $(n - m, n)$. The number of hole trajectories crossing this diagonal line is equal to the number of particles overtaken in time n by a particle which starts at $(-m, 0)$ at time 0 and moves to the right with unit velocity. This is the difference the number of particles to the right of $x = -m$ at the initial time and those to the right of $x = n - m$ at time n . Both these quantities can be expressed in terms of the height function $h(m, n)$, giving

$$l_{m,n} = \begin{cases} h_{n-m+1/2}(m) + m - n, & \text{for } n < m \\ h_{n-m+1/2}(m), & \text{for } n \geq m \end{cases} \quad (1.23)$$

The height $h_{1/2}(t)$, is simply the number of particles that have crossed the origin in time t , with backward-sequential updating. From eqn. 1.22, this is given as

$$h_{1/2}(t) = l_{t,t} \quad (1.24)$$

$$= \frac{2}{1-p}(\sqrt{p} - p)t + p^{1/6}/(1-p)(1+p-2\sqrt{p})^{2/3} t^{1/3} \xi_{GUE} \quad (1.25)$$

Thus the height at the dual lattice site with co-ordinate $1/2$ grows linearly with time, and the fluctuations for large times scale as $t^{1/3}$, a proof that this height model is in the KPZ universality class.

For more examples of models which can be exactly mapped to each other and finally to a random matrix model, see the reviews by Kriecherbauer and Krug [62] and Majumdar [63].

Appendix: The Tracy-Widom distribution

This distribution was introduced by Tracy and Widom in 1993 [70] as the probability distribution of the largest eigenvalue of a random hermitian matrix. It has since found applications in various problems, most prominently ones related to the Kardar-Parisi-Zhang universality class. See [62] and [63].

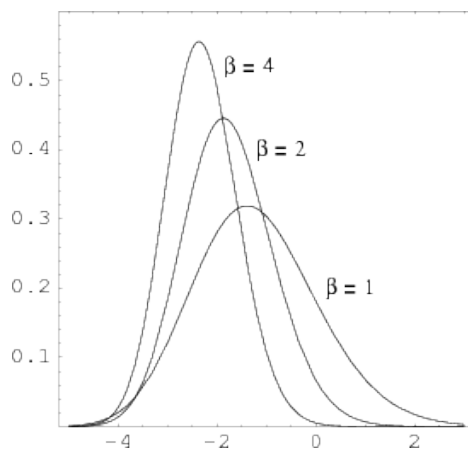


Figure 1.16: The probability density for the largest eigenvalue, for Gaussian Orthogonal ($\beta = 1$), Gaussian Unitary ($\beta = 2$) and Gaussian Symplectic ($\beta = 4$) Ensembles.

The cumulative distribution function of the Tracy-Widom distribution is given by the formula

$$F_2(s) = \exp\left(-\int_s^\infty (x-s)q^2(x)dx\right) \quad (1.26)$$

where $q(s)$ is the solution of the type II Painleve equation

$$q''(s) = sq(s) + 2q(s)^3 \quad (1.27)$$

which satisfies the boundary condition $q(s) \sim \text{Ai}(s)$ as $s \rightarrow \infty$, where $\text{Ai}(s)$ is the Airy function. One can numerically evaluate

$$\langle s \rangle = -1.2065335746\dots, \quad \langle s^2 \rangle - \langle s \rangle^2 = 1.6077810346\dots \quad (1.28)$$

and other higher moments. Similar cumulative distributions $F_1(s)$ and $F_4(s)$, related to F_2 , can be defined for the distributions of the largest eigenvalues of random symmetric and quaternionic matrices respectively.

Although the exact form of the distribution can be evaluated numerically (plotted in fig 1.16), the behaviour of the tails can be determined via a simple scaling argument for the ASEP (refer to [61] for details). As given earlier the number of particles crossing the origin in time t , in a TASEP with backward-sequential updates, is given as

$$N(t) = a(p)t + b(p)t^{1/3}\xi_{GUE} \quad (1.29)$$

where $a(p)$ and $b(p)$ are p -dependent functions. We set $p = 1/2$, and approximate the probabilities for N very large and very small. $N(t) = 0$ corresponds to the situation in which none of the particles move in time t . This means that the first particle does not move at all times $1, 2, \dots, t$, giving us a probability $P(N(t) = 0) = 2^{-t}$. To get $N = 0$ involves

setting $\xi_{GUEsim} - t^{2/3}$, giving

$$P_{GUE}(\xi) \sim \exp(-c_- |\xi|^{3/2}) \quad \text{for } \xi \rightarrow -\infty \quad (1.30)$$

Similarly, not set $N(t) = t$, the maximum number of walkers which can be moved past the origin in time t . The probability of this is (since, at each time step, all particles after the origin must be moved one more step to the right)

$$\frac{1}{2} \times \frac{1}{2^2} \times \cdots \times \frac{1}{2^{(t-1)}} \times \frac{1}{2^t} = \frac{1}{2^{t(t+1)/2}} \quad (1.31)$$

Note that setting $N(t) = t$ involves setting $\xi_{GUE} \sim t^{2/3}$, thus giving

$$P_{GUE}(\xi) \sim \exp(-c_+ \xi^3) \quad \text{for } \xi \rightarrow \infty \quad (1.32)$$

The values of the constants c_+ and c_- can be determined by an analysis of the random matrices based on, for example, a mapping to a logarithmically interacting gas on a line, to be $c_+ = 1/12$ and $c_- = 4/3$.

Bibliography

- [1] T. Viscek, Fractal growth phenomena Vol. 4. (World scientific, Singapore) (1989).
- [2] H. J. Hermann, Phys. Rep. **136** 153 (1986).
- [3] M. C. Cross and P. C. Hohenberg, Rev. Mod. Phys. **65** 851 (1993).
- [4] M. Eden, Proc. Fourth Berkeley Symp. on Mathematical Statistics and Probability, ed. F. Neyman (Univ. of Claif. Press, Berkeley) Vol. IV, p. 223 (1961).
- [5] D. E. Wolf and J. Kertesz, J. Phys. A **23** L257 (1987) (exponents in $d=2,3,4$).
- [6] D. Dhar, Phys. Rev. Lett., **54** 2058 (1985).
- [7] M.T. Batchelor and B.I. Henry, Phys. Lett. A, **157** 229 (1991).
- [8] T. Williams and R. Bjercknes, Nature **236** 19 (1972).
- [9] Z. Alexandrowicz, Phys. Lett. **80A** 284 (1980)
A. Bunde, H. J. Hermann, A. Margolina and H. E. Stanley, Phys. Rev. Lett. **55** 653 (1985).
- [10] R. Chandler, J. Koplik, K. Lerman and J. F. Willemsen, J. Fluid. Mech. **119** 246 (1982)
D. Wilkinson and J. F. Willemsen, J. Phys. A **16** 3365 (1983)
B. Nickel and D. Wilkinson, Phys. Rev. Lett. **51** 71 (1983).
- [11] O.Haggstrom, Y.Peres and R.H.Schonmann: *Perplexing Problems in Probability. Festschrift in honor of Harry Kesten*. M. Bramson, R. Durrett, ed. (Birkhauser, 1999), pp. 69-90
- [12] T. A. Witten and L. M. Sander, Phys. Rev. Lett. **47** 1400, 1981.
- [13] P. Meakin, Phys. Rev. Lett. **51** 1119 (1983) (dla exponents).
- [14] J. W. Lyklema, C. Evertsz and L. Pietronero, Europhys. Lett. **2** 77 (1986).
- [15] F. Family, Physica A, **168** 561 (1990) (defines exponents for growing surfaces).
- [16] T. Halpin-Healy and Y-C Zhang, Phys. Rep. **254** 215 (1995).

-
- [17] S. F. Edwards and D. R. Wilkinson, Proc. Roy. Soc. Lond. A. Math. Phys. Sci. **381** 17 (1982).
- [18] K. Kardar, G. Parisi, and Y.Z. Zhang, Phys. Rev. Lett. **56** 889 (1986).
- [19] M. J. Vold, J. Coll. Sci., **14** 168 (1959).
- [20] M. Prahofer and H. Spohn, Phys. Rev. Lett **84** 4882 (2000)
M. Prahofer and H. Spohn, J. Stat. Phys. **108** 1071 (2002)
- [21] K. Johansson, Comm. Math. Phys. **242** 277 (2003)
- [22] M. Kolb, R. Botet and R. Jullien, **51** 1123 (1983)
- [23] F. Leyvraz, J. Phys. A **18** 321 (1985)
- [24] T. Sadhu and D. Dhar, J. Stat. Mech. P11006 (2013).
- [25] P. Bak, C. Tang and K. Wiesenfeld, Phys. Rev. Lett. **59** 381 1987.
- [26] D. Dhar, Phys. Rev. Lett. **64** 1613 (1990).
- [27] D. Dhar, Physica A **369** 29 (2006).
- [28] S. Ostojic, Physica A **318** 187 (2003).
- [29] D. Dhar, T. Sadhu and S. Chandra, Europhys. Lett. **85** 48002 (2009).
- [30] T. Sadhu and D. Dhar, J. Stat. Phys. **138** 815 (2010).
- [31] T. Sadhu and D. Dhar, J. Stat. Mech. P03001 (2011).
- [32] M. Creutz, Comput. Phys. **5** 198 (1991).
- [33] S. Caracciolo, G. Paoletti and A. Sportiello, J. Phys. A: Math. Theor. **41** 495003 (2008).
- [34] G. F. Lawler, M. Bramson and D. Griffeath, Ann. Probab. **20** 2117 (1992).
- [35] L. Levine and Y. Peres, J. d'Analyse Math. **111** 151 (2010).
- [36] J.-F. Gouyet, *Physique et structures fractales*, Elsevier Masson, 1992.
- [37] T. Sadhu and D. Dhar, Phys. Rev. E **85** 021107 (2012).
- [38] R. Dandekar, Pattern formation in diusive sandpiles, 2011 Proc. Conf. Dynamics of Phase Transformations (Bangalore) www.jncasr.ac.in/dpt/abstract_poster.pdf
- [39] L. Lovasz, Discrete Analytic Functions: An Exposition, <http://www.cs.elte.hu/lovasz/analytic.pdf>
- [40] L. Levine, W. Pegden and C. K. Smart arXiv:1208.4839 (2012).

- [41] V. B. Priezzhev, D. Dhar, A. Dhar and S. Krishnamurthy, Phys. Rev. Lett., **77** 5079 (1996).
- [42] R. R. Scherbakov, Vl. V. Papoyan, and A. M. Povolotsky, Phys. Rev. E, **55** 3686 (1997).
- [43] A. M. Povolotsky, V. B. Priezzhev, and R. R. Scherbakov, Phys. Rev. E, **58** 5449 (1998).
- [44] C. G. Langton, Physica D, **22** 120 (1986)
https://en.wikipedia.org/wiki/Langton's_ant
- [45] Th. W. Ruijgrok and E. G. D. Cohen, Phys. Lett. A **133** 415 (1988)
- [46] L.A. Bunimovich, S. E. Troubetzkoy, J. Stat. Phys., **67** 289 (1992)
- [47] H. Freund and P. Grassberger, Physica A, **190** 218 (1992)
- [48] J. Propp, Chaos, **20** 037110 (2010).
- [49] A. E. Holroyd and J. Propp, Contemporary Mathematics, **520** 105 (2010)
arXiv:0904.4507
- [50] A. E. Holroyd, L. Levine, K. Meszaros, Y. Peres, J. Propp and D. B. Wilson, Progress in Probability, **60** 331 (2008). arXiv:0801.330
- [51] L. Levine, *The rotor-router model*, Harvard University Senior Thesis (2002).
arXiv:0409407
- [52] A. Z. Broder, Generating random spanning trees, Foundations of Computer Science 442 (1989).
- [53] T. Friedrich and L. Levine, Fast simulation of large-scale growth models, Random Structures & Algorithms **42** 185 (2013)
- [54] S. P. Vadhan, Pseudorandomness, preprint available from
<http://people.seas.harvard.edu/~salil/pseudorandomness/>.
- [55] L. Florescu, S. Ganguly, L. Levine and Y. Peres, arXiv:1301.3521
- [56] M. Kleber, The Mathematical Intelligencer, **27** 55 (2005).
- [57] L. Levine and Y. Peres, Indiana Univ. Math. J., **57** 431 (2008). arXiv:0503251.
- [58] L. Levine and Y. Peres, Potential Analysis, **30** 1 (2009), arXiv:0704.0688.
- [59] Matt Cook, <http://paradise.caltech.edu/cook/Warehouse/ForPropp/>
- [60] R. Kapri and D. Dhar, Phys. Rev. E, **80** 051118 (2009).

-
- [61] P. L. Krapivsky, S. Redner, and E. Ben-Naim, *A kinetic view of statistical physics* (Cambridge University Press, Cambridge) (2010)
- [62] T. Kriecherbauer and J. Krug, *J. Phys. A: Math. Theo.* **43** 403001 (2010), arXiv:0803.2796 (2008).
- [63] S. N. Majumdar, *Les Houches lecture notes*, 2006, arxiv:0701193.
- [64] V. B. Priezzhev and G. M. Schutz, *J. Stat. Mech.* P09007 (2008).
- [65] J. Boutet de Monvel, *Eur. Phys. J. B* 7, 293 (1999); *Phys. Rev. E* 62, 204 (2000).
- [66] T. Seppalainen, *Ann. Appl. Probab.* 7, no. 4, 886 (1997).
- [67] S.N. Majumdar and S. Nechaev, *Phys. Rev. E* 72, 020901(R) (2005).
- [68] S.N. Majumdar, K. Mallick and S. Nechaev, arXiv:0710.1030v1 [cond-mat.stat-mech] (2007).
- [69] R.Rajesh and D.Dhar, *Phys.Rev. Lett.* 81, 1646 (1998).
- [70] C.A. Tracy and H. Widom, *Commun. Math. Phys.* 159, 151 (1994); 177, 727(1996).

Chapter 2

Introduction to Active-Absorbing Phase Transitions

In this chapter, we will review the phenomenon of absorbing phase transitions, in systems with and without a conserved number of particles. Absorbing states are states which the dynamics can lead to but cannot escape from. In Absorbing (or active-absorbing) phase transitions, as an external parameter is tuned, the long-time limit of the system changes from an active fluctuating steady-state to an absorbing state where no further changes occur. Some useful reviews are the lecture notes by Grinstein and Munoz [1], the review articles by Hinrichsen [2] and Lubeck [3] (the latter focuses on the study of scaling relations and scaling functions), and the recent book by Henkel, Hinrichsen and Lubeck [4]. These transitions are characterized by static and dynamical critical exponents which obey well-known scaling relations. We will also discuss the phenomena of universality, wherein transitions in many diverse systems nevertheless show the same critical exponents near the transition. The classification of universality classes of absorbing phase transitions, especially those in systems with a conserved number of particles, has been a topic of particular interest in the recent literature [5, 6, 7, 8].

2.1 Absorbing phase transitions

Absorbing states are configurations of the system in which no further transitions are possible. In the following we give some, admittedly idealized, models of real systems which exhibit transitions between an absorbing phase and a fluctuating active phase.

(i) An epidemic disease spreading through the population might die out if the infection rate is low, that is, infected individuals at a particular time do not infect anyone else before they die or recover. A simple model for this is an that an infected person infects everyone he or she comes in contact with a given probability p and recovers from the disease at a unit rate. Once the disease dies out it cannot regenerate, and hence this is an absorbing state.

Whether the disease dies out or proliferates depends on the mean number of other people a single infected person infects before dying or recovering, which depends on p . As p is varied, there is transition between eventual dying out and a phase where there are always some infected individuals in the population [9, 10, 11]. More realistic models of epidemics have been proposed, among them the Generalized Epidemic Process, which is a model where individuals infected earlier have a different susceptibility to the disease the next time round (for example, they might become immune after a given number of infections). Similar to the epidemic models are models of forest fires where the state where the fire dies out is absorbing [12].

(ii) The Ziff-Gulari-Barshad (ZGB) model [13] for the catalytic oxidation of carbon monoxide (CO) to carbon dioxide (CO₂) on a substrate, is defined as follows: Consider the substrate to be a 2D lattice. A CO atom gets adsorbed to an empty site on the surface at a rate y . The two atoms of an O₂ molecule get adsorbed to an adjacent pair of empty sites at a rate $1 - y$. The difference between the two rates represents the different concentrations of the gases in the air above the substrate, and is a tunable parameter. If a CO molecule and an O atom find themselves on adjacent sites, they merge to form a CO₂ molecule and desorb from the surface. This model has two absorbing states - one (for low y) where the entire lattice is filled with O atoms, and one (for high y) where it is entirely filled with CO atoms. Note that this is because both these species cannot desorb on their own. Simulations show correspondingly that there are two transitions and three phases in this model - an active phase sandwiched between the two absorbing phases mentioned above. The transition for low y which is continuous and the one for high y which is first-order [13, 14].

(iii) Water injected at one end of a porous medium percolates under the influence of an external force, and either stops percolating at some point or continues percolating down ‘forever’, depending on the porosity of the medium. If one (in modelling this system) forbids flow of water against gravity, then whether the pores at some level are occupied by water depends on the state of the previous level. The downward direction can be seen as the time axis, and hence the state of the a pore (wetted or not) can be said to depend on the state of its neighbours at the ‘previous time-step’. As one varies the porosity of the medium, it changes the probability of neighbouring pores being connected by downward channels, and one gets a transition from an absorbing state where after a certain time (or level, going downward) in the long-time limit (same as long-distance in the downward direction in the porous material) there is no water in the pores, to a state where there is always a finite density of wet pores arbitrarily downwards. Note that here only also assumes that the structure of the pores does not change as one moves down, so that it also remains same in ‘time’.

One observes from the above examples that the ‘activity’, whether it is the presence of a diseased individual or desorption from the surface or presence of a wetted pore, does not

occur spontaneously in the dynamics, but is only reproduced from active elements already present. The essential competition is between the death of activity and its proliferation. The presence of absorbing states indicates that these are truly non-equilibrium systems, because for a state which can be entered but never exit from, detailed balance is necessarily broken. It must be noted that the descriptions given of the above systems fall somewhere between simple, idealized models and experimental realizations of absorbing phase transitions. Experimental realizations of the systems above, and quantitative measurements on them, are complicated by the presence of disorder as well as the fact that the presence of even a slight amount of spontaneous activity wipes out the transition - for example, slight desorption of the CO or O species would destroy the absorbing state. This makes it hard to experimentally measure critical exponents [4]. However, recently it has been found that liquid crystals undergoing transitions between two intermittently turbulent phases provide a clean system where quantitative measurements can be made [15].

2.1.1 Simple models showing absorbing phase transitions

In this subsection we discuss three paradigmatic and simple models showing absorbing phase transitions.

Directed percolation and the contact process

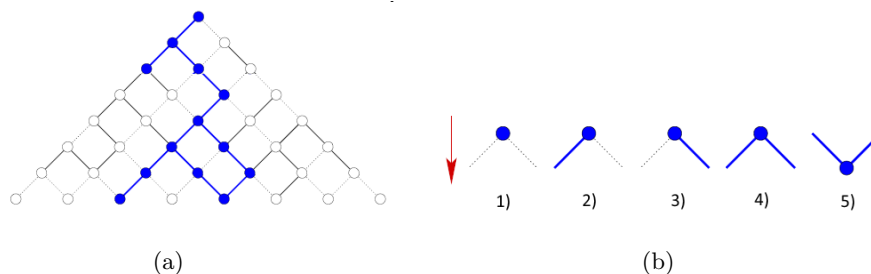


Figure 2.1: (a) Directed bond percolation cluster starting from a single seed. (b) The directed bond percolation rules interpreted as 1) death, 2),3) diffusion, 4) reproduction and 5) coagulation.

Directed bond percolation (DP) [16] is a caricature of the water-percolating-under-gravity system described in the previous section. It is defined on an oriented square lattice, as shown in fig 2.1 (a). Bonds on the square lattice are present with a probability p . Sites become wet if and only if they are connected to wet sites by occupied bonds in the layer above them. Since the bonds are present with a probability p , the various possibilities for evolution are shown in fig. 2.1 (b). These include death (1), diffusion (2,3) and proliferation (4). The ‘activity’ in a layer is defined as the number of occupied bonds in that layer. Starting with some configuration of wet sites in the first layer and a given p , one observes

whether the activity dies out or survives in the long-time limit. This model has not been solved analytically, but numerical studies show that for a 2D square lattice, the transition point $p_c = 0.644700185(5)$ [17]. The universal properties of the model such as the critical exponents (in an expansion around the higher critical dimension) and the structure of the phase diagram can be determined by field theoretic analysis. Reviews of the field theory approach to DP are [18, 19, 20, 2]. [1] discusses renormalization starting from a Langevin equation. We will not discuss the field theory approach in this thesis.

The ‘contact process’ is a continuous-time version of the directed bond percolation model, and is defined by the following rules [21, 22, 23]: sites on a d -dimensional lattice can be occupied or empty. Empty sites which have an occupied nearest neighbouring site can get occupied at rate λ , and occupied sites become unoccupied at rate 1. This is also a simple model for the spread of epidemics discussed in the previous subsection.

For the contact process in the mean field approximation, it is easy to see that the transition between proliferation and death happens at $\lambda = 1/2d$ for a cubic lattice in d dimensions. Close to the critical point, the density of infected individuals in the steady state grows as $(\lambda - 1)^\beta$, giving the critical exponent value $\beta = 1$. MFT also gives $\nu_{\parallel} = 1$ and $\nu_{\perp} = 1/2$ ([23]). (See section 2.2 for the definitions of these exponents.) In 1D, the transition point is however $\lambda = 3.29785(8)$ [24]. This model falls in the same universality class as directed percolation (as do many other models, see section 2.3).

Infinitely many absorbing states: pair contact process

All the models discussed so far have only a single absorbing state on the absorbing side of the transition. (The ZGB model had two, but they were associated with different transitions.) Some models of catalysis, in particular models where two species can co-exist without desorption, like the examples given below, have an exponentially large number of absorbing states.

A simple model of this kind is Jensen’s ‘pair contact process’ [27]. The process is similar to the contact process, except that isolated occupied sites can no longer proliferate or die. If there is a pair of occupied nearest-neighbour sites, however, they can infect one of the vacant neighbours around them at random at rate λ . A pair of such sites can also become unoccupied, at rate 1. For low $\lambda \lesssim 0.08$ occupied pairs of sites eventually die out, leaving a configuration with only isolated particles - that is, occupied sites with no occupied nearest neighbours - which cannot move or evaporate from the surface. Every configuration with only isolated occupied sites is thus an absorbing state. The number of such configurations grows exponentially with the volume of the system.

More complicated models with infinitely many absorbing states include the ‘dimer-dimer model’ for the catalytic formation of water on a substrate [25, 26], in which the isolated hydroxyl group and isolated oxygen atoms are the two species which can co-exist without desorption from the substrate. The steady-state properties of the pair contact process and other models with infinitely many absorbing states, surprisingly, scale with the same critical exponents as directed percolation, and thus the models can be said to fall in the same universality class as directed percolation [27, 28, 29]. However, the time-dependent relaxation properties such as the spreading exponents defined in section 2.3 show a deviation from the DP values.

The conserved lattice gas

The study of absorbing phase transitions in models with a conserved number of particles [31, 32, 35] was motivated by their connection to self-organized critical models like the Manna sandpile [36] (described later in this section). They are long conjectured to fall in a distinct universality class from directed percolation, but recently this claim has been disputed [6]. It is of interest, therefore, to have simple models of such transitions with a well-understood phase space structure, and whose properties can be exactly calculated.

The simplest model with a conserved number of particles which shows an absorbing phase transition is the conserved lattice gas (CLG), first defined in [32]. One considers d -dimensional lattice filled with a given average density of particles ρ . Every site can hold at most one particle, hence $\rho < 1$. Particles which have at least one occupied neighbouring sites are active, and jump to a random empty neighbouring site at rate unity. Isolated particles, meaning particles whose nearest neighbouring sites are all empty, cannot move. At low densities, particles move away from each other till they are all isolated and thus reach an absorbing state. The number of absorbing states grows exponentially with lattice volume - it is simply the number of ways to fill L^d sites with ρL^d particles such that there are no pairs of nearest-neighbour occupied sites. Simulations in 2D starting from a randomly occupied lattice indicate that an active-absorbing transition happens at density $\rho \approx 0.23$, although there are absorbing states till density $\frac{1}{2}$. The measured critical exponents [32, 7] seem to indicate that this model, unlike the ones above, falls in a class distinct from directed percolation - the so-called conserved DP (CDP) class.

The mean field theory of the CLG was worked out by Lubeck and Hucht [33]. The upper critical dimension is $d = 5$. The mean field values for the critical exponents are $\beta = 1$ and $\delta = \frac{1}{2}$. Simulations of the CLG in $d \leq 5$ were carried out by Lubeck in [34], which confirm that the mean field results for $d = 5$. Values of critical exponents for the CLG in dimensions 2 to 5 are given in [4] and recent estimates for $d = 2$ can be found in [8].

In 1D, the steady-state of the CLG turns out to be exactly determined [37], and properties such as the density of active particles, that is, particles which can be moved at a particular time-step, can be calculated as a function density. The 1D models showing an active-absorbing phase transition that we study in the Chapter 5 are closely related to the CLG, and hence we give the 1D solution of the CLG in some detail. Denote the 1D configurations of the CLG on a ring of length L by strings of 1s and 0s, where the 1s denote occupied sites and 0s denote empty sites. We call a contiguous clusters of occupied or empty sites as 1-clusters or 0-clusters respectively. The transitions of the CLG in 1D are

$$110 \rightarrow 101, \quad 011 \rightarrow 101 \quad (2.1)$$

where both the transitions happen at rate unity. It is easy to see that under the dynamics the number of 0-clusters of length > 1 cannot decrease. Also, as long as an activity is present in the system, if there are 0-clusters of length > 1 , the activity will soon diffuse to the location of the 0-cluster and break it up. The long-time result of this depends on whether the 0-clusters dominate or the activity dominates - below density $\rho = 0.5$ eventually there are only isolated 1s left in the system, whereas above this density there are only isolated 0s. Hence the transition density is $\rho_c = 0.5$. Above this density there is an active steady state with allowed configurations being those with only isolated 0s. Configurations which have 0-clusters of length > 1 are transient and are not revisited by the dynamics once the number of such 0-clusters decreases.

In the active steady-state sector, since there are only isolated 0s, transitions are reversible and happen with unit rate in both directions: $1011 \rightleftharpoons 1101$. This implies that there is detailed balance within the steady-state sector of the configuration space, such that all allowed configurations are equally likely. Note that this is still a non-equilibrium system, and irreversible transitions occur when one starts with a configuration outside the steady-state sector. To determine any property in the steady-state, only simply has to average over all configurations with N particles on a ring on length L and with only isolated 0s. Let $C(N, L)$ denote the number of allowed configurations with N particles on L sites. To determine $C(N, L)$, we here use the generating function approach (see Appendix I for an introduction to generating functions). We define:

$$C_L(x) = \sum_{N=0}^L C(N, L)x^N \quad \text{and} \quad (2.2)$$

$$C(x, y) = \sum_{L=1}^{\infty} C_L(x)y^L \quad (2.3)$$

where x is the fugacity of particles and y is the fugacity of sites. The properties of a system of length L' with N' particles for large L' and N' are obtained from $C(x, y)$ by adjusting the values of x and y such that in $\langle L \rangle = L'$ and $\langle N \rangle = N'$. We are simply counting the set of

all strings generated by concatenating the elementary strings 1 and 10. (See the Appendix for an introduction to generating functions.) This gives

$$C(x, y) = (1 - xy - xy^2)^{-1} \quad (2.4)$$

Expanding in partial fractions and then expanding as a Taylor series in y , we see that $C_L(x) \sim y_-(x)^{-L}$ for large L , where

$$y_-(x) = \frac{1}{2}(-1 + \sqrt{1 + \frac{4}{x}}) \quad (2.5)$$

is the smaller root of the equation $1 - xy - xy^2 = 0$. Once we have $C_L(x)$, we can find the fugacity x by setting $x \frac{d}{dx} \log C_L(x) = \langle N \rangle / L$ equal to ρ . This gives, in the thermodynamic limit,

$$\rho = \frac{x}{y_-(x)} \frac{d}{dx} y_-(x) = \left(2 - \frac{1}{2y_-(x) + 1} \right) \quad (2.6)$$

We find that the near-critical limit is taken by the small- x limit of the above expression. This is because as $x \rightarrow 0$ implies $\rho \rightarrow \frac{1}{2}$. The activity density is calculated by modifying the generating function so that it counts the active particles too. Define

$$C(x, y, h) = \sum_{N_a, N, L} C(N_a, N, L) x^N y^L (1+h)^{N_a/2} \quad (2.7)$$

The counting for $C(x, y, h)$ must be done in a way which distinguishes the active and passive particles, and the generating strings used earlier, '1' and '01', cannot do this. We change the set of generating strings to '110', '010' and '1'. Fugacities for the three types of strings are set to $(1+h)x^2y^3$, xy^3 and xy respectively. The fugacity for strings of the type 110 is multiplied by $(1+h)$, so that the new generating function is then

$$(2.8)$$

$$= (1 - xy(1 + y^2 + (1+h)xy^2))^{-1} - 1 \quad (2.9)$$

where N_a denotes the number of active particles in a configuration. We calculate the activity density in the steady-state by the formula

$$\rho_a \equiv \left\langle \frac{N_a}{L} \right\rangle = 2 \frac{d}{dh} C(x, y, h) |_{h=0} \quad (2.10)$$

(This is simply counting the configurations in proportion to the activity - a configuration with n active sites gets the factor $\frac{d}{dh}(1+h)^n|_{h=0} = n$.) Setting the values of x and y so that we are in the thermodynamic limit with density ρ , we get a formula for the activity in terms of the density (for $\frac{1}{2} \leq \rho \leq 1$):

$$\rho_a = \frac{(1-\rho)(2\rho-1)}{\rho} \quad (2.11)$$

The behaviour of the activity near the critical point is the subject of the next section, and here we only note that $\rho_a \sim (\rho - \rho_c)^\beta$, with $\beta = 1$.

The Conserved Manna Model

The Manna Model is a model of Self-Organized Criticality closely related to the sandpile model described in Chapter 1. The 2d Manna Model [36] is a model of particle dynamics defined on an $L \times L$ square lattice by the following rules: (i) If any site has 2 or more particles, 2 particles from this site are transferred to its neighbouring sites, each particle to a randomly chosen neighbour (so some neighbours might get more than 1 particle, unlike the deterministic abelian sandpile model). The transfers are done either in parallel at all sites, in the simplest version of the model. (ii) Particles which move to the boundary sites of the lattice are taken out of the lattice. (iii) Once the system enters a state where the height everywhere is less than 2, and there can be no more topplings, a particle is added at a randomly chosen site, and if necessary, the system is relaxed again following rules (i) and (ii).

Thus the Manna model is a model with threshold dynamics, slow external drive (since one waits for the relaxation to complete before adding a new particle), and boundary dissipation. The steady-state of the model shows power-law correlations in the height variables, and power-law distributions for avalanche sizes and other related variables (avalanche size is defined as the total number of relaxations that occur after step (iii) to get to an absorbing state). Such a state is called self-organized critical, the power laws being evidence of the lack of an intrinsic macroscopic length scale in the system.

The states with all heights less than 2, in the absence of external drive, would be absorbing states for the toppling dynamics. In a series of papers, Vespigiani and collaborators [35] argued that the SOC system can be understood as the critical point of the active-absorbing transition in the conserved version of the model, that is, the one obtained by removing the drive and boundary dissipation (see also [31]). The mechanism for SOC is that the dissipation drives the system towards an absorbing state by decreasing the activity, while the drive generates new activity in the system. The steady-state is when drive and dissipation balance each other, which results in the density being tuned to its critical value ρ_c . The power-law exponents of the steady-state are conjectured to be related to the spreading exponents of the active-absorbing transition (for the definition of spreading exponents see the next section). This prompted research on conserved versions of SOC models, and an important model in this class is the conserved Manna model.

The 2d conserved Manna model is a model of threshold dynamics on a toroidal $L \times L$ square lattice by the following rule: If any site has 2 or more particles, 2 particles from this site are transferred to the neighbouring sites, each to a random neighbour. The transfers

are done in parallel. Note that here the number of particles on the lattice is conserved, and like the CLG the tuning variable is the average density ρ . If ρ is low, successive relaxations eventually result in a state where all heights are less than 2. If $\rho > \rho_c$, there are always active sites, that is, sites with height ≥ 2 , and the activity never dies out. There is controversy over the precise value of ρ_c and the values of the critical exponents, and hence over the universality class of this model. See section 2.3.

2.2 Critical exponents

Systems tuned to be exactly at the transition point of a second order phase transition are known to show scale invariance - the lack of a macroscopic length or time scale, except the size of the system itself [38]. As a result, properties like the equal-time correlation function and the autocorrelation function show power law behaviour for large lengths x or times t . Off-critical properties also show a power-law scaling near the transition point, for example, the magnetisation in a ferromagnet scales as $(T_c - T)^\beta$ for T smaller than but close to T_c . The quantity β is known as a ‘critical exponent’. Models which can be microscopically very different from each other were found to have the same critical exponents, although the behaviour far away from the critical point might be very different [39, 40]. This behaviour is known as universality, and models which share the same scaling properties near the critical point are said to fall in the same universality class. The ultimate explanation of both the power-law scaling and the universality of the exponents of these power laws was provided by the renormalization group, first proposed for equilibrium systems and later extended to non-equilibrium systems as well, including directed percolation [41].

In the following, we state the main quantities of interest in studying the near-transition behaviour of systems showing absorbing phase transition[2]. We also define the critical exponents of interest from the scaling of these quantities near the transition point.

Away from the critical point, the equal-time activity-activity correlation function $C(r) \equiv \langle \rho_a(0, t) \rho_a(r, t) \rangle$ and the single-site activity autocorrelation function in the steady-state (on the active side of the transition) $A(t) \equiv \langle \rho_a(0, 0) \rho_a(0, t) \rangle$ show an exponential decay for long lengths and times respectively: $C(r) \sim \exp -(r/\xi_\perp)$ and $A(t) \sim \exp -(t/\xi_\parallel)$. Both these correlation lengths diverge as one approaches the critical point from the active side:

$$\xi_\perp \sim |p - p_c|^{-\nu_\perp} \quad (2.12)$$

$$\xi_\parallel \sim |p - p_c|^{-\nu_\parallel} \quad (2.13)$$

where p stands for the tuning parameter in the system and p_c is the transition point. This defines the critical exponents ν_\perp and ν_\parallel .

The activity density in the steady-state is usually taken to be the order parameter for

absorbing phase transitions. It is zero in the absorbing phase and non-zero in the active phase, and near the critical point it scales as a power law:

$$\rho_a \sim |p - p_c|^\beta \quad (2.14)$$

Right at the critical point, one can start with a specially prepared homogenous initial condition in which the activity is much higher than in the steady-state, and measure the decay of the activity to zero. This decay also follows a power law, which defines the relaxation exponent α :

$$\rho_a \sim t^{-\alpha} \quad (2.15)$$

Spreading exponents: Spreading exponents are measured by starting with an absorbing state, prepared according to some prescription, on or near the transition point. Activity is then created at a single site or a pair of sites (depending on the model), and the spread of this activity to other sites is observed. The quantities of interest now are the probability $P(t)$ that the activity survives till time t , the average number $N(t)$ of active sites at time t , and the radius of gyration of the positions of active sites, $R(t)$. $R(t)$ is defined as $\frac{1}{M} \sqrt{\langle \sum_i R_i^2 \rangle}$, where R_i is the distance of the i^{th} active site from the center of mass, the sum being over the M occupied sites of the system, and the average is not conditioned on survival [42]. Both $N(t)$ and $R(t)$ scale as power laws at the critical point:

$$P(t) \sim t^{-\alpha'} \quad (2.16)$$

$$N(t) \sim t^\theta \quad (2.17)$$

$$R(t) \sim t^{\nu'} \quad (2.18)$$

The exponents α', ν' and θ are called spreading exponents. As mentioned earlier, they can be related to the SOC exponents in the driven-dissipative version of the model, if the model is a conserved particle one (the argument can be found in [35]). It is also found that they can depend on the particular absorbing state on which the spreading is measured (see section 2.3). $P(t)$ in the limit $t \rightarrow \infty$ is non-zero in the active phase and can be seen as an order parameter for seed simulations, defining another order parameter exponent β' by $P(\infty) \sim |p - p_c|^{\beta'}$. It turns out that for directed percolation a special symmetry called ‘rapidity reversal’ [42] ensures that $\beta = \beta'$, but in general they could be different.

Scaling functions and scaling relations:

The renormalization group framework also provides one with the understanding that universality is not restricted to scaling exponents, but extends to scaling functions as well. Scaling functions [41] are universal functions that describe the off-critical and finite-size

behaviour of quantities like the activity density and the survival probability:

$$\rho_a(t, p, L) \sim t^{-\alpha} f(|p - p_c| t^{1/\nu_{\parallel}}, Lt^{-1/z}) \quad (2.19)$$

$$P(t, p, L) \sim t^{-\alpha'} g(|p - p_c| t^{1/\nu_{\parallel}}, Lt^{-1/z}) \quad (2.20)$$

For the system to have the known scaling with respect to $|p - p_c|$, t and L , the scaling functions f and g have to have the following $t \rightarrow \infty$ (the long-time limit where the system reaches the steady state) and $L \rightarrow \infty$ (the thermodynamic limit) limits:

$$f(x, 0) \sim x^{\beta} \quad (2.21)$$

$$g(x, 0) \sim x^{\beta'} \quad (2.22)$$

These conditions are to ensure that ρ and $P(t \rightarrow \infty)$ vary as $|p - p_c|^{\beta}$ and $|p - p_c|^{\beta'}$ respectively, in the thermodynamic limit. The second arguments of f and g are zero since to reach the thermodynamic limit we need to ensure that we take the limits $L \rightarrow \infty$ and $t \rightarrow \infty$ such that the systems still have time to equilibrate, that is, $Lt^{-1/z} \rightarrow 0$. Since the powers of t have to cancel, we have the following relations between the various critical exponents, known as scaling relations:

$$\alpha = \beta/\nu_{\parallel} \quad (2.23)$$

$$\alpha' = \beta'/\nu_{\parallel} \quad (2.24)$$

For further discussion of scaling relations and the study of scaling functions, see the review of Lubeck [3]. We will discuss the validity of scaling relations for the CLG in chapter 5.

2.3 Universality classification

As explained in the previous section, based on experimental observations and renormalization group arguments, systems undergoing continuous phase transitions show universality of near-critical properties, wherein several models with quite different microscopic dynamics can share the same critical exponents. The theoretical basis for this is the idea that the dynamics of mesoscopic observables obtained in a coarse-grained description is independent of the microscopic details, such that the lattice structure or the precise details of the transitions. (For example, on large scales, the relevant equation for several models for spreading fluids or gases is the diffusion equation, irrespective of the precise interaction potential or the constituent particles.) The mesoscopic description can be written in terms of either a field theory description or a Langevin equation description [2]. Near the critical point, the scaling properties of the mesoscopic variables (an example is the average activity on the scale of a correlation length) depend only on the symmetries of the system and whether the hydrodynamic variables are scalar, vectors, etc. They are independent of the microscopic details. This large-scale theory is what governs the properties near the critical point, when

the correlation lengths and times are large.

The task of identifying the major classes of absorbing phase transitions has been a challenge for the past twenty or so years. The Directed Percolation (DP) class seems to be the most ubiquitous. Janssen and Grassberger [44, 43] conjectured the under the following quite general conditions, an absorbing state transition belongs to the DP class: (i) the phase transition is a continuous one between a unique absorbing phase and a fluctuation active phase, (ii) the order parameter for the transition is positive and has a single component, (iii) the dynamics only involve short-range processes, (iv) there are no other symmetries in the system, and (v) there is no quenched randomness.

Sometimes some of these conditions can be relaxed. For example, systems with infinitely many absorbing states but no additional symmetries, for example Jensen's Pair Contact Process discussed earlier, also show DP exponents in the steady-state. (For a heuristic argument in support of this, based on the Langevin equation, see Grinstein and Munoz [1].) However, the relaxation dynamics, in particular the spreading exponents, might be depend on the initial configuration. Study of the spreading dynamics requires starting with a single active site; however, in systems with infinitely many absorbing states, the inactive background configuration can be changed. For example, in the pair-contact process, one can start with randomly generated configurations of occupied isolated sites. Dickman and collaborators [45] studied spreading in the PCP in 1D by varying the density ϕ of the isolated sites in the background at various values of λ . They found that the deviation of the exponents ν' and δ' from their DP values depends linearly on the difference $\phi - \phi_\lambda$, where ϕ_λ is the steady-state value of the isolated particle density at λ . The critical point in 1D was not dependent on the initial density. However, studies on a related model in 2D [46] showed that not only the exponents, but also the critical point depends on the initial starting density. In both 1D and 2D however, starting from a so-called natural initial condition gives the DP values for the spreading exponents. Natural initial conditions are prepared by relaxing a smaller system than the one being studied at the critical value of λ until it falls into an absorbing state, then constructing the starting configuration on the bigger lattice by tiling it with copies of the smaller-lattice absorbing state.

A later study by Odor et al [47] showed that the fluctuations of the isolated particle density in the 1D PCP diverge with DP exponents at the same point where the active-absorbing transition occurs. The isolated particle density also relaxes very slowly near this critical point, and this might be the reason for the discrepancy between the values of the relaxation exponents between natural and unnatural initial conditions.

Other classes are possible when the system has extra symmetries. For example, the parity-conserved (PC) universality class comprises models where the parity (odd/even-ness)

of the number of particles is conserved by the dynamics [48, 49]. The pair contact process with diffusion (PCPD) [50] is another conjectured universality class, where the reproduction and death dynamics is the same as the pair contact process discussed earlier, but now individual particles can also diffuse (but they cannot reproduce or die). The model has just two absorbing states: the empty lattice and the same with a single diffusing particle. Although this process has been studied for the long time, being first suggested by Grassberger in [44] the determination of its universality class is still a subject of controversy. It might represent a new universality class, or it might be shown to fall in the same class as DP on simulation times longer than the ones available currently [51, 52, 53].

Another conjectured universality class which has recently been the subject of debate is the universality class of absorbing phase transitions in systems with a conserved number of particles. Models with a conserved number of particles (or, in general, a conserved background field) share many characteristics with models with infinitely many absorbing states, which are basically models with a non-conserved background field. In the simplest case (CLG) at least, the relaxation to the steady-state has been shown initial-condition-dependent ([30, 54], see also section 5.6).

As mentioned earlier, it was conjectured that the conservation of the background field shifts the exponents away from DP and changes the universality class. Studies of the 2D CLG, and of related models like the conserved Manna model seemed to confirm this [35], and led to the creation of a new universality class, the conserved DP (CDP) or the Manna class. However, Basu et al [6] recently studied the Manna model in 1D, and showed that the dynamics was affected by long transients, on timescales longer than ones probed by previous studies had probed. Here too it was found that the background inactive field (the local fluctuations in density of sites with heights 1, 2 or 3) took a long time to relax, and this might be what leads to the long transients. Starting with a ‘natural initial condition’ measure, closer to the steady-state measure, gets rid of the long transients and gives values of the exponents closer to the DP values. This claim has been challenged studies by S. B. Lee and collaborators who, following Basu et al, also started with natural initial conditions, and studied the evolution with random sequential dynamics rather than parallel dynamics, in 1D and in 2D, as this seemed to relax faster [7, 8]. They found exponent values different from Basu et al, and closer to the earlier known Recent studies by Lee on 2D models [8] give exponent values that are not equal to the DP ones. Thus, the question of whether CDP models fall in the DP class is a question not yet settled. The exact method of relaxation of the background field, and the nature of this field in the steady-state, seem crucial to understanding how it affects the relaxation and the steady-state of the active field [58].

In one dimension, the CLG is simpler than the Manna model, and can be exactly solved, as given in section 2.1.1. Unlike the Manna model and other known conserved models which

show active-absorbing transitions, like the Conserved Threshold Transfer Process (also introduced in the same paper as the CLG, [32]), it does not have absorbing states above its transition density, only an active steady-state. In recent years, many solvable models showing an active-absorbing transition in 1D have been studied as well [55, 56, 57]. They have the same exponents as the CLG, and thus the CLG can be said to define a universality class by itself. We expect that all models in 1D which show an active-absorbing phase transition, such that (i) there is a single-component order parameter, (ii) there are no absorbing states above the transition density, belong to the CLG universality class.

Da Silva and de Oliveira in [59] introduced several exactly solvable 1D models showing an absorbing phase transition. In one of their models (Model 3 in the paper), the system does have absorbing states above the critical density, and a critical exponent different from the CLG, $\beta = 2$. The transitions in the model are:

$$110 \rightarrow 101, \quad 011 \rightarrow 101 \quad (2.25)$$

$$1100 \rightarrow 1001, \quad 0011 \rightarrow 1001 \quad (2.26)$$

$$10101 \rightarrow 11001, \quad 10101 \rightarrow 10011 \quad (2.27)$$

where all transitions occur with rate unity. The first process is the same as in the Conserved Lattice Gas. In the second process, active particles can also hop over a distance of two units, although not over an occupied site. The third process guarantees that the hops $11001 \rightarrow 10101$ and $10011 \rightarrow 10101$, occurring due to the first line, are also reversible.

In da Silva and de Oliveira's model 3, reasoning similar to the CLG, they observed that the number of 0-clusters of length ≥ 3 cannot increase with time. However, clusters of two zeros can be formed by the dynamics, by the transitions in the third line. The active steady-state configurations thus only contain 0-clusters of lengths 1 and 2. The active steady-state configuration with the lowest density is thus $1001001001 \dots$ (with a 11 active cluster somewhere on the lattice), which has density $1/3$ in the thermodynamic limit. However, a state such as $1010010100 \dots$ does not contain any active particles, and is thus absorbing. But it has density $2/5$. Thus there are absorbing configurations above the critical density as well, upto density $2/5$, in fact. This is unlike the CLG, where there are no absorbing configurations above the transition density $\rho_c = 1/2$. The steady-state configurations near $\rho_c = 1/3$ in this model can contain long sections which look like absorbing states with approximately that density. This means that the average activity in the steady-state can get very low, and in fact counting similar to the one performed for the CLG shows that $\rho_a \sim (\rho - \frac{1}{3})^2$, near ρ_c .

In chapter 5, we extend da Silva and de Oliveira's Model 3 to a class of models of absorbing phase transitions which can be exactly solved. We show that within this class, for each positive integer n , there is a model such that $\beta = n$. These models therefore define

an infinite family of universality classes for 1D active-absorbing phase transitions.

Appendix: A brief introduction to generating functions

Given an infinite sequence G_i , $i = 0, 1, 2, \dots$, one can encode it in a formal power series

$$G(x) = \sum_i G_i x^i \quad (2.28)$$

For example, the Taylor expansion of the function $f(x) = 1/(1 - 2x)$ encodes the geometric sequence $1, 2, 4, \dots$. Given an n -th order linear recurrence relation for a sequence plus n initial values, one can derive a polynomial equation for the generating function. As an example, consider the Fibonacci series defined by $f_n = f_{n-1} + f_{n-2}$ with initial conditions $f_0 = 0$ and $f_1 = 1$. After multiplying both sides of the recurrence by x^n and summing over n ,

$$f(x) - x = xf(x) + x^2 f(x) \quad \text{implying} \quad (2.29)$$

$$f(x) = x/(1 - x - x^2) \quad \text{giving} \quad (2.30)$$

$$f_n = \frac{\phi^n - (-\phi)^{-n}}{\phi + \phi^{-1}} \quad (2.31)$$

where $\phi = (1 + \sqrt{5})/2$ is the golden ratio, and $\phi^{-1} = (\sqrt{5} - 1)/2$.

Now consider the set of all strings of length n generated by arbitrary concatenations of a given set of elementary strings (we simply call this set the set of all strings generated by the elementary strings). Call the number of such strings of length n as C_n . Given the length l of each elementary string, one associates with it a weight x^l , and the generating function for C_n is given by

$$C(x) = \frac{1}{1 - (\sum_{\text{elementary strings}} x^l)} \quad (2.32)$$

This can be easily proved by expanding the function as a geometric series, after which the elementary strings combine in all possible combinations to generate the required sequences, with the correct weights. To give a simple example, consider all strings of a 's and b 's generated by a and ba (that is, no word contains the sequence bb). (Putting $a = '1'$ and $b = '0'$, this is the same counting problem as the set of steady-state CLG configurations from Chapter 2, if there one sets $y = 1$.) The generating function is

$$G(x) = \frac{1}{1 - x - x^2} \quad (2.33)$$

In general, if $G(x)$ has the form $N(x)/D(x)$, then factorising the denominator into its roots, call them r_i , so that $D(x) = f(x) \prod_i (1 - x/r_i)$ and expanding in partial fractions,

one arrives at the general form

$$G_n = \sum_i c_i r_i^{-n} \quad (2.34)$$

The constants c_i can be determined from the initial conditions.

The same counting can also be done using a transfer matrix approach as follows: Every linear recursion relation can be converted to a transfer matrix between (G_n, \dots, G_{n-m}) and $(G_{n+1}, \dots, G_{n-m+1})$. If the length of the longest elementary string is m means that the recurrent relation is an m -th order recurrence. The corresponding transfer matrix is then an $m \times m$ matrix. By raising the transfer matrix to the L -th power, one obtains the number of allowed strings of length L as a sum of L -th powers of the transfer matrix eigenvalues: $G_n = \sum_i c_i \lambda_i^L$, where λ_i are the roots of the transfer matrix. Since the values of G_n are the same in both approaches, we get $\lambda_i = r_i^{-1}$, relating the transfer matrix and generating function approaches.

Bibliography

- [1] G. Grinstein and M. A. Munoz, in *Fourth Granada Lectures in Computational Physics*, edited by P. L. Garrido and J. Marro, Lecture Notes in Physics Vol. 493 (Springer, Berlin, 1997), p. 223.
- [2] H. Hinrichsen, *Advances in Physics* **49**, 815 (2000).
- [3] S. Lubeck, *Int. J. Mod. Phys. B* **18**, 3977 (2004).
- [4] M. Henkel, H. Hinrichsen, and S. Lbeck, *Non-Equilibrium Phase Transitions: Vol. 1: Absorbing Phase Transitions*, (Springer, Berlin) (2009).
- [5] G. Odor, *Rev. Mod. Phys.*, **76**, 663 (2004).
- [6] M. Basu, U. Basu, S. Bondyopadhyay, P. K. Mohanty, and H. Hinrichsen, *Phys. Rev. Lett.* **109**, 015702 (2012).
- [7] S. B. Lee, *Phys. Rev. E* **89**, 060101(R) (2014).
- [8] S. B. Lee, *Phys. Rev. E* **89**, 062133 (2014).
- [9] J. L. Cardy, *J. Phys. A* **16**, L709 (1983).
- [10] J. L. Cardy and P. Grassberger, *J. Phys. A* **18**, L267 (1985).
- [11] H. K. Janssen, *Z. Phys. B* **58**, 311 (1985).
- [12] K. Chen, P. Bak and M. H. Jensen, *Phys. Lett. A* **149**, 207 (1990).
- [13] R. M. Ziff, E. Gulari and Y. Barshad, *Phys. Rev. Lett* **56**, 2553 (1986).
- [14] P. Meakin and D. J. Scalapino, *J. Chem. Phys.* **87**, 731 (1987).
- [15] K. A. Takeuchi, M. Kuroda, H. Chat, and M. Sano, *Phys. Rev. E* **80**, 051116 (2009),
K. A. Takeuchi, M. Kuroda, H. Chat, and M. Sano, *Phys. Rev. Lett.* **99**, 234503 (2007);
103, 089901 (2009).
- [16] S. R. Broadbent and J. M. Hammersley, *Proc. Camb. Philos. Soc.* **53**, 629 (1957).
- [17] I. Jensen, *J. Phys. A* **37**, 6899 (2004).

-
- [18] V. N. Gribov, Sov. Phys. JETP **26** 414 (1968).
- [19] H. D. I. Abarbanel *et al.*, Phys. Rep. **21C**, 120 (1975).
- [20] J. L. Cardy and R. L. Sugar, J. Phys. A **13**, L423 (1980).
- [21] T. E. Harris, Ann. Prob. **2**, 969 (1974).
- [22] T. M. Liggett, *Interacting Particle Systems* (Springer-Verlag, N.Y.), (1985).
- [23] J. Marro and R. Dickman, *Nonequilibrium Phase Transitions and Critical Phenomena* (Cambridge University Press, Cambridge) (1997).
- [24] R. Dickman and J. K. da Silva, Phys. Rev. E **58**, 4266 (1998).
- [25] E. V. Albano, J. Phys. A **25**, 2557 (1992).
- [26] A. Maltz and E. V. Albano, Surf. Sci. **277**, 414 (1992).
- [27] I. Jensen, Phys. Rev. Lett. **70**, 1465 (1993)
- [28] I. Jensen and R. Dickman, Phys. Rev. E, **48** 1710 (1993).
- [29] I. Jensen, Int. J. Mod. Phys. B **8**, 3299 (1994)
- [30] S. B. Lee, and S.-G. Lee, Phys. Rev. E. **78**, 040103(R) (2008).
- [31] G. Grinstein, in *Scale Invariance, Interfaces and Non-Equilibrium Dynamics*, edited by A. McKane et al., NATO Advanced Study Institute, Series B: Physics Vol. 344 (Plenum, New York, 1995).
- [32] M. Rossi, R. Pastor-Satorras, and A. Vespignani, Phys. Rev. Lett. **85**, 1803 (2000).
- [33] S. Lubeck and A Hucht, J. Phys. A: Math. Gen. **34** L577 (2001).
- [34] S. Lubeck, Phys. Rev. E **64**, 016123 (2001).
- [35] A. Vespignani, R. Dickman, M. A. Munoz, S. Zapperi, Phys. Rev. E **62**, 4564 (2000).
R. Dickman, M. A. Munoz, A. Vespignani, S. Zapperi, Braz. J. Phys. **30**, 27 (2000).
- [36] S. S. Manna, J. Phys. A **24**, L363 (1991).
- [37] M. J. de Oliveira, Phys. Rev. E **71**, 016112 (2005).
- [38] J. Cardy, *Scaling and renormalization in statistical physics*, Cambridge University Press (Cambridge) (1996).
- [39] L. P. Kadanoff, Physics **2** 263 (1966),
B. Widom, Physica **73** 107 (1974).
- [40] K. G. Wilson and J. Kogut, Phys. Rep., **12** 75 (1974).

-
- [41] C. Domb and M. S. Green eds., *Phase Transitions and Critical Phenomena*, Vol 6 (Academic, London) (1976).
- [42] P. Grassberger and A. de la Torre, *Ann. Phys. (N.Y.)* **122**, 373 (1979).
- [43] H. K. Janssen, *Z. Phys. B* **42**, 151 (1981).
- [44] P. Grassberger, *Z. Phys. B* **47**, 365 (1982).
- [45] J. F. F. Mendes, R. Dickman, M. Henkel and M. C. Marques, *J. Phys. A: Math. Gen.* **27** 3019 (1994),
I. Jensen and R. Dickman, *Phys. Rev. E* **48** 1710 (1993).
- [46] R. Dickman, *Phys. Rev. E* **53**, 2223 (1996).
- [47] G. Odor, J. F. Mendes, M. A. Santos and M. C. Marques, *Phys. Rev E*, **58** 7020 (1998).
- [48] H. Takayasu, and A. Y. Tretyakov, *Phys. Rev. Lett.* **68**, 3060 (1992).
- [49] J. Cardy, and U. C. Tauber, *Phys. Rev. Lett.* **77**, 4780 (1996).
- [50] M. J. Howard and U. C. Tauber, *J. Phys. A* **30**, 7721 (1997).
- [51] E. Carlon, M. Henkel, and U. Schollwöck, *Phys. Rev. E* **63**, 036101 (2001).
- [52] J. Kockelkoren, and H. Chate, *Phys. Rev. Lett.* **90**, 125701 (2003).
- [53] H. Hinrichsen, *Physica A* **361**, 457 (2006).
- [54] S. Bondyopadhyay, *Phys. Rev. E.* **88**, 062125 (2013).
- [55] K. Jain, *Phys. Rev. E* **72**, 017105 (2005).
- [56] U. Basu, and P. K. Mohanty, *Phys. Rev. E* **79**, 041143 (2009).
- [57] A. Gabel, P. L. Krapivsky and S. Redner, *Phys. Rev. Lett.* **105** 210603 (2010).
- [58] S. D. da Cunha, L. R. da Silva, G. M. Viswanathan and R. Dickman, arXiv:1405.1134.
- [59] E. F. da Silva, and M. J. de Oliveira, *J. Phys. A: Math. Gen.* **41**, 385004 (2008).

Chapter 3

Proportionate growth in patterns formed in the rotor-router model

In this chapter, we will study the growing patterns formed in the rotor-router model by adding N walkers at the center of an $L \times L$ two-dimensional square lattice, starting with a periodic background of arrows, and relaxing to a stable configuration. (See 3.1.) The pattern is made of a large number of triangular and quadrilateral regions, where in each region all arrows point in the same direction. We show that the pattern formed by arrows which have been rotated at least one full circle, may be described in terms of a tiling of the plane by squares of different sizes. The sizes of these squares, and the size of the pattern, grow linearly with N , for $1 \ll N < 2L$. We use the Brooks-Smith-Stone-Tutte theorem relating tilings of squares by smaller squares to resistor networks, to determine the exact relative sizes of these tiles. The scaling limit of the number of visits $\phi(\xi, \eta)$ as a function of the scaled position (ξ, η) is also determined. We also present numerical evidence that the deviations of the sizes of different squares in the tiling from the asymptotic linear growth law are always $O(1)$, and are quasiperiodic functions of N .

The outline of this chapter is as follows: In section 3.1, we state our protocol for creating patterns in the rotor-router model. In section 3.2, we study the pattern obtained from the initial configuration with all arrows parallel. We define the asymptotic pattern, and the scaling limit of the visit function for the pattern. In section 3.3, using the Brooks-Smith-Stone-Tutte (BSST) theorem, we construct the resistor network corresponding to the tiling seen in the pattern and determine the sizes of the tiles. We obtain an exact characterization of the asymptotic pattern, and determine the relative sizes of different elements. Thus we also determine the visit function for the pattern in the large N limit. In section 3.4, we extend the analysis to some other patterns obtained starting from different periodic initial configurations. In section 3.5, we give evidence that the deviations in the diameter and sizes of various elements in the pattern from simple linear dependence on N are bounded and show quasiperiodicity. Section 3.6 contains a summary of our results, and some concluding

remarks. In an appendix, we re-derive the results of section 3.4 C without invoking the BSST theorem.

3.1 Forming Patterns in the Rotor-router model

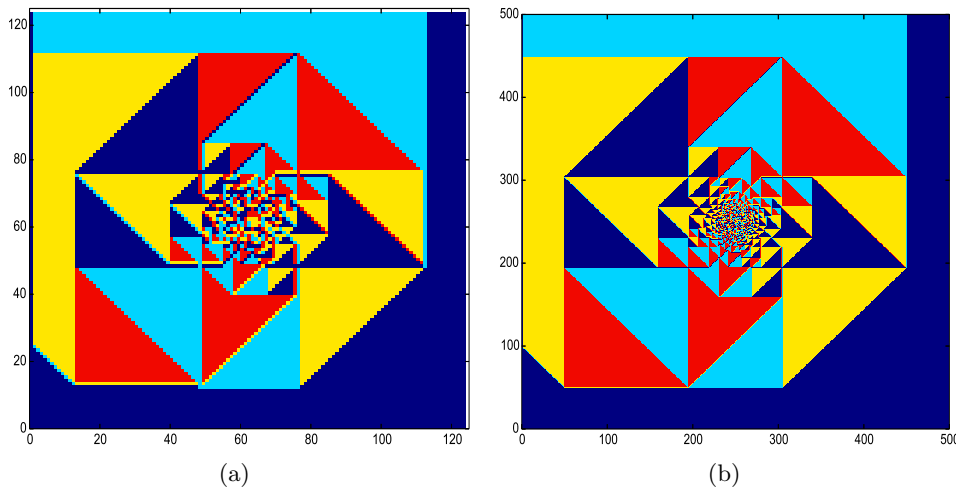


Figure 3.1: Pattern formed by depositing rotor-router walkers at the origin of a square lattice, starting from an initial configuration of all arrows pointing East. (a) the pattern after 200 walkers and (b) after 800 walkers. Note that (b) is scaled down by a factor 4 to make it equal in size to (a). Colour code: dark blue - \rightarrow , light blue - \uparrow , yellow - \leftarrow , red - \downarrow

We consider a finite square lattice, with sites labeled as (x, y) , where x and y are integers, with $|x| \leq L/2$, and $|y| \leq L/2$. The first walker starts at the origin. The arrows attached to the boundary sites can point out of the lattice. The walker then ‘falls off’ the lattice when it follows such an arrow. When this happens, a new walker is introduced at the origin.

We study the configuration of arrows when the N -th walker has just left the system, and the $(N + 1)$ -th walker is not yet introduced. First consider the case where the initial configuration is such that all arrows are parallel, pointing due East. Clearly, the first walker put at the origin would move along the positive y -axis, rotating the arrows it encounters to point North. The second walker rotates the arrow at the origin to point West, and then walks North along the vertical line $x = -1$. The third walker returns to the origin once, before leaving along the vertical line $x = +1$. And so on.

Fig 3.2 shows the configurations left behind by the walker after 2, 5 and 20 walkers. We denote sites having different directions of arrows by small filled squares of different colours. Then the region of the lattice visited at least once by a walker is seen to consist of four distinct regions: (i) a long vertical stripe, with an extra triangular region at one end, in which all arrows are pointed towards north, showing the walkers’ paths before they leave from the top boundary, (ii) a dart-shaped region with all arrows pointing west, (iii) a trian-

gular region where sites have been visited thrice and are hence pointing south, and (iv) a growing octagonal region around the origin. The octagonal region is made of sites where the arrows have undergone at least one complete rotation, while sites on the rest of the lattice have been visited less than four times. We call this octagonal region as the ‘pattern’. We first note that the internal structure of the pattern grows proportionately with the pattern itself. This is seen by comparing Figs. 3.1 (a) and (b), which shows the pattern after the number of walkers $N = 400$ and 1600 respectively. The size of the pattern has grown four times, but the internal structure has not changed much, except for near the origin, where the smaller patches become better-resolved, and some new small patches can be seen.

The diameter D_N of the pattern is defined as the extent of the pattern along the x-axis, after N walkers have exited from the lattice. From the simulations we find that, asymptotically, $D_N = N/2 + \mathcal{O}(1)$. We will take this as an observation based on numerical studies. A rigorous proof is not yet available. The behaviour of D_N as a function of N is discussed in detail in section 3.5.

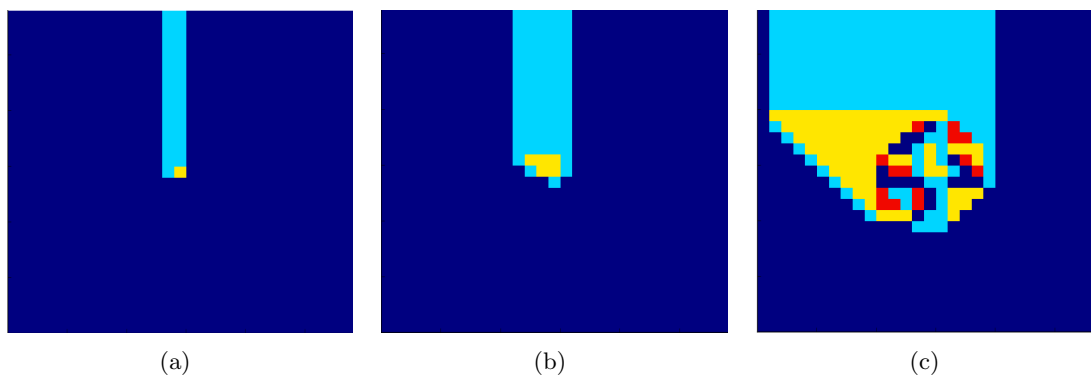


Figure 3.2: The arrangement of the arrows starting from the initial background with all spins pointing East after (a) two (b) five and (c) twenty walkers. The lattice depicted is 50×50 . Colour code: dark blue - \rightarrow , light blue - \uparrow , yellow - \leftarrow , red - \downarrow .

It is seen that the octagon in the figure is made of triangular or dart-shaped quadrilateral regions in which all arrows point in the same direction (shown with the same colour). We call these three- or four-sided polygonal regions ‘patches of constant orientation’. As N is increased, the size of these patches increases, but their shapes and relative sizes remain nearly unchanged. The linear growth cannot be exact, as the coefficient of the linear growth rate is typically irrational, but the diameters of all patches are necessarily integers.

We now describe how a walker explores a single patch after entering it (fig. 3.3). From the evolution rules of the walker, it is easy to check that when a walker enters a patch, it visits all the sites in the patch four times, and the sites on the boundaries one, two or three times, before leaving the patch. Thus, the orientation of arrows in the patch does not

change with N , except at the boundaries of the patch, which may be shifted by one lattice spacing. A new walker, introduced at the origin, moves from one patch to another until it exits the octagonal region, after which it follows a non-self-intersecting path to the sink. As a result of this motion, the boundaries of visited patches shift, and the overall pattern grows in size.

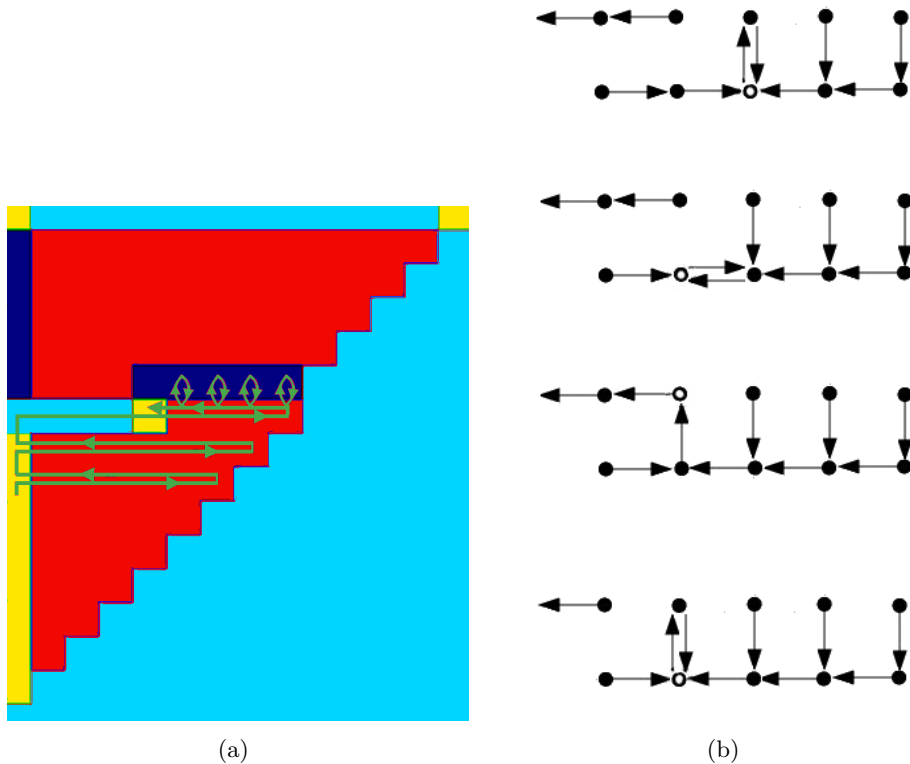


Figure 3.3: (a) A schematic representation of the trail of the walker in a single red patch: When going to the right the path is a straight line, while going to the left, it moves between two adjacent horizontal rows, as indicated in the topmost part of the path. The colour code: dark blue - \rightarrow , light blue - \uparrow , yellow - \leftarrow , red - \downarrow . (b) Successive arrow configurations encountered during the walker's overall leftward motion. The position of the walker is indicated by an unfilled circle.

3.2 The Visit Function

Since we will study the structure of the asymptotic pattern in the limit of large N , we define the asymptotic pattern as follows.

Assign the numerical values 0, 1, 2 and 3 to arrows pointing in the directions East, North, West and South respectively. Call $\rho_N(x, y)$ the numerical value assigned to the direction of the arrow at the site (x, y) after N walkers have exit the lattice. We define scaled coordinates $\xi = x/D_N, \eta = y/D_N$. The asymptotic pattern is defined by the discrete function $\rho(\xi, \eta)$ in

the unit square centered at the origin, given by the limit

$$\rho(\xi, \eta) = \lim_{N \rightarrow \infty} \rho_N(\lfloor D_N \xi \rfloor, \lfloor D_N \eta \rfloor) \quad (3.1)$$

The function $\rho(\xi, \eta)$ is a piece-wise-constant integer function of its (real) arguments, and gives the orientation of the arrow at point (ξ, η) in the scaled pattern. We will defer a formal proof of the existence of this limit to future studies. For the sandpile patterns, the existence of the asymptotic pattern has been proved for the initially empty background by Pegden and Smart in [2].

With our normalization convention and the observation that $D_N = N/2 + O(1)$, and using the fact that the pattern is symmetric about the y-axis, the left and right boundaries of the scaled pattern are at $|\xi| = 1/2$. From the observation that the pattern is in the shape of an octagon, and has equal extent in horizontal and vertical directions, we infer that the upper and lower boundaries of the scaled pattern lie along the lines $|\eta| = 1/2$.

From fig 3.1, it can be seen that the outer patches are bigger and hence are well-formed even for small N , while one has to increase N in order to distinguish patches with smaller diameters. The asymptotic pattern as defined above has well-resolved triangular or dart-shaped patches at all levels, with sharp boundaries. The boundaries between well-resolved patches seem to be of width at most 2 in the original unscaled units. (This may be checked by zooming into fig. 3.1 in the electronic file of this thesis.)

The exact characterization of the sandpile patterns was given in terms of the toppling function $\Phi_N(x, y)$ which gives the number of topplings at any lattice point (x, y) , when N particles are added at the origin and the configuration is relaxed. For the rotor-router model, the corresponding function, which we also denote $\Phi_N(x, y)$ is the so-called visit function, which counts the total number of full rotations undergone by the arrow attached to the site (x, y) due to the first N walkers. The region where Φ_N is non-zero is just the octagonal region which we have earlier defined as our pattern. Define the scaled visit function $\phi(\xi, \eta)$ by

$$\phi(\xi, \eta) = \lim_{N \rightarrow \infty} \frac{\Phi_N(\lfloor D_N \xi \rfloor, \lfloor D_N \eta \rfloor)}{D_N} \quad (3.2)$$

Note that the total number of visits to the site (x, y) is given by $4\Phi_N(x, y) + \rho_N(x, y)$.

Now we argue that Φ_N in every patch is the sum of a linear function of x and y and a periodic part, with the periodicity same as that of the initial background. (For examples of patterns on backgrounds where the unit cell is 2×2 , see section V, and figs. 10, 11 and 13.) Let us take a patch of constant orientation, where the basis vectors of the periodic arrow configuration within the patch are \hat{e}_1 and \hat{e}_2 . Define $\Delta_j \Phi(\vec{R})$ for $j = 1, 2$ as the finite

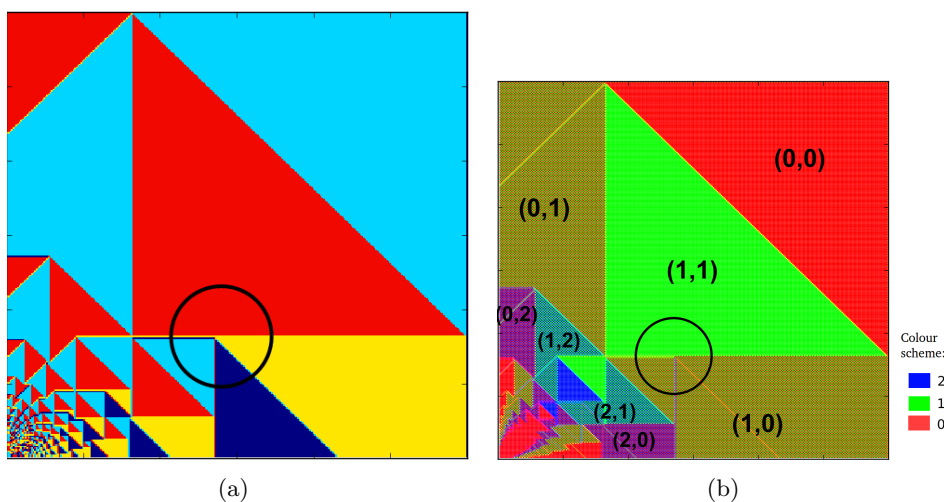


Figure 3.4: (a) The first quadrant of the pattern in Fig. 1 showing patches of constant orientation, and (b) the the same area showing the visit-function-patches. Within a single visit-function-patch, $\nabla\phi$ is constant. We plot the two components of $\nabla\phi$ using a two-color checkerboard code, with the colour on odd pixels showing $\nabla_x\phi$, and the even pixels showing $\nabla_y\phi$. The values of $\nabla\phi$ are also directly displayed in the patch. Note that there are four patches of different arrow orientation within the circle shown in (a), whereas only two regions with different values of $\nabla\Phi_N$ in the corresponding circle in (b). The color code in (a) is: dark blue - \rightarrow , light blue - \uparrow , yellow - \leftarrow , red - \downarrow .

difference $\Phi_N(\vec{R} + \hat{e}_j) - \Phi_N(\vec{R})$. The key observation that enables full characterization of the pattern is that whenever \vec{R} and $\vec{R} + \hat{e}_j$ are both within a given patch of constant orientation, $\Delta_j\Phi(\vec{R})$ is independent of \vec{R} and N . The non-dependence on N comes from the Eulerian property of the walkers illustrated in fig. 3.3: whenever a walker comes to a patch, it visits all sites in the patch same number of times. The translation invariance within a patch, namely that $\Delta_j\Phi(\vec{R})$ does not depend on \vec{R} , comes from the fact that the boundary between two different patches of constant orientation shifts by the same amount each time a new walker visits the patch. Since all sites along the boundary are visited the same number of times whenever the boundary is shifted, this gives rise to translation invariance in the direction along the boundary. Since the shift of boundary is always the same, this gives rise to the invariance of finite differences in the direction normal to the boundary. Hence $\Delta_j\Phi(\vec{R})$ must be same for all sites \vec{R} in the same patch, equivalent under translations by \hat{e}_1 and \hat{e}_2 .

The argument above does not apply for two sites \vec{R}_1 and \vec{R}_2 within the same unit cell. We now argue that $\Delta_j\Phi(\vec{R})$ cannot be different for two such sites either. Consider two adjacent sites \vec{A} and \vec{B} , within the same unit cell. Now, for s such that sites $\vec{A} + s\hat{e}_1$ and $\vec{B} + s\hat{e}_1$ are still within the patch, $\Phi(\vec{A} + s\hat{e}_1) - \Phi(\vec{A}) = s\delta_A$ and $\Phi(\vec{B} + s\hat{e}_1) - \Phi(\vec{B}) = s\delta_B$, which gives $\Phi(\vec{A} + s\hat{e}_1) - \Phi(\vec{B} + s\hat{e}_1) = s(\delta_A - \delta_B)$. This difference grows with s , but since $\vec{A} + s\hat{e}_1$ and $\vec{B} + s\hat{e}_1$ are adjacent sites, the difference between the number of visits at both

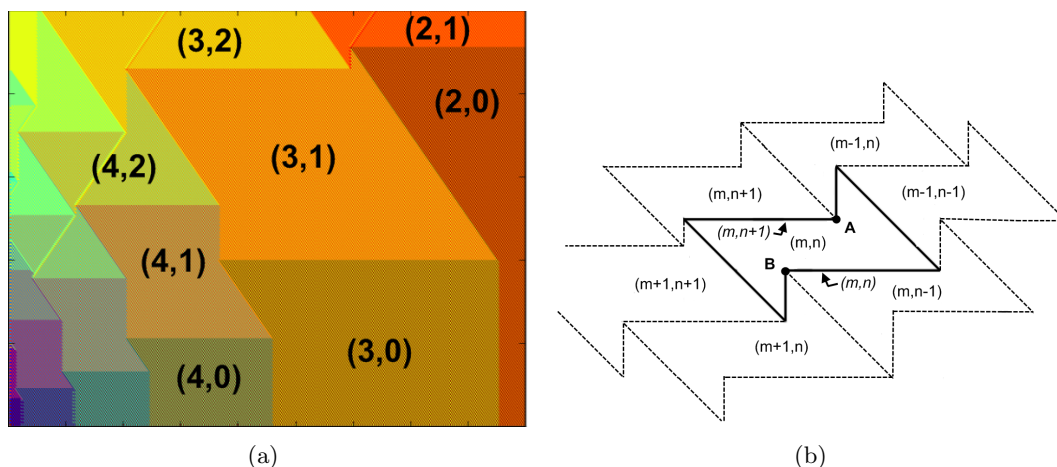


Figure 3.5: (a) A zoomed-in figure of some patches in the first quadrant in Fig. 5 (b), illustrating the arrangement of visit-function-patches, labeled by their (m,n) values. Note that the vector $\nabla\Phi_N$ changes by $(0,1)$ across a horizontal boundary, by $(1,0)$ across a vertical one, and by $(1,1)$ across a diagonal boundary. (b) The patch (m,n) and its neighbours. The points A and B lie on a line of slope ± 1 . In section IV (C), we assign the co-ordinate (m,n) to the lower boundary of the patch (m,n) , to make a correspondence between visit-function-patches and a tiling of the pattern by squares.

sites cannot be arbitrarily large. This is possible only if $\delta_A = \delta_B$. Hence we must have δ_R same for all sites \vec{R} within a single patch of constant orientation.

We note that for a linearly growing pattern, this result also follows from the scaling property of proportionate growth. This argument is an adaptation of the one for linearly growing sandpiles. Consider the scaled toppling function $\phi(\xi, \eta)$ within a patch of constant orientation. We expand $\phi(\xi, \eta)$ about a point (ξ_0, η_0) within the patch (not at the boundary), assuming that the scaled visit function is a twice-differentiable function within a given patch. We also assume that the vector of finite differences $\Delta\Phi \rightarrow D_N \nabla\phi(\eta, \xi)$ point-wise, as $N \rightarrow \infty$, where both sides are expressed in the basis formed by the basis vectors of the unit cell in the patch. One gets $\phi(\xi_0 + \Delta\xi, \eta_0 + \Delta\eta) = \phi(\xi_0, \eta_0) + v_1\Delta\eta + v_2\Delta\xi + v_3(\Delta\eta)^2 + v_4(\Delta\xi)^2 + \dots$, where v_1, v_2, v_3, v_4 are finite constants. Rescaling back to the visit function $\Phi_N(x, y) = D_N\phi(\xi, \eta)$, and using $\Delta\xi = \Delta x/D_N, \Delta\eta = \Delta y/D_N$, we find that near the point (x, y) , $\Phi_N(x_0 + \Delta x, y_0 + \Delta y) = \Phi_N(x_0, y_0) + v_1\Delta x + v_2\Delta y + (v_3\Delta x)^2/D_N + v_4(\Delta y)^2/D_N + \dots$. In this expansion, the second order terms scale as $1/D_N$, and can be made arbitrarily small for large D_N . But, Φ_N has to be an integer valued function for integer values of Δx and Δy for arbitrary D_N however large. and this implies that v_3, v_4 and all higher coefficients have to be exactly zero. Therefore, within each patch, $\phi(\xi, \eta)$ is a linear function of ξ and η .

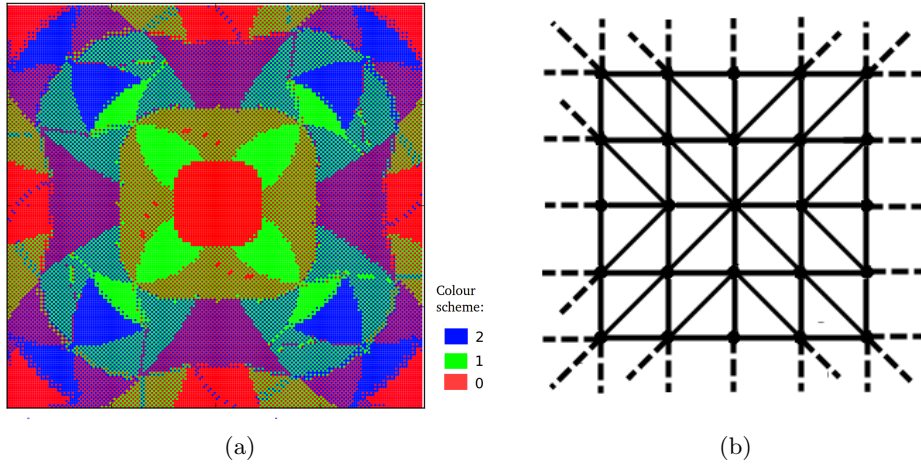


Figure 3.6: (a) The $1/r$ transform of the plot of $|\nabla\Phi_N|$, of which fig. 3.4 (b) is the first quadrant. As in that figure, the odd and even sites give $|\nabla_x\Phi_N|$ and $|\nabla_y\Phi_N|$ respectively. The red spots in the patches next to the central patch are artifacts caused by the $1/r$ transform of the diagonal lines within patches of the visit function in fig. 3.4 (b). (b) Central part of the adjacency graph of the visit function, the first quadrant of which corresponds to the patches shown in Fig. 5 (b). The central node is the vertex $(0,0)$ corresponding where $\phi(\xi, \eta) = 0$.

The above discussion implies that within a single patch

$$\Phi_N(x, y) = f_{per}(x, y) + F_N + v_1x + v_2y \quad (3.3)$$

where f_{per} is a periodic function on the lattice with zero mean, v_1 and v_2 are constants which depend on the patch. The constant F_N is an N -dependent integer. The periodicity of f_{per} would be expected to be the same as the periodicity of the starting background configuration. To get the continuum limit function $\phi(\xi, \eta)$, we have to average $\Phi_N(x, y)$ over a ‘coarse-graining scale’ much larger than 1. Then, since mean value of f_{per} may be assumed to be zero without any loss of generality, it does not contribute to $\phi(\xi, \eta)$, and we get

$$\phi(\xi, \eta) = f + v_1\xi + v_2\eta, \quad (3.4)$$

where $f = \lim_{N \rightarrow \infty} F_N/D_N$. Thus f measures the mean increase in the number of rotations at a site (x, y) in the patch, per unit increase of diameter, as long as it stays within the patch.

Let $\vec{\delta x}$ be a basis vector of the superlattice of the background pattern. Within a single patch, this difference $\Phi_N(\vec{x} + \vec{\delta x}) - \Phi_N(\vec{x}) = (v_1, v_2) \cdot \vec{\delta x}$ has to be an integer. For the present pattern, the periodicity in both directions is 1, and $\vec{\delta x}$ equals $(1, 0)$ or $(0, 1)$. Hence v_1, v_2 can only take integral values, and $f_{per}(x, y)$ may be taken to be 0. Thus, within a patch, $\Phi_N(\xi, \eta)$ is of the form

$$\Phi_N(x, y) = F_N(m, n) + mx + ny \quad \text{and} \quad (3.5)$$

$$\phi(\xi, \eta) = f_{m,n} + m\xi + n\eta \quad (3.6)$$

where m and n are integers depending on the patch, and $F_N(m, n)$ is an integer. The coefficients of x and y in eq. (3.5) have no N -dependence, as long as the point (x, y) stays within a given patch.

For the pattern in Fig. 1, within a given patch, $\nabla\phi(\xi, \eta) = (m, n)$ and hence is constant. However, its value might change discontinuously across patch boundaries (but it does not always, as is shown in fig. 3.4). Since $\nabla\phi$ does not always change across boundaries between patches of constant orientation, we define patches of constant gradient of the visit function, or more briefly ‘visit-function-patches’ as the regions across which $\nabla\phi$ is the same constant. By the continuity of the scaled visit function $\phi(\xi, \eta)$, the value of the constant part $f_{m,n}$ also does not change across boundaries when m and n don’t change. It is convenient to label a visit-function-patch using the value of $\nabla\phi$ in the patch. Then the patch (m, n) refers to the visit-function patch for which $\nabla\phi = (m, n)$. To compare visit-function-patches with patches of constant orientation, compare figs. 3.4 (a) and (b).

Consider two adjacent patches with scaled visit functions $\phi_1 = a_1 + m\xi + n\eta$ and $\phi_2 = a_2 + m'\xi + n'\eta$. Then from the continuity of ϕ implies that the equation of the boundary is $(m - m')\xi + (n - n')\eta = a_2 - a_1$. Since the slopes of the boundaries in fig 3.1 are either 0, ± 1 or ∞ , the vector $(m - m', n - n')$ has to be an integer multiple of $(0, 1)$, $(1, 0)$ or $(1, 1)$. The results of our numerical study show that the multiplicative constant is unity, that is, (m, n) only changes by $(0, \pm 1)$, $(\pm 1, 0)$ or $(\pm 1, \pm 1)$ across a patch-boundary in this pattern. Since we do not observe patches with only diagonal boundaries, we conclude that all values of (m, n) are present. Figs 3.5 shows the arrangement of these patches in the actual figure.

We note that there is a crowding of different patches near the origin in the pattern. One way to avoid this, and be able to see details of the pattern near the origin, is to take a $1/r$ transform of the picture. Such a transformation was first used in [3] for sandpile patterns. Under this transform, a point with polar coordinates (r, θ) is mapped to the point $(1/r, \theta)$ in the transformed picture, and the colour in the transformed picture is given the colour of the corresponding point in the original pattern. Taking a transform of a pattern produced on the 1000×1000 lattice, we get fig. 3.6 (a). The colours in the picture are chosen to show $\nabla\phi(\xi, \eta)$, of which fig. 3.4 (b) shows the first quadrant. Under this mapping, straight line boundaries map to non-straight arcs. However, the transformation preserves the adjacency structure of different patches (i.e. which patches share a boundary). In the

transformed picture, we can notice more easily a rectangular grid-like structure, such that the visit-function-patch with label (m, n) is found in the neighbourhood of the point with Cartesian coordinates (m, n) in the transformed picture. This is shown in Fig. 7b, where we have shown the adjacency graph of visit-function-patches in the pattern. Here a node in the graph denotes a patch, and we draw an edge between two nodes only if they share a common boundary.

Thus, we see that the adjacency graph for patches of the visit function is an infinite graph which takes the form of a square lattice with extra diagonal bonds, of which fig. 3.6 (b) shows the neighbourhood of the node corresponding to the patch at infinity.

3.3 Characterizing the Pattern as a Tiling

In this section we will determine the sizes of the different patches in the pattern, using as input the observed arrangement of these elements in the pattern. We do this by noting that the observed pattern may be thought of as a tiling of a square by smaller squares, where each square tile is made of two triangles of different colours (compare figs. 3.1 and 3.8 (a)). We will ignore the colours, and focus on the sizes and the adjacency relations between different tiles.

We consider the asymptotic pattern defined by eqn 3.1 (fig 3.1). This rescaled asymptotic pattern has diameter $D = 1$, and has features at arbitrarily small scales. From this pattern one constructs a tiling of the unit square as follows: we take each diagonal boundary between patches, and construct its bounding square. The bounding square of a diagonal line is the square for which this line is the diagonal. Drawing these bounding squares for each diagonal line, and then erasing these diagonal lines, one gets from fig. 3.1 to fig. 3.8 (a). If one assumes that the asymptotic pattern is fully tiled by patches of constant orientation, it follows that the squares tiles so constructed also tile the pattern without overlaps or voids, as each patch of constant orientation is fully covered by one square (when the patch is a triangle), or by two squares (when it is a dart). Each square tile thus overlaps two patches of constant orientation. Alternatively, one could start from the six-sided visit-function-patches, and construct squares as above from the two slanted boundaries. Then the remaining area of the patch forms a single square. That is, a patch of the visit function is made of three squares, two shared with other patches, and one lying entirely within the patch. See fig. 3.4 (b).

3.3.1 The Brooks-Smith-Stone-Tutte Mapping

The Brooks-Smith-Stone-Tutte (BSST) mapping [4] between square tilings and resistor networks allows one to find the sizes of all the squares in a square tiling knowing only their arrangement in the tiling. We first recapitulate the BSST mapping and then use it to cal-

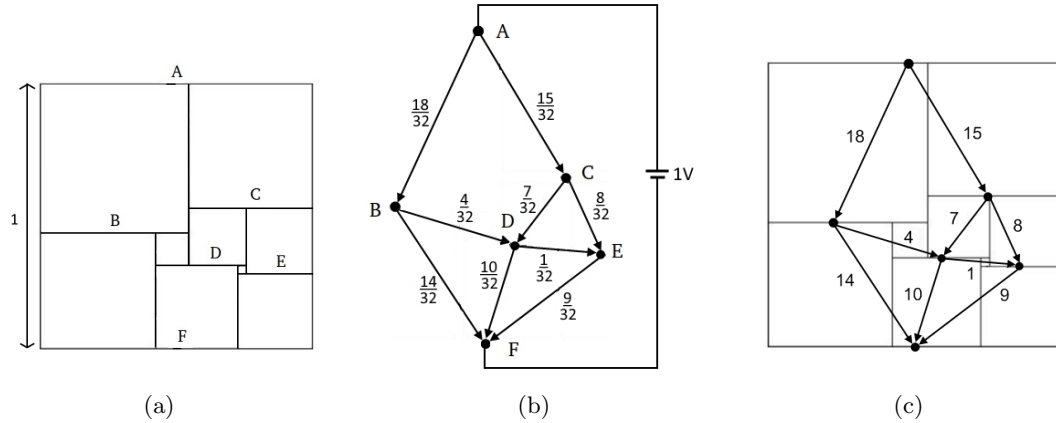


Figure 3.7: An application of the BSST theorem. (a) A tiling of a rectangle by squares (b) The resistor network constructed from the tiling. All the edges of the graph have unit resistance. We put a voltage source across the graph equal to the height of the rectangle and determine the currents produced in each edge. (c) The lengths of squares determined from the values of currents in (b), converted to integers by multiplying by 32. (The height of the big square becomes 32. Its width can be calculated from the currents to be 33.) Note that the arrows only denote the direction of the current (from top to bottom, in the tiling).

culate the properties of the pattern in fig. 3.1.

Consider the tiling of a rectangle by squares shown in Fig. 3.7. We refer to the outer rectangle as the ‘bounding’ rectangle. We associate with a given tiling a resistor network as follows: With each horizontal line, we associate a node of a resistor network. Two nodes are joined by a (1Ω) resistor if parts of the corresponding segments form opposite edges of a tiling square. The resistors (that is, the edges) in the network thus correspond to squares. We associate a voltage $V(v)$ with the nodes v of the network, where $V(v)$ is the vertical height of the horizontal edge corresponding to the node v in the tiling. Assigning unit resistance to all resistors, the current between nodes v and u is $V(v) - V(u)$, and this equals the length of the side of the square joining the corresponding horizontal lines in the tiling. Then the Kirchoff current balance conditions of the resistor network corresponds to the condition that the total horizontal length $L(v)$ of the segment v is the same whether calculated using its set of upper neighbours $\{u\}$ or the set of lower neighbours $\{\ell\}$

$$\sum_{\{u\}} [V(u) - V(v)] = \sum_{\{\ell\}} [V(v) - V(\ell)] = L(v) \quad \text{or,} \quad (3.7)$$

$$\sum_n [V(n) - V(m)] = 0 \quad (3.8)$$

where the summation in the second line is over all neighbours n of the node m in the graph. Denoting by L and U the vertices corresponding to lower and upper edges of the bounding

square, we define $V(U) = 1$ and $V(L) = 0$. Then, the unique solution for the voltage developed on the nodes of the resistor network constructed in the above way gives the heights (in the original tiling) of all the horizontal segments.

Note that when four squares meet at a point, the horizontal segment going through the point can be considered as one segment or two. An example is the meeting point of segments G and B in fig. 3.8 (a)). In such cases, we will always choose the latter, more general, option. (The former case corresponds to the degenerate case when the voltages at B and G are equal.)

3.3.2 The tiling as a resistor network on a square grid

The resistor network corresponding to this tiling, to a depth of three layers starting from the outer boundary, is shown in 3.8 (b). Drawing more layers of the resistor network, one will get an infinite graph with an infinite number of nodes. Most of these edges correspond to the very tiny square tiles near the center of the pattern.

The main simplification that allows us to analyse this problem exactly is the fact that the resistor network graph has a very simple structure: it is equivalent to the resistor-network formed by connecting unit resistors to make a square grid, with only one missing bond between nodes A and K (Fig. 3.8 (c)). One can easily verify that the networks in figs. 3.8 (b) and (c) are equivalent, being different pictorial representations of the same graph. For the present, we will take this crucial observation as an induction from the features of the observed pattern.

For the resistor network shown in Fig. 3.8 (c), it is convenient to label nodes by their integer coordinates (m, n) . We will choose the coordinates so that the node A has the Euclidean coordinate $(0, 0)$ and the node K has the coordinate $(0, -1)$. The boundary conditions for the voltage on this resistor network are given by the positions of the upper and lower horizontal segments of the bounding square. Since the pattern has been rescaled to be of unit diameter centered at the origin, this gives $V(0, 0) = 1/2$, and $V(0, -1) = -1/2$.

Then Eq.3.8 in our case becomes

$$V(m, n) = \frac{1}{4}[V(m + 1, n) + V(m - 1, n) + V(m, n + 1) + V(m, n - 1)] \quad (3.9)$$

for $(m, n) \neq (0, 0)$ or $(0, -1)$.

The solution of the resistor network problem for this graph is well known, $V(m, n)$ being given by the following superposition of Green's functions for an infinite square lattice $G_{sq}(m, n)$

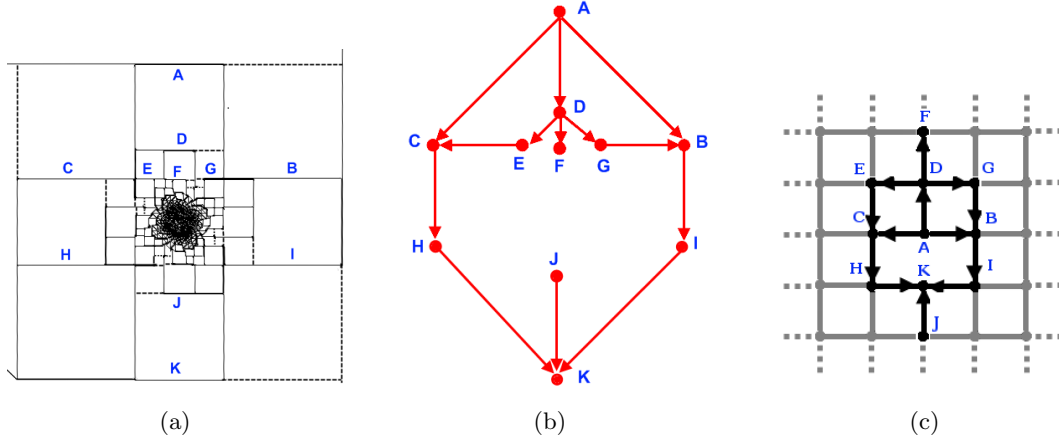


Figure 3.8: (a) The pattern in fig. 1 as a square tiling. The dashed lines indicate segments not present in the pattern in fig. 1, but drawn to help visualisation. The first few levels of the corresponding network are shown. (b) Part of the resistor network corresponding to the tiling in (a). (c) The graph in part (b), showing the different labeled nodes, redrawn as a square lattice. The edges between nodes labeled in (a) by capital letters are in black, with arrows indicating the direction of the current flow. Note that some nodes (for example B and G) correspond to horizontal segments which lie at the same height, but have not been grouped together as a single segment. The arrows only denote the direction of the current.

$$V(m, n) = 2(G_{sq}(m, n + 1) - G_{sq}(m, n)) \quad (3.10)$$

where

$$G_{sq}(m, n) = \int_{-\pi}^{\pi} \frac{dk_1}{2\pi} \int_{-\pi}^{\pi} \frac{dk_2}{2\pi} \frac{1 - \cos(k_1 m + k_2 n)}{2 - \cos k_1 - \cos k_2} \quad (3.11)$$

It can be verified that indeed $V(0, 0) = 1/2$. For finite values of m and n , this integral can be evaluated in closed form, and the result is of the form $a_{m,n} + b_{m,n}/\pi$, where $a_{m,n}$ and $b_{m,n}$ are rational numbers [5]. A computationally efficient formula for $G_{sq}(m, n)$, which can be used in MathematicaTM to get exact expressions for the first few $V(m, n)$, is given in [6],

$$G_{sq}(m, n) = \int_0^{\pi} \frac{dy}{2\pi} \frac{1 - e^{|m|s} \cos(ns)}{\sinh(s)} \quad (3.12)$$

with $\cosh(s) = 2 - \cos(y)$.

From this solution we get the sizes of various elements in the pattern. For example, the size of the big squares at the four corners of Fig. 3.8 (a) is given by the difference in the vertical co-ordinates of lines A and B. From Fig. 3.8 (c) this is equal to $V(A) - V(B) = V(0, 0) - V(1, 0)$. Using the values $V(1, 0) = \frac{2}{\pi} - 1/2$ and $V(0, 0) = 1/2$, the size of these largest squares in the pattern relative to the size of the pattern is $1 - \frac{2}{\pi}$.

For $m, n \gg 1$, the corresponding horizontal lines get closer and closer to the origin of the original pattern. On the resistor network for large m, n , $V(m, n)$ looks like the electric potential due to a dipole at the origin, and tends to zero for large m, n . $V(m, n) \sim \frac{\cos \theta}{(m^2 + n^2)^{1/2}} = \frac{n}{(m^2 + n^2)}$ in this region. Consider moving along the y -axis of the resistor network. Then $V(m = 0, n) \sim 1/n$. In the tiling, this gives the distance from the origin of the n^{th} ring of squares (counted from the outside inwards) is $r_n \sim 1/n$. Then the size of the squares in this ring varies as $\frac{\partial r_n}{\partial n} \sim \frac{1}{n^2}$.

3.3.3 Determining the visit function

In the previous section, we were able to determine the sizes of patches by solving the Kirchoff equations for a resistor network that was a square lattice. In Fig. 3.6, we also encountered the square lattice as the adjacency graph for the patches. These are somewhat different constructions, in that the nodes in the adjacency graph are patches, but nodes in the BSST construction are horizontal line segments in the pattern. This difference is resolved by noting that we can associate a unique horizontal segment to each visit-function patch, which we choose to be its lower horizontal boundary. Label this horizontal boundary by the same label as the patch, that is, (m, n) . The choice of the lower boundary for this association ensures that the labels on the adjacency graph and the resistor network are the same. (For instance, the lower boundary of the bounding square is the lower horizontal boundary of the patch $(0, -1)$, and also the node $(0, -1)$ in the resistor network in figs. 3.8 (b) and (c).)

To determine the visit function for the scaled pattern, we have to determine $f_{m,n}$ for all (m, n) in eqn. 3.6. The visit function in the patch with label (m, n) is $\phi_1(\xi, \eta) = m\xi + n\eta + f_{m,n}$. For two adjacent patches with labels (m, n) and $(m, n + 1)$, continuity of the visit function along the horizontal boundary between them gives the position of the boundary as

$$y = f_{m,n} - f_{m,n+1} \quad (3.13)$$

Since this is the lower boundary of the patch (m, n) , we can make the identification $y = V(m, n)$ in eqn. 3.10, giving

$$f_{m,n} = -2G_{sq}(m, n) \quad (3.14)$$

This gives $f_{0,0} = 0$ and $f_{0,1} = -1/2$, which is consistent with the normalisation that the upper boundary of the pattern (the boundary between patches $(0, 1)$ and $(0, 0)$) lies along the line $x = 1/2$. The f 's are negative because patches with positive m, n lie in the upper right quadrant of the pattern. For large m and n , $f_{m,n} \sim -\log(m^2 + n^2)$.

3.4 Other starting backgrounds

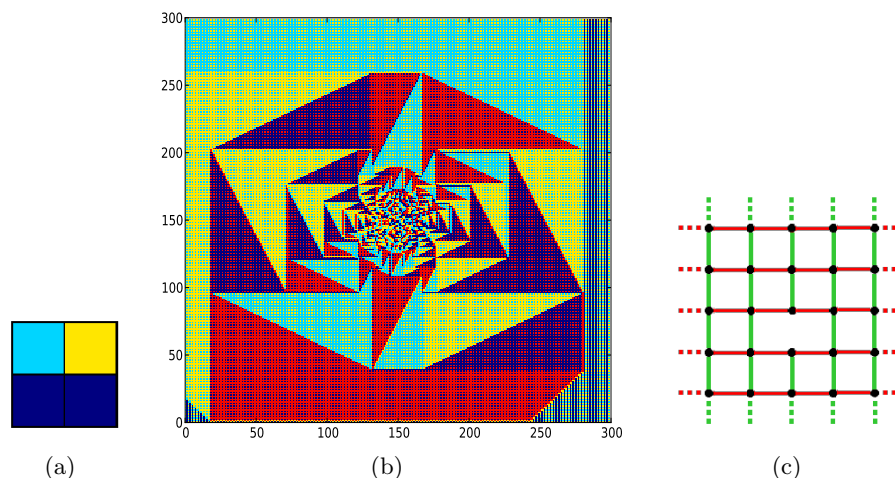


Figure 3.9: Pattern formed on the initial background generated by the 2×2 unit cell given in (a) is shown in (b) after 700 walkers put at the origin have left the lattice. Colour code: dark blue - \rightarrow , light blue - \uparrow , yellow - \leftarrow , red - \downarrow . (c) The resistor network for the pattern, where black bonds denote a resistance of 1Ω , red that of 0.5Ω and green a resistance of 2Ω .

In this section, we study the patterns formed by walkers deposited on the origin of backgrounds formed by periodic repetition of unit cells of size 2×2 . Using the symmetries of rotation, reflection and translation to classify all the 2×2 unit cells, we get 18 inequivalent classes of unit cells. However, the number of different asymptotic patterns (classified according to the adjacency structure of their patches) is only 4. The reason for this is not clear. For example, the unit cell $(\rightarrow \uparrow)$ clearly belongs to a different symmetry class from the unit cell $(\rightarrow \rightarrow)$, which forms the background with all arrows parallel, and forms the pattern in fig. 3.1. Yet the pattern formed on the former background has the same structure. We call this the type I pattern. This pattern has already been discussed in the previous two sections. We will discuss the remaining three inequivalent pattern types in this section.

3.4.1 Type II

We first consider the background formed starting from the unit cell in fig. 3.9 (a). The pattern generated on this background is shown in fig. 3.9 (b). We see from the picture generated that this pattern can be seen as a tiling of the unit square by rectangles with aspect ratio 1:2. The BSST mapping is easily generalised to a tiling by rectangles: the resistor in the network corresponding to a rectangle with vertical to horizontal side ratio p/q has resistance $R = p/q$. The corresponding resistor network is drawn in Fig. 3.9 (c). Interestingly, this network has the same structure as the one for the pattern studied in section IV, with different resistances along the bonds depending on the aspect ratio of the tile. The vertical bonds have $R_1 = 2\Omega$ and horizontal bonds have $R_2 = \frac{1}{2}\Omega$. The solution

for the potential on such a lattice is given by the so-called rectangular lattice Green's function $G_{rect}(R; m, n)$, which is the generalization of the square lattice Green's function to a lattice with resistance $R\Omega$ along the vertical bonds and Ω along the horizontal bonds. This lattice is equivalent to the present lattice provided all resistances are scaled down by a factor 2; here this is built into the scale factor Q in eqn. (3.16). The computationally efficient formula for $G_{rect}(m, n)$ is [6]

$$G_{rect}(R; m, n) = \int_0^\pi \frac{dy}{2\pi} \frac{1 - e^{|m|s} \cos(ny)}{\sinh(s)} \quad (3.15)$$

where s is defined implicitly $\cosh(s) = 1 + \frac{1}{R} - \frac{1}{R} \cos y$.

The solution of $V(m, n)$ with $V(0, 0) = \frac{1}{2}$ and $V(0, -1) = -\frac{1}{2}$ is given by the superposition of two Green's functions:

$$V(m, n) = Q(G_{rect}(R = 4; m, n + 1) - G_{rect}(R = 4; m, n)) \quad (3.16)$$

The charge Q is determined by the condition that $V(0, 0) = \frac{1}{2}$, which gives $Q = 1/[4 - \frac{8}{\pi} \tan^{-1}(2)]$. The height of the big rectangles at the corners *relative to the height of the figure* is hence given by $l = V(0, 0) - V(0, 1) = \frac{1}{2} - \frac{Q}{2}(1 - \frac{2}{\pi} \tan^{-1} \frac{1}{2}) \approx 0.259286$.

We can also determine the aspect ratio of the figure, by also using the BSST mapping for the pattern rotated by 90° . The structure of the resistor network is again the same (Fig. 3.9 (c)), except that the 0.5Ω and 2Ω bonds are interchanged. Hence, for the new network, $V'(m, n) = V(n, m) \frac{Q'}{Q}$, where Q' is determined by the condition that $V(0, 0) = \frac{1}{2}$. This gives $Q' = (1 - \frac{2}{\pi} \tan^{-1} \frac{1}{2})^{-1}$. One can then calculate the breadth of the big rectangle at the corner *relative to the width of the figure* as $b' = \frac{1}{2} - \frac{Q'}{2}(2 - \frac{4}{\pi} \tan^{-1}(2)) \approx 0.43433$. One then uses the condition that $2lH = b'W$ to determine the aspect ratio of the figure to be $H/W \approx 0.83755$.

3.4.2 Type III

Now consider the initial periodic structure having the unit cell in fig. 3.10 (a). The resulting pattern after 900 walkers is shown in fig. 3.10 (b). The characterization and analysis of this pattern is very similar to previous cases. The corresponding resistor network is given in fig. 3.11 (a). It is also a square lattice, but the bonds connecting sites $(i, 0)$ and $(i, -1)$ for all integers i have $R' = 2\Omega$ whereas the rest of the bonds have $R = \Omega$. Fig. 3.11 (b) gives an equivalent square lattice structure for this network.

Using the BSST mapping, the vertical positions of horizontal lines with respect to the center of the figure in the upper left half of Fig. 3.10 (b) are given by the voltages in the first quadrant in the square lattice in Fig. 3.11 (b), taking the point with $+\frac{1}{2}$ as the origin.

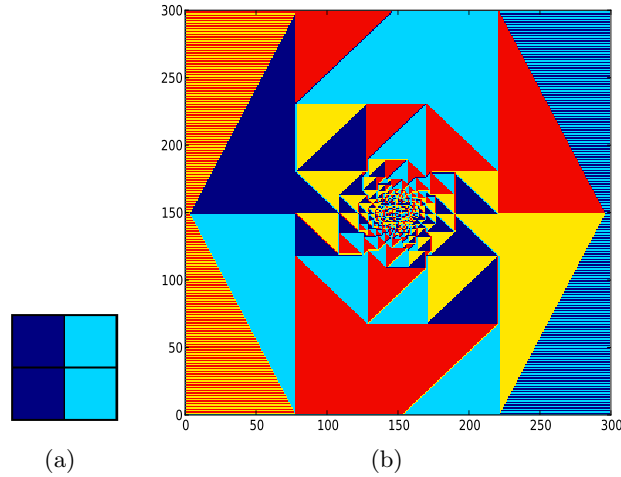


Figure 3.10: Pattern formed by the initial background generated by the 2x2 unit cell given in (a) is shown in (b) after 900 walkers put at the origin have left the lattice. Colour code: dark blue - \rightarrow , light blue - \uparrow , yellow - \leftarrow , red - \downarrow .

In terms of the square lattice Green's function $G_{sq}(m, n)$, eqn. (3.12),

$$V_1(m, n) = Q_1(G_{sq}(m, n+2) - G_{sq}(m, n)) \quad (3.17)$$

The condition $V(0, 0) = \frac{1}{2}$ then gives $Q_1 = (2 - \frac{4}{\pi})^{-1}$. To determine the aspect ratio of the figure, one determines the positions of the horizontal lines with labels $(m, n) = (0, 1)$ and $(1, 0)$, call them l_1 and l_2 . The size of the big squares at the boundary is then $(\frac{1}{2} - l_2)$ and that of the square between then is $(\frac{1}{2} - l_1)$. The horizontal extent of the pattern is then $(\frac{1}{2} - l_1) + 2(\frac{1}{2} - l_2) = (\pi - 2)^{-1}$. Since the voltages are normalized such that the vertical extent of the pattern is 1, This gives the aspect ratio as $H/W = (\pi - 2)^{-1}$.

3.4.3 Type IV

Holroyd and Propp [1] classify initial backgrounds on infinite lattices into two types. 'Transient' backgrounds are those where the walker visits all sites only finitely many times before reaching infinity, while 'recurrent' backgrounds are those where it visits each site infinitely many times before reaching infinity. For periodic backgrounds on a lattice of size $L \times L$, we will call a background as transient, if the first walker exits in a time of order $\mathcal{O}(L)$, and recurrent if the time is $\mathcal{O}(L^3)$. The backgrounds we have studied so far in this chapter were all transient. For the backgrounds studied so far, after N walkers have been put on an $L \times L$ lattice, the total time taken for all the walkers to reach the sink is, for $N \gg 1$, $AN^3 + BNL + \mathcal{O}(N^2)$. For $1 \ll N \ll L$, this is linear in L . When the size of the pattern becomes comparable to the lattice, this becomes $\mathcal{O}(L^3)$. A and B are constants for a given background.

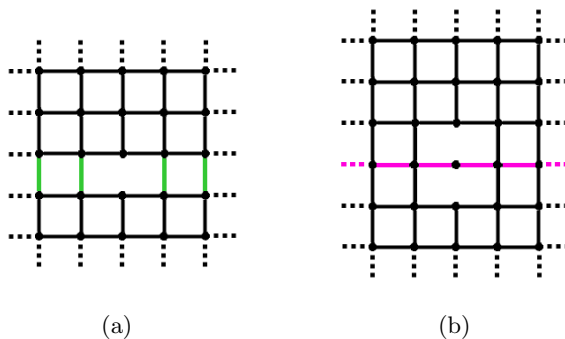


Figure 3.11: (a) The resistor network for the pattern in fig. 3.10 (b), where black bonds denote a resistance of 1Ω , red that of 0.5Ω and green a resistance of 2Ω . (b) The resulting network, when we replace the 2Ω resistors, by a series combination of two 1Ω resistors, and connect the new added neighboring nodes by 1Ω resistors (shown as pink bonds in figure). Since in our problem, the end points of pink bonds are at same potential, this does not change the currents. In this new network, all resistors have equal resistance.

Now we consider the initial periodic structure having the unit cell in fig. 3.12 (a). Here, on an $L \times L$ lattice, the first walker takes $\mathcal{O}(L^3)$ steps to get to the sink, and hence this background is recurrent. Fig. 3.12 (b) shows the pattern left behind by the first walker. This resulting background is no longer recurrent, and the next walker takes just $L/4$ steps to reach the boundary. Putting more walkers at the origin after the first walker has exit, one gets the pattern observed in Fig. 3.12 (c).

The resistor network for this tiling is shown in fig. 3.13 (a), and is again a square lattice with not all resistances equal to 1Ω . Thus, at least starting from 2×2 unit cells, we find that the adjacency graph of patches is the same for all types of patterns formed, and the corresponding resistor networks differ not in their structure, but only in the values of resistances. Fig. 3.13 (b) gives an equivalent square lattice structure for this network.

The voltages in the first quadrant of 3.13 (a) are given by

$$\begin{aligned}
 V_2(m, n) = Q_2(G_{sq}(m, n-2) &+ G_{sq}(m+1, n-2) \\
 -G_{sq}(m, n) &- G_{sq}(m+1, n))
 \end{aligned} \tag{3.18}$$

where Q_2 is determined by the condition that $V(1, 0) = \frac{1}{2}$. The aspect ratio for this pattern can be observed from the symmetry of the pattern itself to be unity.

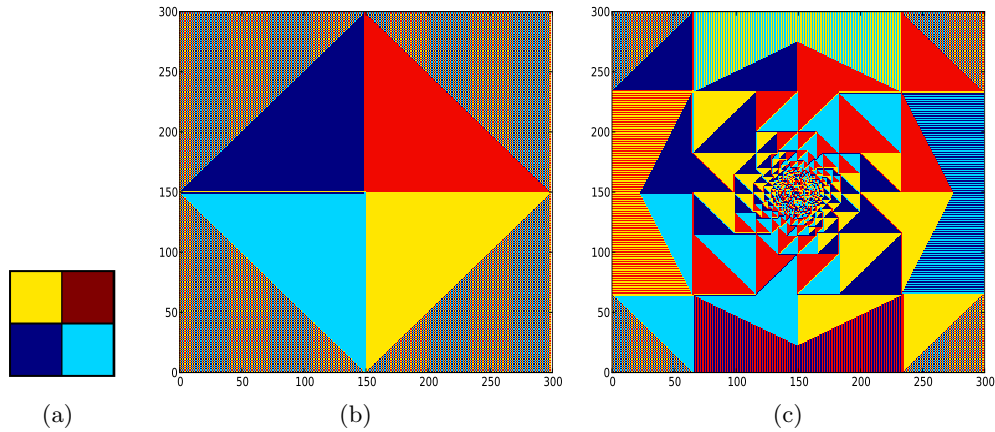


Figure 3.12: The pattern formed starting from the (recurrent) initial background shown in (a) by (b) a single walker (c) 1200 walkers on a 600x600 lattice. Colour code: dark blue - \rightarrow , light blue - \uparrow , yellow - \leftarrow , red - \downarrow .

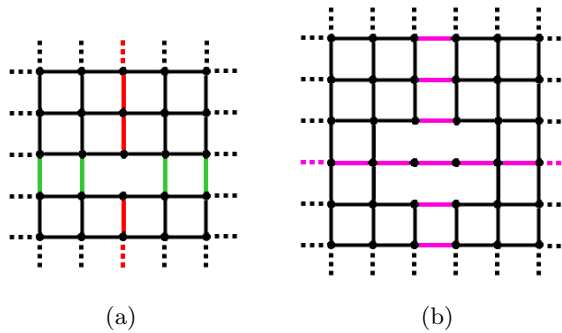


Figure 3.13: (a) The resistor network for the pattern in fig. 3.12 (c), where black bonds denote a resistance of 1Ω , red that of 0.5Ω and green a resistance of 2Ω . (b) An equivalent resistor network, obtained by (i) replacing a 2Ω resistor by a series combination of two 1Ω resistors (ii) replacing a $.5 \Omega$ by a parallel combination of two 1Ω resistors, (iii) adding some extra 1Ω resistors (shown with pink bonds) between nodes at equal potential.

3.5 Bounded Fluctuations and Quasiperiodicity

In this section we examine the growth with N of the horizontal and vertical extent of the full pattern in fig. 3.1, and the sizes of the different patches which comprise it. As the pattern shows proportionate growth, each of these would grow as $\alpha_P N$ for large N , where α_P is in general an irrational number, which depends on the patch. We would like to study how much the actual size at a given value of N differs the linear growth expectation. Our surprising observation is that for the patterns studied here, for all patches that we looked at, the actual value of the diameter of patch stays very close to the linear growth as is possible, differing from $\lfloor \alpha_P N \rfloor$ by not more than $O(1)$.

As the first example, consider the horizontal extent (distance of the boundary from the origin) of the pattern along the positive x-axis. Denote this extent after N walkers have left

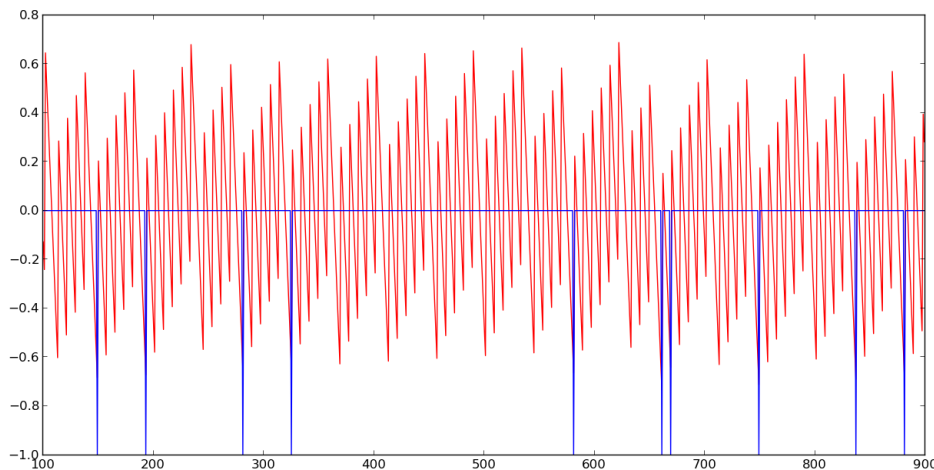


Figure 3.14: For the pattern in Fig. 1, (in red) the deviation of $H_1(N)$, the horizontal extent of the second-farthest vertical line along the positive x-axis measured every fourth step from the asymptotic linear value $(3/4 - 2/\pi)N$, and deviation from $\lfloor N/4 \rfloor$ (in blue). On the x-axis is $\lfloor N/4 \rfloor$ ($H_1(N)$ only changes every fourth step).

the lattice, by $H(N)$. Similarly, let $H_1(N)$ be the distance from the origin of the vertical boundary of the patch of constant orientation $(1, 0)$ (the largest dark blue triangle in the fig. 3.4 (a)). In section IV, we showed that, for large N ,

$$\lim_{N \rightarrow \infty} H(N)/N = 1/4, \quad (3.19)$$

$$\lim_{N \rightarrow \infty} H_1(N)/N = \left(\frac{3}{4} - \frac{2}{\pi}\right)N. \quad (3.20)$$

We find that, after an initial transient, $H(N)$ increases exactly periodically, increasing by 1 every fourth step. In fact, we can write down an exact formula for $H(N)$: $H(N) = \lfloor (N + 1)/4 \rfloor$ for $N \geq 3$.

Now consider the behaviour of $H_1(N)$ with N . We find that $H_1(N)$ increases only when $H(N)$ increases, but, clearly, as the the average rate of increase is lower, sometimes $H(N)$ will increase, but $H_1(N)$ would not. In fig. 3.14, we have plotted $H_1(N) - (3/4 - 2/\pi)N$ every fourth step vs. $\lfloor N/4 \rfloor$. For all N in the range plotted, these deviations from the linear growth are always of magnitude strictly less than 1, but have a complicated dependence on N .

Thus, we have seen that the exact value of $H_1(N)$ is very well approximated by $(3/4 - 2/\pi)N$, and the actual value is either the integer just above or just below this real approximant.

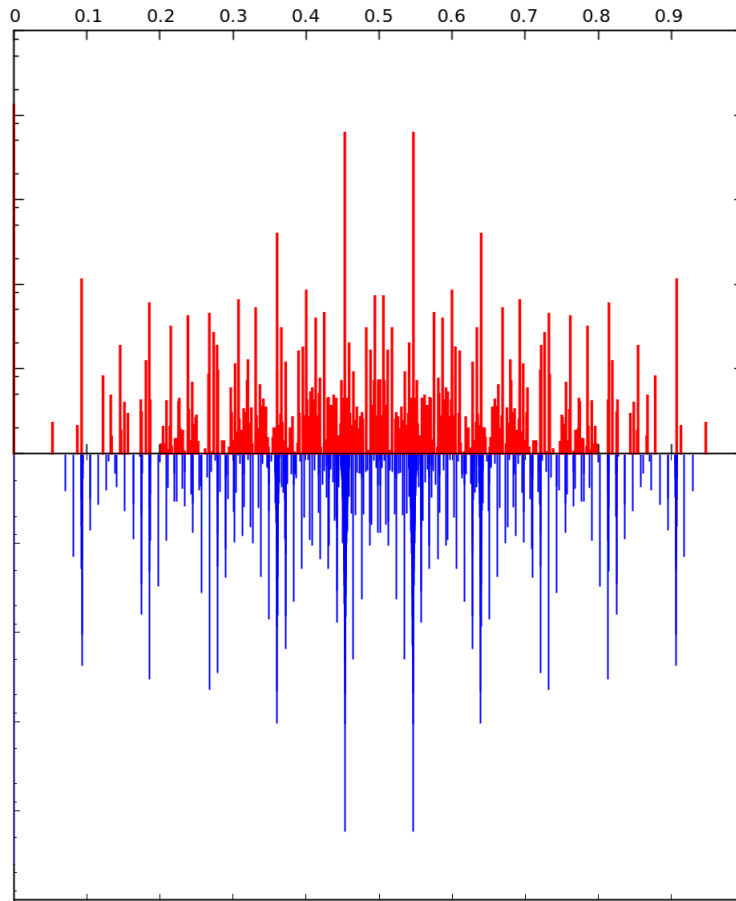


Figure 3.15: The power spectra (on a log scale and arbitrary units) of (in red) the actual sequence $h'_{N/4}$ for the pattern and (in blue) the Fourier transform of the sequence $\text{Nint}[(3 - \frac{8}{\pi})i]$

As a simple exercise, we considered the sequence $g_N = \text{Nint}(f(N - a))$, where $\text{Nint}()$ is the nearest-integer function, $f = (3/4 - 2/\pi)$, and a is an adjustable constant. Fig 3.14 shows that the difference between the actual sequence and this sequence, in the range plotted, is non-zero only about 1% of the time, for the choice $a = 3$. Also, when it is not zero, it takes the value -1 . The Fourier transform for g_N is shown in fig. 3.15 along with the Fourier transform of the actual sequence. It is seen that the peaks (when the Brillouin zone of frequencies is scaled to go from 0 to 1) for the sequence are at multiples of $f = 3 - 8/\pi$ to as close an accuracy as the finite length of the sequence allows. While most of the peaks for the real sequence fall at the same frequencies, their heights are slightly smaller. There are also additional peaks which are not there in this approximating sequence. In the next few paragraphs we examine the origin of these extra peaks by taking a closer look at the difference between the actual sequence and this simple approximant.

The growth of $H_1(N)$ may be encoded in a binary sequence $\{h_i\}$ defined as follows:

Let h'_j denote the increase in $H_1(N)$ when $H(N)$ increases from $j - 1$ to j . Clearly, $H_1(N) = \sum_{j=0}^{N/4} h'_j$. Also, asymptotically, $\sum_{j=0}^N h'_j = (3 - 8/\pi)N$. The power spectrum for the sequence $\{h'_j\}$ obtained from the pattern is plotted in fig. 3.15. There are a number of peaks of various magnitudes, which is the typical behaviour of quasiperiodic sequences.

We now construct a sequence of 1's and 0's which has growth rate $3 - 8/\pi$, using a different deterministic rule: the best rational approximant to $(3/4 - 2/\pi)$ using the nearest-integer continued fraction representation. The sequence of continued fractions obtained by truncating the expansion at different orders is easily seen to be

$$1/2, 5/11, 39/86, \dots \quad (3.21)$$

Denote the string '01' by A. For $N < 11$, the best sequence of 0s (no growth during the time-step) and 1s (denoting growth by one unit), which best approximates the irrational growth rate $(3/4 - 2/\pi)$ would be the sequence AAA..., that is, 010101..., such that the total length is less than N . For $N > 11$, one would need to have five 1's for every six 0's, and hence the best sequence (for $N < 86$) would be $(A^50)(A^50)(A^50)\dots$. Compare this with the actual sequence $h'_{N/4}$ from $N/4 = 242$ to $N/4 = 511$:

$$(A^50)(A^50)(A^50)(A^50)(A^50)(A^50)(A^40)(A^60)(A^40)(A^50)(A^40)(A^60)(A^50) \quad (3.22)$$

$$(A^40)(A^60)(A^40)(A^50)(A^50)(A^50)(A^50)(A^50)(A^50)(A^40)(A^60)(A^40)$$

It is seen that sometimes the string $(A^50)(A^50)$, in the simplest rational approximant at this order, is replaced by the string $(A^40)(A^60)$. We have no good explanation of why this should occur, except to say that this is probably caused by steric effects of nearby patches.

This effect of nearby patches is felt even at the boundary of the pattern. Let $V(N)$ denote the vertical extent of the pattern along the positive y-axis after N walkers. Figs. 3.16 (a) shows $V(N) - \frac{N-3}{4}$ vs. N and we plot its power spectrum in Fig. 3.16 (b). This sequence is not periodic, unlike the horizontal extent, although the associated growth rate is the same rational number $\frac{1}{4}$. Again, we note that the magnitude of the difference is always $O(1)$, in fact being ≤ 1 in the range plotted.

Our numerical studies suggest that this behaviour, where deviations from the exact linear growth are bounded and quasiperiodic, is a general property of the positions of all patch boundaries in the pattern.

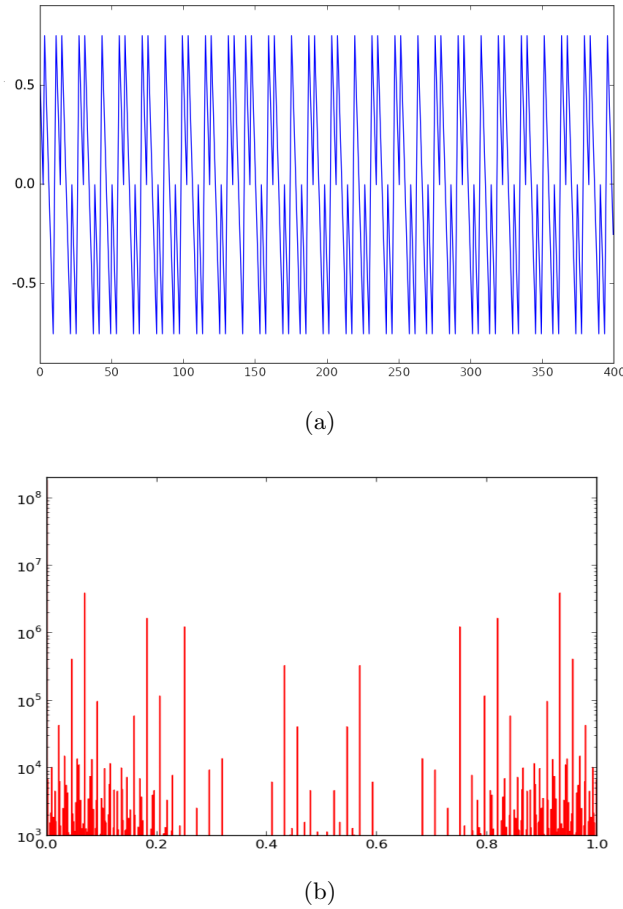


Figure 3.16: (a) Plot of the deviation of the vertical boundary along the positive y-axis from exact linear variation, $V(N) - \frac{N-3}{4} + 1.5$, against N and (b) its power spectrum (on a log scale, arbitrary units)

3.6 Summary and concluding remarks

In this chapter, we studied the growing patterns formed by depositing rotor-router walkers on the origin of a finite two-dimensional lattice, starting with periodic background configurations of arrows. We find that the patterns show rich internal structure which scales proportionately with the size of the pattern. We characterized this structure by mapping it to a resistor network and solving the Kirchoff equations on the network. We make some reasonable assumptions that the regularities seen in the observed patterns continue to hold for larger N , and this allows us determine the exact asymptotic scaling limit of the visit function $\phi(\xi, \eta)$. We find that the function $\phi(\xi, \eta)$ is a piece-wise linear function of its arguments, with integer slopes. We presented numerical evidence that the magnitude of deviation of the pattern size from the linear growth estimate remains less than 1, and is a quasiperiodic function of the number of walkers.

Another interesting set of systems which grow self-similar growth are known as Lin-

dermayer or (L-) systems [7], which are defined by a set of objects, and iterative rules to generate larger systems made of these objects, from smaller ones. Interestingly, one-dimensional L-systems can generate sequences generated from the continued fraction expansions of algebraic numbers, like the ones studied in section 3.5. (Note, however, that the irrationals which characterize the growth of the patterns in chapter 3 depend on π , which is not an algebraic number.) Perhaps an L-system construction in 2D can be constructed to approximate the growth of rotor-router patterns.

Appendix: Derivation on eqn. (3.9) from matching of boundary conditions

Consider the arrangement of six-sided visit-function-patches shown in Fig. 3.5 (b). We note that the point A lies on the boundary of patches labeled (m, n) and $(m - 1, n)$. Continuity of ϕ across the boundary implies that

$$\phi(A) = f_{m-1,n} + (m - 1) \xi_A + n \eta_A = f_{m,n} + m \xi_A + n \eta_A, \quad (3.23)$$

where $A \equiv (\xi_A, \eta_A)$. Thus

$$\xi_A = f_{m-1,n} - f_{m,n}. \quad (3.24)$$

Similar arguments give

$$\eta_A = f_{m,n} - f_{m,n+1}, \quad (3.25)$$

$$\xi_B = f_{m,n} - f_{m+1,n}, \quad (3.26)$$

$$\eta_B = f_{m,n-1} - f_{m,n}.$$

Now, we note that the line AB was a boundary of a patch of constant orientation, and has a slope that can only take one of the values $0, \pm 1, \infty$. In this case, it must be 1. Hence we get

$$f_{m+1,n} + f_{m-1,n} + f_{m,n-1} + f_{m,n+1} - 4f_{m,n} = 0 \quad (3.27)$$

which is the Eq. (3.9), obtained earlier using the BSST theorem.

Bibliography

- [1] A. E. Holroyd and J. Propp, *Rotor Walks and Markov Chains*, Contemporary Mathematics, **520** 105 (2010) arXiv:0904.4507
- [2] W. Pegden and C. K. Smart. *Convergence of the Abelian sandpile*, Duke Mathematical Journal **162** 627 (2013)
- [3] S. Ostojic, Physica A **318** 187 (2003).
- [4] R. L. Brooks, C. A. B. Smith, A. H. Stone and W. T. Tutte, *The Dissection of Rectangles into Squares*, Duke Mathematical Journal **7** 312 (1940).
- [5] F. Spitzer, *Principles of Random Walk*, pp. 124, 148-51, (Van Nostrand, Princeton, 1964);
- [6] J. Cserti, *Application of the lattice Green's function for calculating the resistance of an infinite networks of resistors*, Am. J. Phys., **68** 896 (2000).
- [7] Aristid Lindenmayer, *Mathematical models for cellular interaction in development*, J. Theoret. Biology, **18** 280 (1968)
<https://en.wikipedia.org/wiki/L-system>

Chapter 4

Rotor-router Patterns on Noisy Backgrounds

In this chapter, we will consider the patterns formed by rotor-router walkers on backgrounds which are not perfectly periodic, but are perturbations of periodic backgrounds with the arrow directions changed at some randomly chosen sites. Consider the simplest periodic starting background, with all arrows pointing to the left. The pattern formed on this background was studied in the previous chapter. Now suppose a fraction p of these sites, randomly chosen, are flipped to point up instead of left. Fig 4.1 shows the pattern after $N = 500$ walkers with $p = 0.01$. We see that the noise has created ‘defect lines’ in some of the patches, which also affect the shapes of the patch boundaries. Here we study perturbations on particular starting backgrounds, and also study how the presence of the noise affects the shapes of the patches in the pattern and how these properties vary as the noise strength p is varied.

We find that the consideration of two simple but instructive cases of noise (i.e., perturbations of the periodic background) helps us study how the defect lines can be drawn given the particular realization of noise, and the effect of these lines on the shape of the patch. The study of these two cases will occupy us for most of the chapter. We begin this chapter with a definition of Transient and Recurrent backgrounds in section 4.1, along with a simple example of a periodic recurrent background. In section 4.2 we describe the method used to study the perturbed background, based on a method developed by Friedrich and Levine [1]. In section 4.3, we describe the two noisy backgrounds we have studied. These are discussed in detail in sections 4.5 and 4.6 respectively. We state our conclusions in section 4.6 with remarks about growth on more general noisy backgrounds.

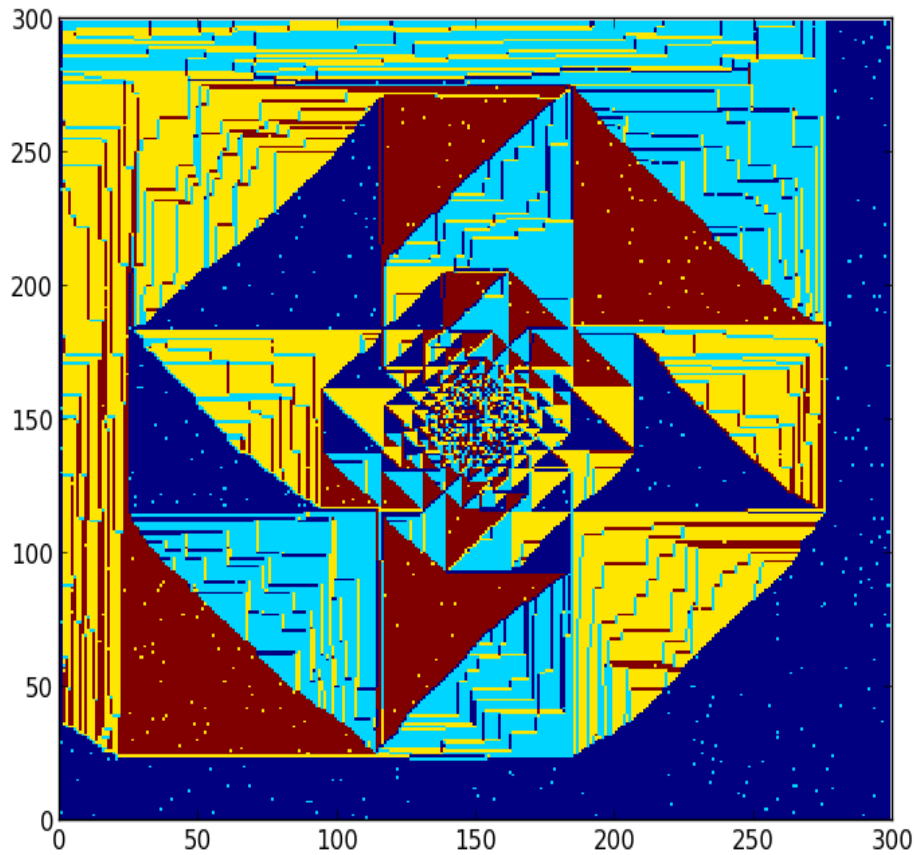


Figure 4.1: Pattern formed by depositing 500 rotor-router walkers at the origin of a square lattice, starting from an initial configuration where 99% of the arrows point East and 1% point North. Colour code: dark blue - \rightarrow , light blue - \uparrow , yellow - \leftarrow , red - \downarrow

4.1 Recurrent and Transient Backgrounds

4.1.1 Recurrence and Transience

As discussed in the previous chapter, every background configuration of arrows on an infinite lattice (or, in general, any infinite strongly connected graph) can be classified into two types, Recurrent or Transience, depending on the path followed by the first walker [4].

An example of a recurrent background, where a walker dropped at the origin keeps coming back to the origin, is given by the background formed by repeating the unit cell $\begin{pmatrix} \rightarrow & \downarrow \\ \uparrow & \leftarrow \end{pmatrix}$ periodically in the x- and y-directions. We recall the matrix notation introduced in the previous chapter to write unit cells. The (i, j) -th ($i = 0, 1$) element of this 2×2 matrix denotes the direction of the arrow attached to the lattice site $(2m + i, 2n + j)$, where m and n are arbitrary integers. As before, we will use the numbers 0, 1, 2 and 3 to refer to arrows pointing in the directions \rightarrow , \uparrow , \leftarrow and \downarrow respectively. The same background can thus be denoted by the unit cell $\begin{pmatrix} 0 & 3 \\ 1 & 2 \end{pmatrix}$. Fig. 4.1.1 shows the pattern formed by the first walker on this background after the walker has visited the origin for the 40-th time. The walker

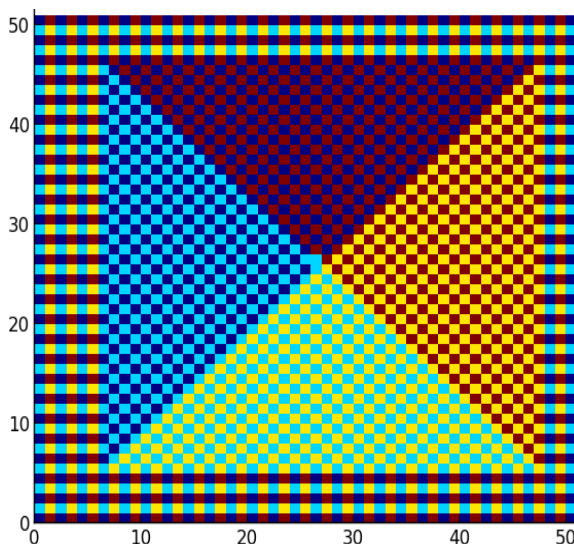


Figure 4.2: Pattern formed on the background $\begin{pmatrix} 0 & 3 \\ 1 & 2 \end{pmatrix}$ after the first walker is stopped after visiting the origin 40 times. Colour code: dark blue - \rightarrow , light blue - \uparrow , yellow - \leftarrow , red - \downarrow

keeps coming back to already-visited sites - in fact, for every increase of the diameter of the pattern by 4, all inner sites are visited four more times. Fig 4.1.1 shows the pattern when the walker has been stopped at the origin on its 40-th visit.

This simple pattern is made of just four patches. The configuration within each of the patches is a periodic tiling by the 2×2 unit cells $\begin{pmatrix} 0 & 3 \\ 3 & 0 \end{pmatrix}$, $\begin{pmatrix} 0 & 1 \\ 1 & 0 \end{pmatrix}$, $\begin{pmatrix} 2 & 1 \\ 1 & 2 \end{pmatrix}$ and $\begin{pmatrix} 2 & 3 \\ 3 & 2 \end{pmatrix}$ respectively. The boundary between patches $\begin{pmatrix} 0 & 3 \\ 3 & 0 \end{pmatrix}$ and $\begin{pmatrix} 0 & 1 \\ 1 & 0 \end{pmatrix}$ consists of a diagonal line of left-pointing arrows. (This shows as a diagonal line of dark blue sites in the figure.) There are similar diagonal boundaries between every pair of neighbouring patches.

The visit function for this pattern is linear in each of the four patches. After the walker has returned to the origin for the D^{th} time, the visit function is given by $V_D^0(x, y) = D - 2|x|$ in patches 1 and 3, and $V_D^0(x, y) = D - 2|y|$ for patches 2 and 4. The superscript 0 stands for the fact that this is the unperturbed visit function.

The following theorem allows us to classify backgrounds according to the time taken to reach infinity in the above two types:

Theorem: [4] Every background on a strongly connected graph is either recurrent or transient.

This theorem follows from the observation that if a site is visited infinitely many times, so are its neighbours, and this implies there are no backgrounds where some sites are visited infinitely many times while others are visited only finitely many times. It also implies that

the recurrence or transience of a background is independent of the choice of the site that the first walker is dropped on.

Given a periodic background, we study the effect on the pattern as the arrow directions at randomly chosen sites are flipped. If one starts with a recurrent background, and flips a certain fraction of sites, when this fraction is large the background might become transient. Such cases, where there is a transition from recurrence to transience at a certain fraction p , turn out to be the most interesting cases, and we focus on them in this chapter. It could also happen that the background retains its transience/recurrence even as we vary p from 0 to 1.

4.1.2 Notation and Protocol

We will be constructing background arrow configurations out of 2×2 unit cells. Unit cells, and the backgrounds made by periodic repetition of them, will both be specified by a 2×2 matrix.

We extend the notation to random backgrounds as follows: $\{A, B|p, 1 - p\}$ denotes an ensemble of starting backgrounds where each unit cell on the lattice is of type A with probability p or of type B with probability $(1 - p)$. Thus, a background $\{(\begin{smallmatrix} 2 & 3 \\ 0 & 1 \end{smallmatrix}), (\begin{smallmatrix} 1 & 0 \\ 0 & 1 \end{smallmatrix}) | 0.8, 0.2\}$ denotes the ensemble of backgrounds in which, for a typical background in the ensemble, about 80% of the unit cells are $(\begin{smallmatrix} 2 & 3 \\ 0 & 1 \end{smallmatrix})$ and 20% are $(\begin{smallmatrix} 1 & 0 \\ 0 & 1 \end{smallmatrix})$.

The protocol for constructing patterns, given a background, is as follows: starting with a given background specification, say $\{A, B|p, 1 - p\}$ we generate a random starting background on an $L \times L$ lattice. For transient backgrounds, we then drop N walkers at the center of the lattice, and wait till they have all exit the lattice, and study the resulting pattern. For recurrent backgrounds, we study the pattern after stopping the walk at a specified stopping time, usually the $4N$ -th time the walker visits the origin.

Defining the final configuration of arrows that have undergone at least one full rotation as ‘the pattern’, we now have an ensemble of patterns for a given starting background specification (ie, for given A, B and p). We will focus on calculating the averages of various properties taken over this ensemble.

4.2 From Approximate to Exact Visit function

Given a starting random background, we need a method for calculating the resulting patterns that allows for analytical treatment. Our aim is to determine the final visit function once the walker has returned to the origin for the $4N$ -th time. We will start with an approximate guess for final visit function - our guess will be the visit function for the periodic

unperturbed background ($p = 0$).

In this section we outline Friedrich and Levine's [1] method for getting better and better approximations to the visit function, starting from an initial approximation, and eventually culminating in the exact answer. They use the method in [1] to efficiently simulate patterns formed in an aggregating version of the rotor-router model. First we outline the method itself, and in the next subsection we use it to determine the rules for the generation and interaction of defect lines created by perturbations on a particular periodic background configuration.

Consider starting with a number of walkers on a given background, and consider the state of the arrow configuration when the walkers might not have yet reached the sink. As in the previous chapter, $\rho(x, y)$ denotes for the direction of the arrow at site (x, y) . $\sigma(x, y)$, called the walker configuration, denotes the number of walkers on site (x, y) . Call the starting arrow and walker configurations as ρ_i and σ_i respectively. Let $u(x, y)$ denote the total number of times the site (x, y) is visited - the visit function (or 'odometer function') at the point (x, y) . Then ρ and σ at any time obey the equation

$$\mathcal{L} [u, \rho_i](x, y) = \sigma(x, y) - \sigma_i(x, y) \quad (4.1)$$

where the 'stack Laplacian' \mathcal{L} is defined as follows [1]:

$$\mathcal{L} [u, \rho_i](x, y) = \nabla^2 u(x, y) + \sum_{(x', y') \sim (x, y)} f_{(x', y')}(\rho_i, \rho_f) \quad (4.2)$$

where the summation is over the neighbours of site (x, y) . The function $f_{(x', y')}(\rho_i, \rho_f)$ counts the number of times the arrow at site (x', y') points towards site (x, y) when one rotates it from $\rho_i(x', y')$ to $\rho_f(x', y')$. This f_j is either 0 or 1. (ρ_f is not independent of ρ_i and u , but follows from $\rho_f = \lfloor (\rho_i + u)/4 \rfloor$).

In a region which does not contain any walkers at starting and ending times, $\mathcal{L} u = 0$. If $\mathcal{L} u < 0$ at a site, this indicates that walkers initially at the site have not returned to it, while $\mathcal{L} u > 0$ indicates that more walkers are present at the site at the ending time than at the start.

Another property of the arrow configuration once all walkers have reached the sink is that arrows in the region visited by the walker do not form any loops. For one walker, this follows from an old theorem by Broder [2] which says that the graph formed by the last exit edges at all the sites visited by a walker is a tree rooted at the current position of the walker. The proof of this theorem is simply that any graph with N vertices and $(N-1)$ edges is a tree. For more walkers, one uses the fact (true for rotor-routers) that if a walker vis-

its a site which is part of a loop, the loop is finally broken after a certain number of steps [3].

If a loop, or ‘cycle’, exists in an arrow configuration, we can define an operation called ‘reverse cycle popping’, where all the arrows which form the cycle are rotated 90° clockwise (that is, reverse of the anti-clockwise direction in which they are moved by the walkers). This destroys the original loop, but might create new loops. It is useful to extend the definition of reverse cycle popping to a set of arrows which do *not* form a loop as simply doing nothing to the arrow configuration. Friedrich and Levine show that the procedure of reverse cycle-popping a set of sites commutes with the operation of starting a walker at a site and letting it walk until it reaches the sink. That is, reverse-popping the loop before starting the walk will result in the same final configuration once the walker has reached the sink as performing the reverse-popping after the walker has reached the sink - if the loop still exists, that is. (If the walker visits any site on the loop, the final configuration will not contain that loop, and reverse-cycle popping will do nothing.)

The Friedrich-Levine procedure finds the exact solution of the equation 4.1, given the following information:

- (i) Initial arrow and chip configurations, ρ_i and σ_i ;
- (ii) The final condition is that all chips have ended up at the sink;
- (iii) An initial guess for the visit function, $u_0(x, y)$.

The steps of the procedure are as follows:

1. Evaluate the initial guess for the final arrow configuration, $\rho_0 = \lfloor (\rho_i + u_0)/4 \rfloor$
2. Evaluate $\mathcal{L} [u_0, \rho_i](x, y)$ at all sites. This gives a $\sigma_0(x, y)$, an initial guess for the final chip configurations. Sites at which $\sigma_0 > 0$ are said of be hills of height σ_0 , and sites at which $\sigma_0 < 0$ are called holes of depth $|\sigma_0|$.
3. Place walkers at each hill site equal in number to the height of the hill, and let them walk until they reach the holes. When a walker reaches a hole, the height of the hole decreases by 1.
4. Once all these hills have been moved to the holes, scan the lattice for any loops in the part of the lattice where u_0 is non-zero, and reverse-cycle-pop them. Rescan and repeat until no more loops are left.

At the end of the this procedure, one gets an updated guess for $u(x, y)$, because $u(x, y)$ changes every time a cycle containing the point (x, y) is reverse-popped or when an extra walker visits (x, y) , according to the following rules:

- Extra walkers - extra walkers walking from hills to holes *add* to u on the sites along the path followed by the walker, in the usual way.

- While reverse-popping a cycle, u is decreased by 1 for all sites on the cycle.

The final $u(x, y)$ one gets after completing the procedure is an acyclic background where $\mathcal{L} u = 0$ everywhere but at the sink - the unique solution given the stated conditions [1].

4.2.1 Point perturbations

We call a perturbation in which only a single unit cell of a periodic background is changed a ‘point perturbation’. Consider a point perturbation of the background $\begin{pmatrix} 0 & 3 \\ 1 & 2 \end{pmatrix}$ such that only a single arrow is rotated 90° anticlockwise, changing a single unit cell in the pattern from $\begin{pmatrix} 0 & 3 \\ 1 & 2 \end{pmatrix}$ to $\begin{pmatrix} 0 & 3 \\ 1 & 3 \end{pmatrix}$. We want to determine the final configuration we get after a single walker started at the origin walks until it has visited the origin N times, where N is such that the region visited by the walker contains the perturbed site. For the case shown in fig 4.3, a four unit cells of the initial background are changed in the above fashion, and N is 40.

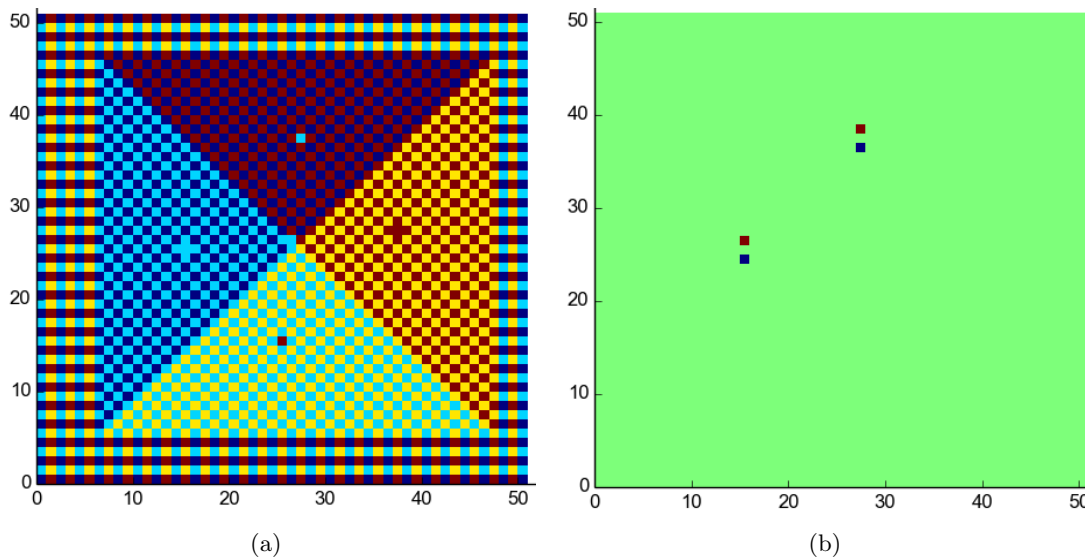


Figure 4.3: (a) The initial approximation to the final arrow configuration. The differently colored cells in the four patches are where the arrow is flipped from the periodic background. Colour code: dark blue - \rightarrow , light blue - \uparrow , yellow - \leftarrow , red - \downarrow (b) $\mathcal{L} u_0(i, j)$ for initial approximate visit function $u_0(i, j)$. Color code: red = 1, blue = -1, green = 0.

We start with the visit function for the unperturbed pattern as the initial guess: $u_0(x, y) = 40 - 2|x|$ in the top and bottom patches and $40 - 2|y|$ in the right and left patches. $\mathcal{L} u_0$ evaluated at all sites is shown in fig 4.3 (b). There is a hill of height 1 at the site above the perturbed site and a hill of hole 1 at the site below the perturbed site. Putting a walker at the hill and letting it walk to the hole gives the final configuration in fig 4.4 (a), and changes u as given in fig 4.4 (b). Scanning the final configuration for cycles, we find none. Thus, the effect of the perturbation is creating the ‘lightcone’ inside which sites are visited 4 more times than they would be in the unperturbed case.

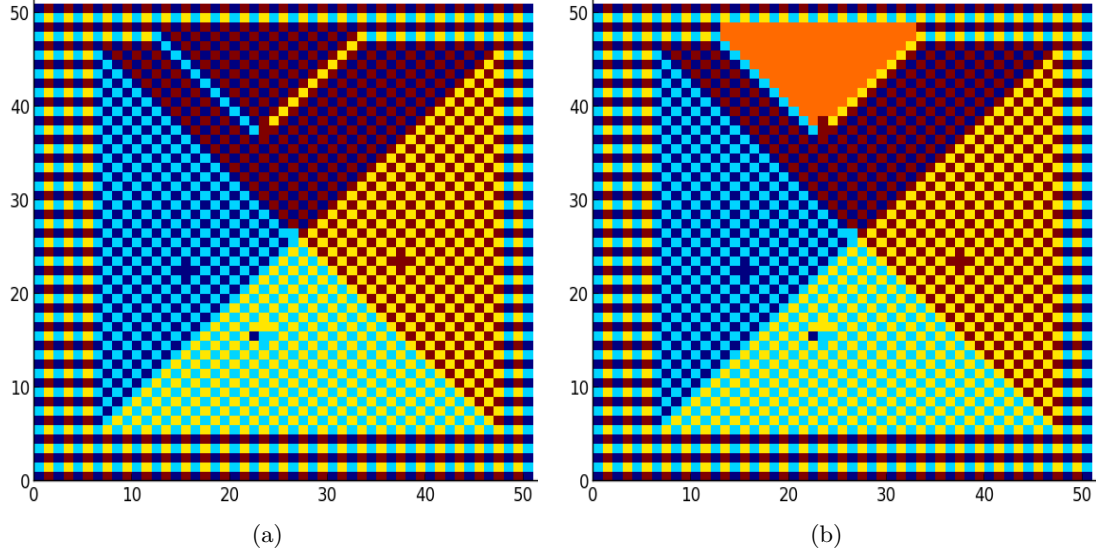


Figure 4.4: (a) The final pattern after the Friedrich-Levine procedure with point perturbations in all four patches. Figure (b) shows the sites visited by the additional walker put in the top patch - the sites in orange are visited four times, while those in blue and yellow lines bounding the orange region are visited twice. Colour code: dark blue - \rightarrow , light blue - \uparrow , yellow - \leftarrow , red - \downarrow

We call the above specific procedure - for the hill-hole pair created by the defect, putting an extra walker at the hill and letting it walk to the hole - as ‘firing a defect’. We use the nomenclature ‘lightcone’ throughout this chapter to denote the V-shaped formation created by this procedure in this case. The sites on the diagonal (which are here colored yellow or light blue) will be called ‘sites *on* the lightcone’.

One can also place a perturbed unit cell $\begin{pmatrix} 0 & 3 \\ 1 & 3 \end{pmatrix}$ in each of the other three patches and use the Friedrich-Levine procedure to calculate the final configuration. This is also shown in fig - there are no lightcones generated in the other patches, and the perturbations have only a local effect.

Now consider the effect of several point perturbations of the same type in the top patch (change several unit cells from $\begin{pmatrix} 0 & 3 \\ 1 & 2 \end{pmatrix}$ to $\begin{pmatrix} 0 & 3 \\ 1 & 3 \end{pmatrix}$ in the initial configuration). Each defect creates a single hill and a single hole as if acting independently, since \mathcal{L} is a local operator. (If a hill from one defect falls on top of a hole from another, thus ending up with $\mathcal{L} u = 0$ at that site, we can still treat it as a hill and hole being present at the same site - a walker is stopped when it falls into the ‘hole’, and then a new walker starts walking from the ‘hill’.)

We use the following order of firing the defects to determine the rules of interaction when more than one defect is present: fire the defects in the farthest layer from the origin

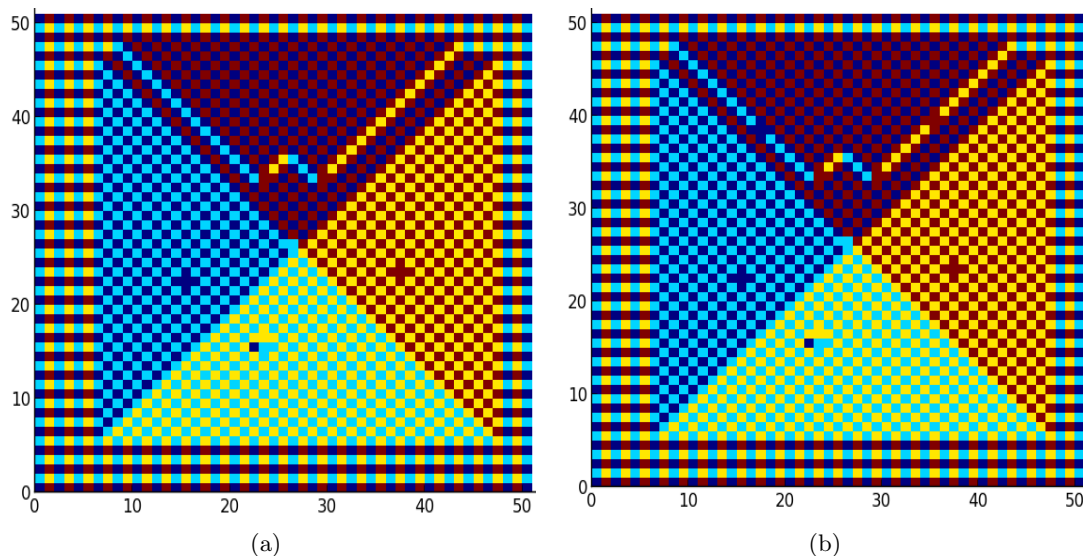


Figure 4.5: The final pattern formed by type (i) point perturbations: (a) Two intersecting lightcones (b) Perturbed unit cells on lightcones have no effect. Colour code: dark blue - \rightarrow , light blue - \uparrow , yellow - \leftarrow , red - \downarrow

first, then fire the defects in the layer below it, and so on. This procedure ensures that when we fire a defect, there are no other holes in the region that the walker from this defect explores (the lightcone region), and hence no other holes that this walker can fall into. The only hole it falls into is the one which is two sites below its hill. We make the following observations:

(1) It is clear that if the two points create non-intersecting lightcones, they will simply act individually.

(2) If the lightcones are nested, the visit function gets an additive part of +4 every time one crosses from the outside to a lightcone to inside it.

(3) If the lightcones due to two defects intersect (fig 4.5 (a)), they merge to create a single terrace-like structure.

(4) However, if one of the points is on the boundary of a lightcone created by another, it does not create a lightcone of its own, see fig 4.5 (b).

Note that these rules apply for arbitrarily big patches and arbitrary arrangements of defect unit cells. This is because of the fact that \mathcal{L} is a local operator, and the fact that even an arbitrarily long lightcone has the same structure as a small one - the region inside the lightcone that is tiled by the same unit cell as the patch, and one-unit-cell thick boundaries which continue at a 45° angle until they hit the edge of the patch. This argument enables us to deduce the behaviour of larger patterns from the study of patterns formed on small lattices with a few defect sites.

We use this construction in the next two sections to study two particular but illustrative cases of random backgrounds, and to determine the rules to generate defect lines in both cases. Both backgrounds studied are noisy perturbations of the recurrent periodic background $\begin{pmatrix} 0 & 3 \\ 1 & 2 \end{pmatrix}$.

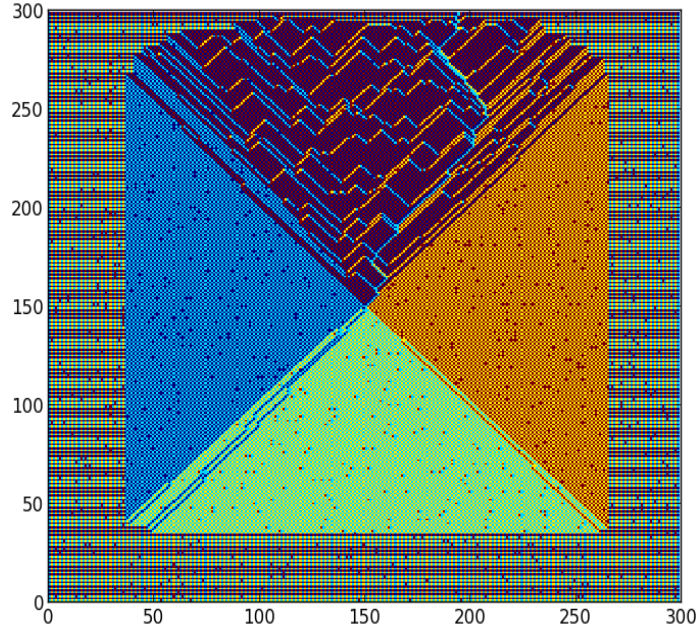


Figure 4.6: Pattern formed on a type I background, with $p = 0.02$. Colour code: dark blue - \rightarrow , light blue - \uparrow , yellow - \leftarrow , red - \downarrow

4.3 Case I

In this section, we study the pattern formed on the background (see fig 4.6).

$$\left\{ \begin{pmatrix} 0 & 3 \\ 1 & 2 \end{pmatrix}, \begin{pmatrix} 0 & 3 \\ 1 & 3 \end{pmatrix}, \begin{pmatrix} 1 & 3 \\ 1 & 2 \end{pmatrix}, \begin{pmatrix} 1 & 3 \\ 1 & 3 \end{pmatrix} \mid (1-p)^2, p(1-p), p(1-p), p^2 \right\} \quad (4.3)$$

On this background, the noise creates defect lines in only one patch, while in other patches the noise has only local effects. For $p = 1$ the background is transient, and we find in the next section that for all $p < 1$ it is recurrent. There are terrace-like structures present in only one patch out of the four.

4.3.1 The rules for drawing defect lines

The unit cells $\begin{pmatrix} 0 & 3 \\ 1 & 2 \end{pmatrix}$, $\begin{pmatrix} 0 & 3 \\ 1 & 3 \end{pmatrix}$, $\begin{pmatrix} 1 & 3 \\ 1 & 2 \end{pmatrix}$ and $\begin{pmatrix} 1 & 3 \\ 1 & 3 \end{pmatrix}$ form the type I background, being present with probabilities $(1-p)^2$, $p(1-p)$, $p(1-p)$ and p^2 respectively.

Calculating the stack Laplacian $\mathcal{L} u_0$ with the initial approximation u_0 being, as before,

the visit function for the unperturbed patch, we find that the $\begin{pmatrix} 1 & 3 \\ 1 & 2 \end{pmatrix}$ unit cells act identically to the $\begin{pmatrix} 0 & 3 \\ 1 & 3 \end{pmatrix}$ ones, both producing hill-hole pairs that, when fired, generate lightcones in the patch, except the lightcones have vertices at sites where x and y are both odd, in one case, and at sites where x and y are both even, in the other. It turns out that the lightcones of the second kind of firing (due to the perturbation $\begin{pmatrix} 1 & 3 \\ 1 & 2 \end{pmatrix}$) interact with the lightcones of the first kind (due to $\begin{pmatrix} 0 & 3 \\ 1 & 3 \end{pmatrix}$, studied in the previous section) according to the rules given in the previous section, without distinguishing which kind of unit cell created the defect line.

Thus the rules for drawing defect lines given the positions of the perturbed unit cells are:

- (i) Start two defect lines at right angles to each other at each noise point.
- (ii) If two defect lines meet, they do not continue beyond that point. This results in a terrace-like structure.
- (iii) Noise points which fall on existing defect lines do not create any new defect lines.

We give a heuristic explanation for rule (iii). The defect lines which form the two arms of a lightcone have the same arrow structure, locally, as the patches on either side of the current patch. That is, the defect line on the right side of a lightcone is made of the same unit cells which tile the patch to the right. We know that \mathcal{L} is a local operator, and that in both these patches the perturbation has only a local effect and does not generate lightcones. Thus we can expect that a perturbation on such a defect line would also have only a local effect, and not generate lightcones either. As shown earlier, this expectation is verified by explicit studies of small systems.

Denote the unperturbed visit function by $V_0(x, y)$, and the visit function for a particular noise realisation by $V(x, y)$. We define a height function $h(x, y)$ in the top patch by $4h(x, y) = V(x, y) - V_0(x, y) = V(x, y) - (D - 2y)$. The value of h at a point (x, y) which does not lie on a defect line is given by the number of terraces crossed in order to get to the region from the origin (or from the boundary of the patch). If (x, y) lies *on* a defect line, $h(x, y)$ is $h' - \frac{1}{2}$, where h' is the value of h for the region inside the defect line. Once we draw the defect lines according to the above rules, we can determine $h(x, y)$ for all points inside the patch, and this determines $V(x, y)$.

Note that the periodicity of the patches and the equivalence proved in the previous section allow us to use calculations of the final state on small-sized patches, as was done in the figures above, to generalise to large patches and arbitrary levels of noise (as long as the background stays recurrent).

4.3.2 The exact visit function and Tracy-Widom fluctuations

In chapter 1 we described the Bernoulli matching problem, and mapped it to a height model in which the height increases in integer steps as one crosses terraces with vertical and horizontal boundaries, situated in the first quadrant of the xy -plane. The height increases monotonically in both x - and y -directions. Here we only recall the basic rules for generating height terraces in the Bernoulli matching problem. We are given two random sequences of characters of length i and j and asked to find the longest increasing subsequence (LCS) : (a) Consider first quadrant of the square lattice. If the x -th character from sequence 1 is the same as the y -th character from sequence 2, draw two lines, one horizontal and one vertical, starting from point (x, y) . (b) Merge these lines to form terraces when they meet. (c) Points on existing defect lines have no effect. (d) The length of the LCS of the first m characters of the first word and the first n characters of the second word, $l(m, n)$ obeys the rules: $l(0, 0) = 0$, and $l(m, n)$ increases by 1 each time you climb a terrace. As noted in Chapter 1, we have that for large x and y ,

$$h_{BM} = \begin{cases} x & \text{if } x < py \\ \frac{1}{1-p}(2\sqrt{pxy} - p(x+y)) + A(p, x, y) \xi_{GUE} & \text{if } py \leq x \leq p^{-1}y \\ y & \text{if } p^{-1}y < x \end{cases} \quad (4.4)$$

where ξ_{GUE} is a random variable distributed according to the Tracy-Widom distribution corresponding to the Gaussian Unitary Ensemble, and $A(p, x, y) = (pxy)^{1/6}/(1-p) \left[(1+p) - \sqrt{p/xy}(x+y) \right]^{2/3}$.

Comparing the rules given in the previous subsection for the perturbations of type (i) and for Bernoulli matchings, we see that if one changes co-ordinates from (x, y) for Bernoulli matchings to $(x+y, x-y)$ for the rotor-router patch, $h(x, y) = h_{BM}(x+y, x-y)$ for the same realization of noise. Note that this correspondence holds for all values of p . (So long as the rotor background is recurrent, which as we show below it is for $p < 1$). Given the one-to-one correspondence between the two problems, we immediately conclude that $h(x, y) = h_{BM}(x+y, y-x)$. In particular, along the y -axis, the visit function goes like (for large $y \gg 1$)

$$V(y) = V(0) - 2y + 4 + h_{BM}(y, y) \quad (4.5)$$

where $V(0)$ is the mean number of visits to the origin. Note that since $h(x, y) \geq 0$, the boundary of the affected patch is extended outwards. We perform simulations on finite lattices with absorbing boundaries, where the walker exits the lattice when the boundary of the affected patch touches the boundary of the lattice. The longest extent of the boundary is, on average, along the y -axis. Working on an $L \times L$ lattice and setting $V(L/2) = 0$, from

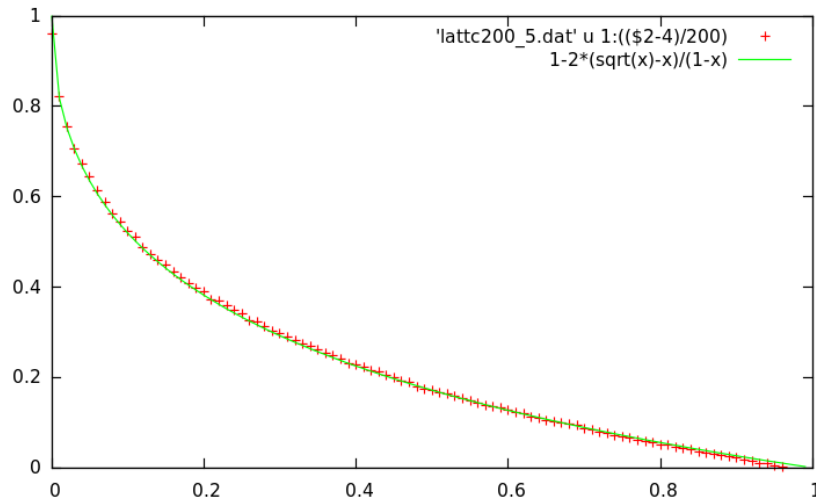


Figure 4.7: Number of visits to origin/ L vs. p : Comparison of theory and simulation results for type (i) backgrounds.

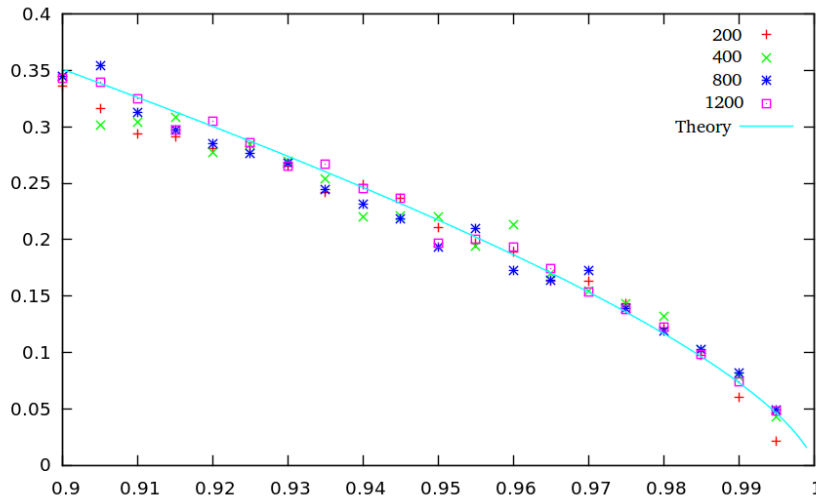


Figure 4.8: $\sigma_{V(0)/L} \times L^{-1/3}$ vs. p : Comparison of theory and simulation for scaled variance of order parameter.

the eqns (4.4) and (4.5), we get

$$V(0)/L = 1 - 2 \frac{\sqrt{p} - p}{1 - p} + A(p, \frac{L}{2}, \frac{L}{2}) \xi_{GUE} \quad (4.6)$$

We can measure the behaviour of this average, and its fluctuations, with p . The results are shown, along with the theoretical predictions, in figs 4.7 and 4.8. The fluctuations scale as $L^{3/2}$, and thus belong to the KPZ universality class. In fact, the Tracy-Widom behaviour of the entire distribution, as was mentioned in chapter 1, is identical across a whole set of models in widely different systems, in apparently unrelated contexts, which can be mapped exactly to each other, including Random Matrices, Anisotropic Directed Percolation, the

Asymmetric Exclusion Process, and many more (see section 1.3). To this diverse list of models we can now add Rotor-Router walks on the background studied in this section.

4.3.3 Lines of constant visit function

In this subsection we present another mapping of the above pattern to a model in the KPZ universality class, discussed in chapter 1 - the Polynuclear growth (PNG) model [6, 7].

Recall that the PNG model concerns the growth of a one-dimensional interface characterised by a function $h(x, t)$, which is the height of the interface at position x and time t . The function $h(x)$ in the PNG model is an integer valued function with discontinuous jumps of ± 1 (see fig 1.6 in chapter 1). The dynamics of the interface is best described in terms of these kinks and antikinks, which are nucleated in kink-antikink pairs at rate unity per unit length. Once nucleated, the kinks move towards the right and the antikinks move towards the left, both at unit velocity, and annihilate upon meeting.

Nucleation of a kink-antikink pair, in the language of the rotor-router patterns, is the formation of a lightcone at a defect site. Note that in the continuum limit, the probability of a nucleation on an existing worldline line is zero. The continuum limit of the rotor-patterns, when taken along with the $p \rightarrow 0$ limit, is precisely the continuum PNG process. Thus we can expect to see KPZ fluctuations in this limit.

Since the dynamics of the rotor-router worldlines is discrete, one might wonder if there is a way to get a discrete version of the PNG model which exactly maps onto the rotor-router pattern. There indeed is, as is seen by considering lines of constant visit function in the rotor-router patterns. In the unperturbed pattern, these lines are horizontal or vertical lines in each patch, which change orientation at the boundaries between the patches. That is, the right-angled change in direction happens on the ‘boundary line’ of sites between each pair of patches, which were described in section 3.1.3. (See fig 4.9). From the figure it is seen that in the perturbed pattern the contours of the visit function jump by a height ± 1 when they cross a defect line, with an antikink when going from the outside of the defect line to the inside and a kink when going from the inside to the outside. If we define value of the visit function on a contour as the time t , the evolution of the lines of constant visit function can be seen as a discrete version of the PNG process - kink-antikink pairs are created with probability p , and spread outwards with a constant velocity. The only subtlety is that new kink-antikink pairs cannot be nucleated co-incident with the edge of another jump, and this the jump at a kink or antikink cannot be of magnitude larger than 1.

A different discrete version of the PNG process gives rise to terraces which arise in the model of Anisotropic Directed Percolation studied by Rajesh and Dhar [8]. In this discrete PNG, defined by Johansson [7], new kink-antikink *can* be nucleated co-incident with an

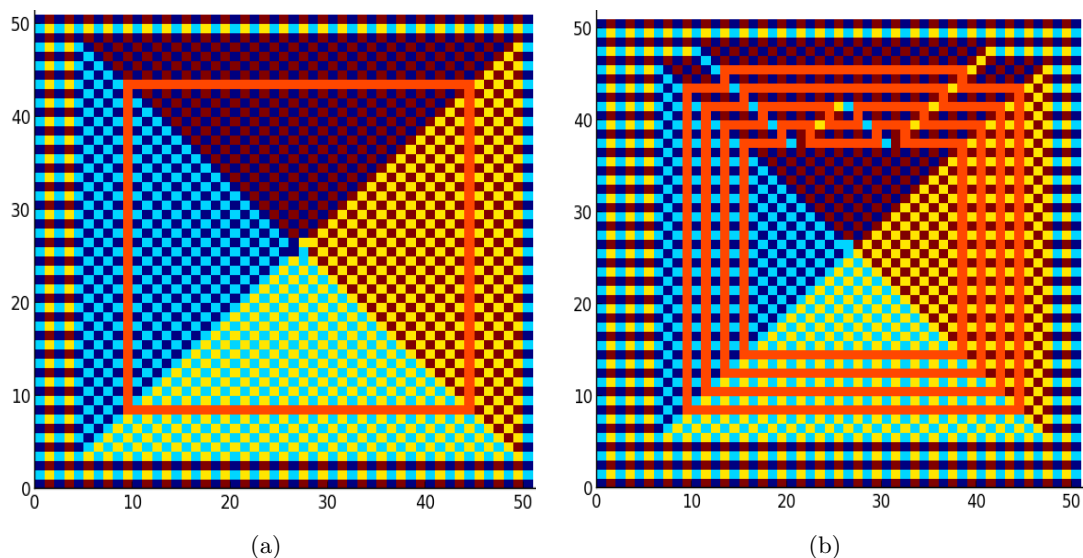


Figure 4.9: The contours of constant visit function with (a) a single type (i) perturbation, and (b) two type (i) perturbations. The visit function along successive contours in the figure differs by 4. Note the resemblance to the PNG model. Colour code: dark blue - \rightarrow , light blue - \uparrow , yellow - \leftarrow , red - \downarrow

existing kink or antikink, and hence jumps in height of the interface can be more than unity in magnitude. Johansson showed that the interface, for all p not just for $p \rightarrow 0$, has KPZ fluctuations, and the distribution of the fluctuations is the Tracy-Widom distribution. The two versions of the discrete PNG described above, Johansson's and the one corresponding to the rotor-routers, are related by the same transformation as the Bernoulli Matchings and Anisotropic Directed Percolation [5].

4.4 Case II

In this section, we study the patterns formed on the background (See fig 4.10).

$$\left\{ \begin{pmatrix} 0 & 3 \\ 1 & 2 \end{pmatrix}, \begin{pmatrix} 0 & 3 \\ 1 & 0 \end{pmatrix} \mid (1-p), p \right\} \quad (4.7)$$

On this background, defect lines are created in two patches, and our studies show that for large p the background is transient. A transition from recurrence to transience happens at $p_c \approx 0.61 < 1$.

The rules for generating the defect lines are different from those in the previous case, and the height function cannot be exactly solved for. We will present numerical evidence that the pattern can be divided into two regions - a region where the fluctuations of the visit function follow KPZ statistics, and a region where the fluctuations follow EW statistics.

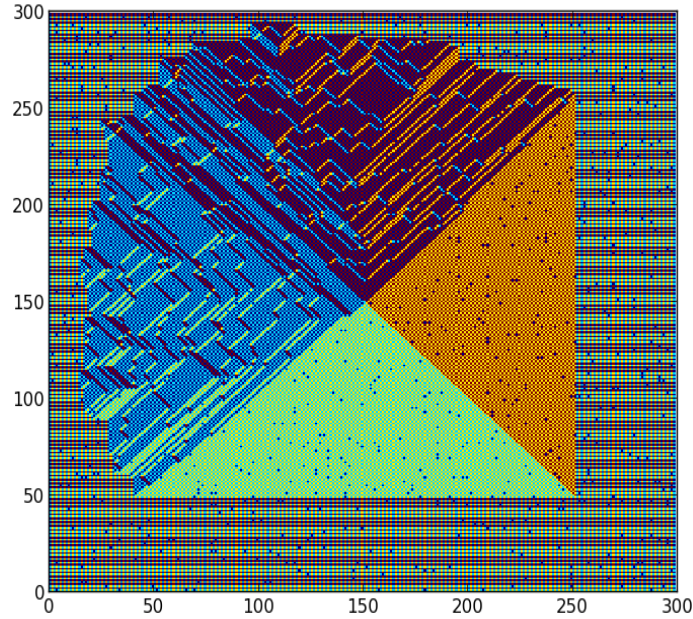


Figure 4.10: Pattern formed on a type II background, with $p = 0.02$. Colour code: dark blue - \rightarrow , light blue - \uparrow , yellow - \leftarrow , red - \downarrow

4.4.1 Rules for drawing defect lines

The unit cells $\begin{pmatrix} 0 & 3 \\ 1 & 2 \end{pmatrix}$ and $\begin{pmatrix} 0 & 3 \\ 1 & 0 \end{pmatrix}$ form the type (ii) backgrounds, being present with probability $1 - p$ and p respectively. The unperturbed ($p = 0$) background is the one tiled by $\begin{pmatrix} 0 & 3 \\ 1 & 2 \end{pmatrix}$, the same as that for case (i).

Now let us consider the effect of a single point perturbation, using the Friedrich-Levine procedure. Fig 4.11 shows the $\mathcal{L} u_0$ calculated when a single defect unit cell is placed in each of the four patches. In the top and left patches there are two pairs of hill-hole pairs created, while in the right and bottom patches there is no effect. In the patch on the left the vertical hill-hole pair, which was also present in the case (i) pattern, has only a local effect. Similarly, the horizontal hill-hole pair has only a local effect in the top patch. However, the vertical hill-hole pair in the top patch creates a lightcone, just like in case (i). The horizontal hill-hole pair creates a lightcone in the left patch. Following some local reverse-cycle-popping, we get the pattern in fig 4.12 (a).

The effect of multiple defect sites is mostly the same as for case (i): the lightcones merge to form terraces, or are nested, and the height function can be defined correspondingly (see fig 4.12 (b)).

However, the type (i) rule that a point perturbation falling on an existing defect line has no effect, is no longer valid. Let us now consider the case where a perturbed unit cell falls on a defect line. The heuristic argument given in the previous section, which implied

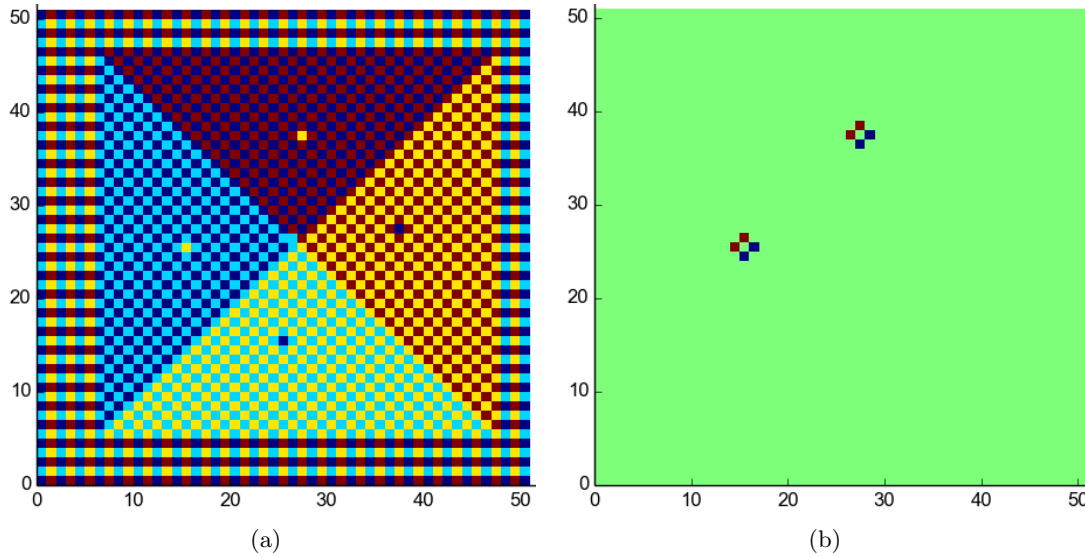


Figure 4.11: (a) The initial approximation to the final arrow configuration for type (ii). The differently colored cells in the four patches are where the arrow is flipped from the periodic background. Colour code: dark blue - \rightarrow , light blue - \uparrow , yellow - \leftarrow , red - \downarrow (b) $\mathcal{L} u_0(i, j)$ for the initial approximate visit function $u_0(i, j)$. Color code: red = 1, blue = -1, green = 0.

that such a perturbation has no effect, relied on the fact that the defect lines locally look like the neighbouring patches of the affected patch, and that the perturbation had no effect in these patches. In the present case too, the defect lines which comprise a lightcone are made of the unit cells which tile the patches on either side of the affected patch. However, in this case the perturbation does create lightcones in one of the neighbouring patches of the affected patches.

The effect of a perturbed unit cell lying on such an arm of the lightcone, as shown in figure 4.12 (b), is (i) to create another lightcone with its vertex at the position of this site, and (ii) this new lightcone displaces the previous position of the arm of the lightcone by two units. One arm of the new lightcone is adjacent to the displaced defect line, creating a defect line of width four. For lightcones created in the adjacent patch, the same effect is seen on the *other* arm.

Now consider a defect line of width $2n$, created by the adjacent arms of many such defect lines. Because the individual defect lines are made of the unit cells which tile the adjacent patch, this line looks like a stripe of the adjacent patch inside this one. We now investigate the effect of a perturbed unit cell being present inside this line. Figs 4.13 (a) and (b) shows two cases: one where the perturbation is at a point along the inside edge of the line, and the second when it is not. In the first case, as for a single defect line, the whole line is displaced two units to the right, and a new lightcone is created. In the

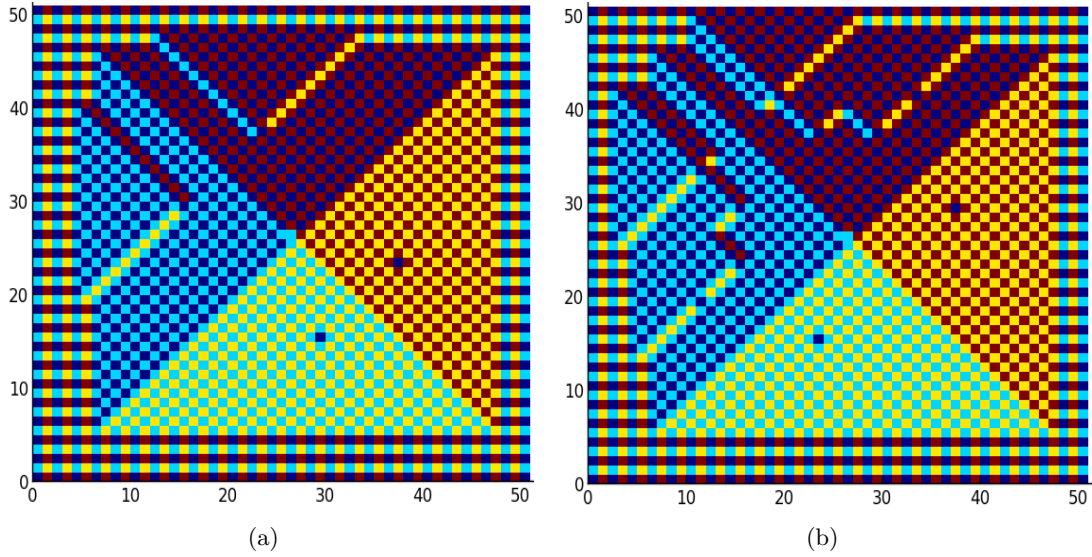


Figure 4.12: (a) The final pattern after the Friedrich-Levine procedure, which shows the effect of single type (i) perturbations in all four patches. (b) Generation of terraces by intersecting lightcones, and the additional lightcones generated by perturbations present on the defect line. Colour code: dark blue - \rightarrow , light blue - \uparrow , yellow - \leftarrow , red - \downarrow

second case, the perturbed unit cell acts effectively like it is in the adjacent patch, and creates a lightcone like the one in the adjacent patch. The effect of this is clear from fig 4.13 (b).

Thus we have determined the rules for how the lightcones are drawn for a given configuration of defects, for case (ii). Now we describe how the lightcones affect the visit function.

4.4.2 Lines of constant visit function

The visit function contours in the current case are shown in figure 4.14. The orientation of the contour in a region of the pattern depends on the local structure of the region: the contours are vertical in regions which are made of unit cells which tile the (unperturbed) left and right patches, and horizontal in regions which are made of unit cells which tile the top and bottom patches. The contours rotate by 90° when crossing the boundary between two kinds of regions. Thus, the rule for drawing contours is to rotate the contours by 90° when crossing the boundary from one kind of region to another, mirroring the way contours change when crossing between patches in fig. 4.9. This works even when, as in this case, there are ‘nested’ lightcones of another orientation within defect lines of the first type. We can imagine the successive contours to be the time-evolution of a growing closed surface, which started at the origin.

In a region around the boundary between the two patches which have lightcones, this sort of nesting eventually leads to a steady-state where a small region can locally look like

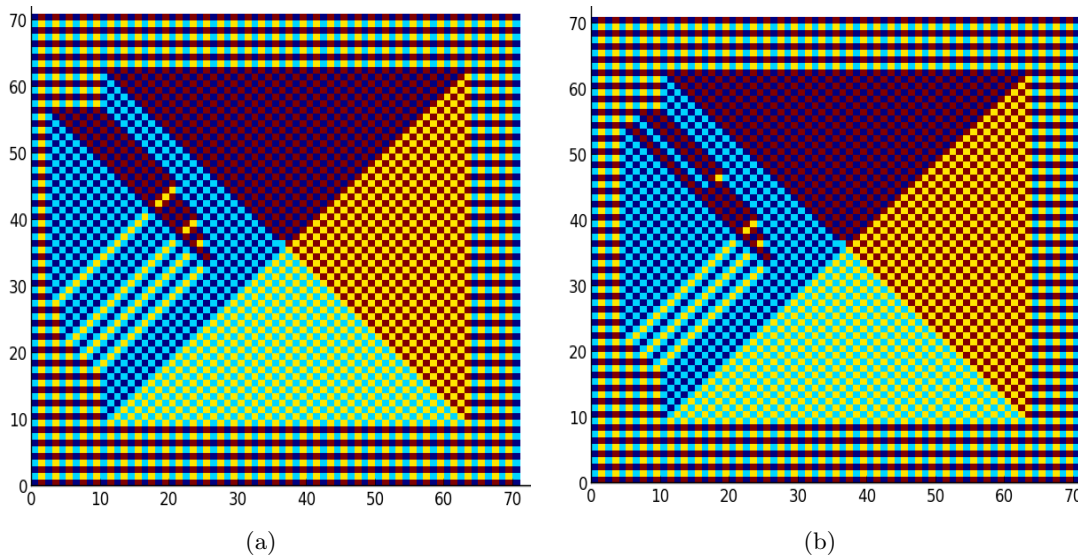


Figure 4.13: A cluster of defect lines, and an additional perturbed unit cell present (a) On the inner edge of the cluster, and (b) Inside the cluster. In the latter case the region acts just like the adjacent patch. Colour code: dark blue - \rightarrow , light blue - \uparrow , yellow - \leftarrow , red - \downarrow

either of the two patches with equal probability. (That this is the steady-state is easy to see since a noise point in a region of either type creates a defect line which looks like the other type.) The width of this region around the 45° boundary between the patches grows with the distance from the origin at least as fast as the width of the region in the previous section which looked like the adjacent patch, that is, at rate p (see paragraph following eqn. (4.4).

In this region, although there is an overall rate of increase of the visit function as one moves away from the origin, the fluctuations around this rate, we believe, are equally likely to be positive or negative. This is based on the observation that these fluctuations in $V(x, y)$ in this region follows Edwards-Wilkinson rather than KPZ scaling. Recalling the universality classes of growing contours discussed in Chapter 1, we see that when fluctuations about the average growth are as likely to be positive as negative, they fall in the Edwards-Wilkinson rather than the Kardar-Parisi-Zhang universality class, and will scale as $L^{1/4}$ where L is the distance from the origin. Fig 4.15 shows a schematic drawing of the pattern near p_c . The visit function in region A is expected to show EW fluctuations, while in regions B and C we expect KPZ fluctuations.

4.4.3 Transition from recurrence to transience

With the type (ii) background, a transition from recurrence to transience happens at a finite p . When the background becomes transient, the analysis performed in the previous subsection does not apply, and properties of the path the walker takes from the origin to infinity are not known.

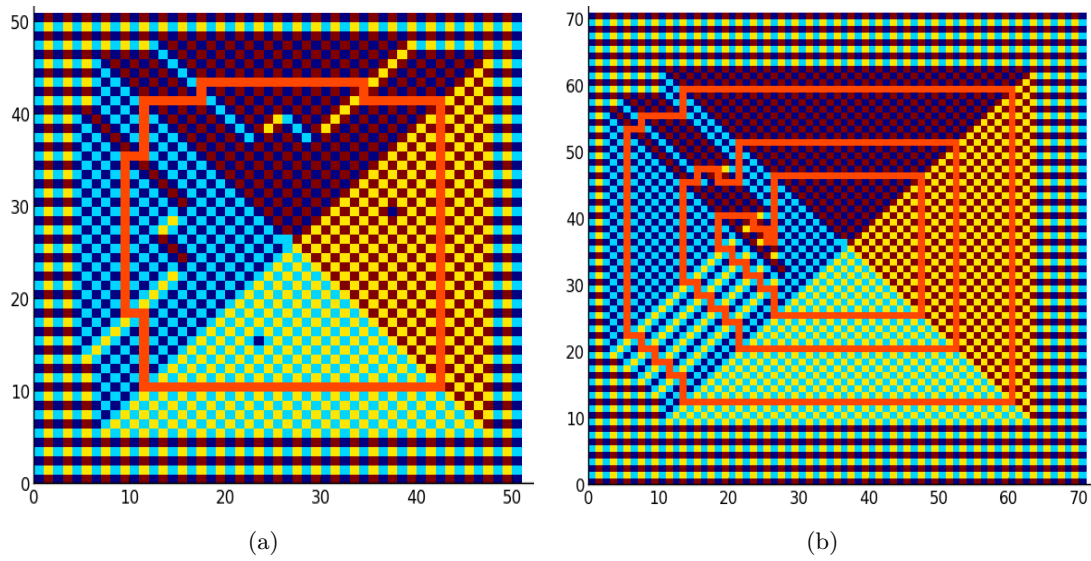


Figure 4.14: Contours of constant visit function for type (ii) perturbations. Note that in this case they cannot be described as a surface without overhangs. Colour code: dark blue - \rightarrow , light blue - \uparrow , yellow - \leftarrow , red - \downarrow .

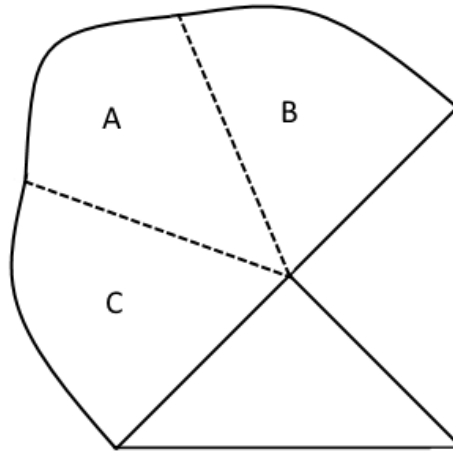


Figure 4.15: Schematic drawing of the pattern for p slightly below the transition. In region A, the height function is expected to show Edwards-Wilkinson fluctuations, while in regions B and C we expect KPZ fluctuations.

In fig. 4.16 we plot the number of visits to the origin, N_O , as a function of p , for various lattice sizes.

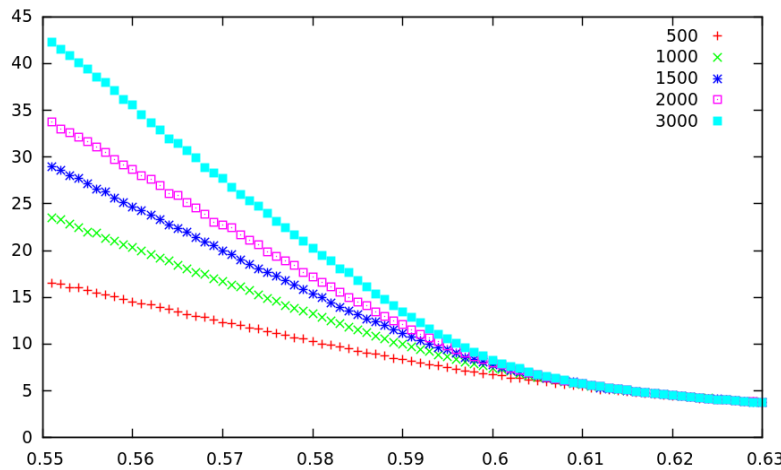


Figure 4.16: Number of visits to origin vs. p for type (ii) backgrounds, for various lattice sizes. Below $p \approx 0.61$, this quantity scales with the lattice size, whereas above this value of p it does not. This indicates a transition from recurrence to transience.

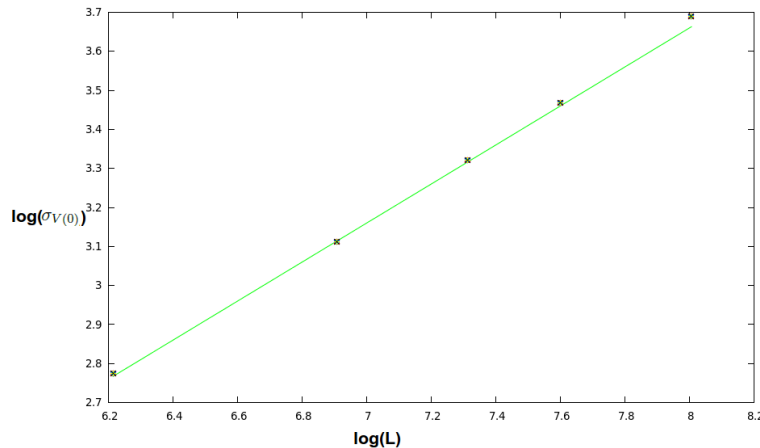


Figure 4.17: A log-log plot of the variance of the number of visits to the origin, at $p = 0.55$, versus lattice size L . The solid line is of slope 0.5.

From the figures one sees that the longest extent of the pattern is along the line $x + y = 0$. To avoid anisotropy effects, we simulate not on an $L \times L$ square lattice, but stop the walker when it reaches a site with $x^2 + y^2 > L^2/4$. As in the previous section, keeping L fixed, we measure the variation of the number of visits to the origin $V(0)$ with the disorder p . Fig 4.16 shows the results: As the lattice size increases, for recurrent backgrounds, the number of visits to the origins increases proportionately to the lattice size, $N_O = n(p)L$. However, for transient backgrounds once the walker leaves a finite region near the origin it does not visit it again. The size of this region might be different for different backgrounds, and might be a function of p . However, this means that N_O does not scale with L , except for finite-size effects. From the figure it can be seen that the transition from recurrence ($V(0)/L$ finite)

to transience ($V(0)/L \rightarrow 0$ as $L \rightarrow \infty$) happens at $p_c \approx 0.61$.

One can also measure the the fluctuations in the number of visits to the origin, $\langle V(0)^2 \rangle - \langle V(0) \rangle^2$, and study the scaling of this quantity with L . Suppose the mean rate of decrease of the visit function along the 45° boundary between patches is M . Then, according to the above considerations,

$$V(-x, y) = V(0) - \sqrt{2}My + y^{1/4}B(p)\xi \quad (4.8)$$

where ξ is a random variable with zero mean and unit variance, and $B(y)$ is some function of p . Hence, setting $V(-L/\sqrt{2}, L/\sqrt{2}) = 0$, we get that $V(0)$ has a mean which scales as L , and a variance that scales as $L^{1/4}$. We measured this variance numerically, and the measured scaling with lattice size is shown in fig 4.17 for $p = 0.55$. It is seen that the exponent is quite close to $1/2$, which confirms that the rms fluctuations scale as $L^{0.25}$, and belong to the Edwards-Wilkinson class rather than the KPZ class.

4.5 Conclusions

In this chapter we studied the growth of patterns formed by rotor-router walkers on two noisy backgrounds. We showed that in one case the visit function of the pattern can be mapped to the height function in a model of Bernoulli Matchings, which shows KPZ fluctuations and where the exact distribution of the fluctuations follows a Tracy-Widom law. In the second case we showed that part of the boundary of the pattern shows not KPZ but EW fluctuations.

The class of models which map to growing discrete PNG interfaces has been studied quite a lot in recent years, as was discussed in chapter 1. Among these models are the Totally Asymmetric Exclusion Process, Directed Polymers at zero temperature with uncorrelated noise, etc. These models are special cases of more general models, namely the Partially Asymmetric Exclusion Process and Directed Polymers at zero Temperature with short-range correlated noise, etc. In these general cases, although the mapping cannot be carried out exactly, the general property of KPZ fluctuations and also that of their distribution being Tracy-Widom is expected to hold. This is based on the fact that the coarse-grained equation for these models is the KPZ equation (see chapter 1) and this has recently been exactly solved [9] and found to give a Tracy-Widom distribution for the height fluctuations.

In the same manner, we expect that the Tracy-Widom distribution is a generic feature of rotor-router patterns growing on noisy backgrounds - earlier studies have found that the fluctuations on a totally random background grow as KPZ, although the distribution of fluctuations has not been measured. However, further studies need to be done to confirm the conjecture of Tracy-Widom universality in cases other than the ones studied here. EW

fluctuations also seem to play a part in some cases. The existence of other backgrounds showing both KPZ and EW fluctuations in different regions is an open question.

Bibliography

- [1] T. Friedrich and L. Levine, Fast simulation of large-scale growth models, *Random Structures & Algorithms* **42** 185 (2013)
arxiv:1006.1003
- [2] A. Z. Broder, Generating random spanning trees, *Foundations of Computer Science* 442 (1989).
- [3] A. M. Povolotsky, V. B. Priezzhev, and R. R. Scherbakov, *Phys. Rev. E*, **58** 5449 (1998).
- [4] A. E. Holroyd, and J. Propp, *Algorithmic probability and combinatorics*, **520** 105 (2010)
- [5] S. N. Majumdar and S. Nechaev, *Phys. Rev. E* **72** 020901 (2005)
- [6] M. Prahofer and H. Spohn, *Phys. Rev. Lett* **84** 4882 (2000)
M. Prahofer and H. Spohn, *J. Stat. Phys.* **108** 1071 (2002)
- [7] K. Johansson, *Comm. Math. Phys.* **242** 277 (2003)
- [8] R. Rajesh and D. Dhar, *Phys. Rev. Lett.* **81** 1646 (1998)
- [9] T. Sasamoto and H. Spohn, *J. Stat. Mech.* P11013 (2010)

Chapter 5

A Class of Active-Absorbing Phase Transitions

In this chapter, we present the construction and analysis of a class of assisted-hopping models which show an active-absorbing phase transition in one dimension. The models are a generalization of the Conserved Lattice Gas (CLG) model defined in the introduction. The steady state for all the models in the class can be exactly determined and various quantities calculated easily with the help of generating functions. We show that, for the model where the particles have a hopping range n , for $n = 1, 2, 3, \dots$, the critical exponent $\beta = n$. The model with $n = 2$ was defined by da Silva and de Oliveira in [1]. The models with $n > 2$ define previously unknown universality classes for active-absorbing phase transitions.

Models with $\beta > 1$ are not typical in equilibrium or non-equilibrium problems. An important issue here is the correct identification of the order parameter. In the percolation problem, the fractional number of sites in the backbone [2], the bulk conductance in a random resistor network [3] or the rigidity modulus in a random spring network [4] could be considered as possible order parameters, but these are known to vanish with different powers than the fractional number of sites in the infinite cluster near the critical point. In the Bose glass-superfluid transition, the superfluid density at zero temperature grows more slowly than the density of the fluid which is the tuning parameter [5]. For the active-absorbing phase transitions we are interested in, this issue is presumably not so contentious, as there is a natural choice of order parameter, viz. the mean density of activity, which is the choice we use in this chapter to define β .

The plan of this chapter is as follows: In section 5.1 we define the generalized model. In section 5.2 we discuss structure of the configuration space for the models. In sections 5.3 and 5.4 we use the technique of generating functions to determine several properties and critical exponents of the models, with and without an external field conjugate to the activity. In section 5.5 we present a mapping to a gas of defects with height restriction, which makes it

easier to calculate certain properties of the models such as critical exponents. In section 5.6 we use this mapping to calculate the non-equilibrium relaxation exponents of the conserved lattice gas, starting from random and what are called ‘natural’ initial conditions. In two appendices we count the number of absorbing configurations which locally look like the steady-state, and show that the scaling of this quantity for large lattice sizes is related to the critical exponent β .

5.1 Definition of the model

The models that we study are defined on a line of L sites with N particles, with sites labelled $1, 2, \dots, L$. These are exclusion models, so at most one particle can occupy one site. A configuration on the lattice is denoted by a binary string $\dots 01001110010\dots$ where the symbol 1 denotes a particle and 0 denotes an empty site. We call a connected cluster of empty sites as a 0-cluster (of that length) and a connected cluster of occupied sites as a 1-cluster. A more compact notation for the binary string which denotes a configuration is of the form $0^{m_1}1^{n_1}0^{m_2}\dots$, with all $m_i, n_j \geq 1$ where 1^m denotes a 1-cluster of length m .

Particles evolve by continuous-time Markov dynamics, and the rate of a move depends on the local neighbourhood of the particle and the size of the jump. When particles move, they cannot hop over each other. Also, we assume ‘assisted-hopping’, that is, particles cannot move unless they are assisted (or ‘activated’) by another particle (in a way given by the transition rules defined precisely below). We define an infinite class of models parameterized by the integer n , which is a measure of the range within which particles can ‘assist’ other particles. The model with range n is defined by the following two types of hopping processes (see Fig. 5.1):

a) The first process is a particle hop of length at most n into the neighbouring 0-cluster, activated by a nearest neighbour occupied site. A hop of length i from a 1-cluster of length > 1 into a 0-cluster of length k takes place with rate $\Gamma_1(i, k)$, to the right or towards the left. This is represented by the processes for all $i \leq k$, and $m \geq 1$:

$$1^{m+1}0^k \xrightarrow{\Gamma_1(i,k)} 1^m0^i10^{k-i}, \quad (5.1)$$

$$0^k1^{m+1} \xrightarrow{\Gamma_1(i,k)} 0^{k-i}10^i1^m, \quad (5.2)$$

For $i < k$, this leads to break-up of a 0-cluster of length k into clusters of length i and $k - i$. We assume that for all $k > n$, there is at least one $i < k$ for which $\Gamma_1(i, k)$ is non-zero. For $k \leq n$, we assume that all $\Gamma_1(i, k)$ are non-zero. Thus all 0-clusters of length > 1 are susceptible to break-up into smaller clusters.

b) The second process is the coalescence of 0-clusters separated by a single particle, only

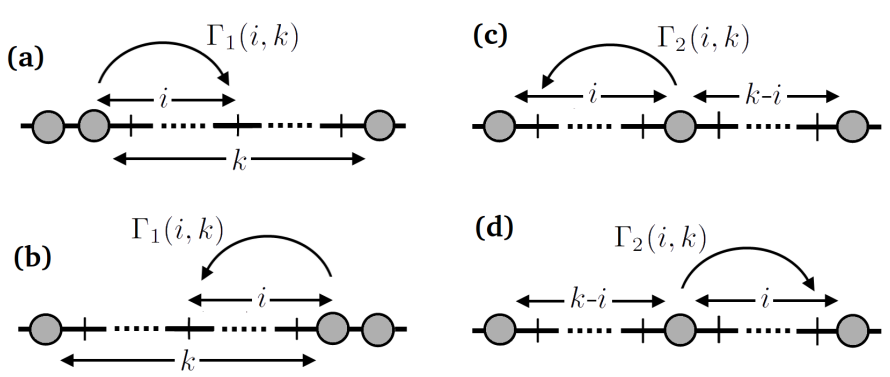


Figure 5.1: The hopping rates for the model with range n . In (a) and (b), a particle activated by an occupied nearest neighbour site jumps a distance i at most $\min(n, k)$ into a neighbouring cluster of empty sites which has length k . The reverse transitions are shown in (c) and (d) respectively and have non-vanishing rates only for $k \leq n$.

when the resulting cluster has total length $\leq n$. An isolated particle between two 0-clusters of length i and i' can jump either to the nearest 1 on the left or to the nearest 1 on the right, with rates $\Gamma_2(i, i + i')$ and $\Gamma_2(i', i + i')$ respectively. This leads to joining of the 0-clusters into a single cluster of length $i + i'$, and is represented by the processes : For all $m, m' \geq 1$, and all i, i' , with $i + i' \leq n$

$$1^m 0^i 1 0^{i'} 1^{m'} \xrightarrow{\Gamma_2(i, i+i')} 1^{m+1} 0^{i+i'} 1^{m'}, \quad (5.3)$$

$$1^m 0^i 1 0^{i'} 1^{m'} \xrightarrow{\Gamma_2(i', i+i')} 1^m 0^{i+i'} 1^{m'+1}, \quad (5.4)$$

All hopping rates $\Gamma_2(i, k)$ are assumed non-zero for all $i \leq k \leq n$, and $\Gamma_2(i, k) = 0$ if $k > n$. That is, the resulting 0-cluster after the particle hop can only be of length $\leq n$. Hence, 0-clusters of length $> n$, in the model with range n , are not reconstructed by the dynamics, and their number steadily decreases. If the system reaches an active steady-state, the steady-state sector only has configurations with 0-clusters of length $\leq n$.

In this sector, since all Γ_1 and Γ_2 rates are non-zero when the second argument is $\leq n$, all transitions are reversible. For simplicity, we set

$$\Gamma_1(i, k) = \Gamma_2(i, k) \text{ for all } 1 \leq i \leq k \leq n \quad (5.5)$$

5.2 Phase Space Picture

It is straightforward to determine some properties of the models, such as the transition density and the structure of the phase space, simply by looking at the possible configurations at a given density.

For the model with range n , as already noted above, the break-up of 0-clusters of length $> n$ due to processes Γ_1 is irreversible, but the break-up of 0-clusters of length $\leq n$ is reversible due to the processes Γ_2 . Thus the number of clusters of length $> n$ decreases monotonically with time (see Figs. 5.2 and 5.3). Configurations with 0-clusters of length $> n$ are thus either transient or absorbing, and cannot be part of an active steady-state if it exists. For $\rho \leq 1/(n+1)$, there are no configurations with all 0-clusters of length $\leq n$, and the system always ends up in an absorbing state after passing through a series of transient configurations. The number of absorbing configurations increases exponentially with the size of the system. For $\rho > 1/(n+1)$, eventually, all 0-clusters that remain are of length $\leq n$. These keep on breaking up, and reforming, as the particles hop, but always remain of length $\leq n$. For an example, see Fig. 5.4. Thus the critical density for the model with range n is $\rho_c = 1/(n+1)$.

For models with range $n > 2$, there also exist absorbing states for densities above ρ_c . For example, consider the configuration $10^{r_1}10^{r_2}10^{r_3}1\dots$, where r_i are any integers with $r_i + r_{i+1} \geq n+1$, for all i . Here, clearly, all 1's are immobile, and the maximum possible density possible in such a configuration is $\rho_{abs}^{max} = 2/(n+3)$. (This corresponds to the state with $r_1 = r_3 = \dots = \lfloor (n+1)/2 \rfloor$ and $r_2 = r_4 = \dots = \lceil (n+1)/2 \rceil$). The structure of the configuration space for these models is shown in Fig. 5.2. The number of absorbing configurations at a particular density grows exponentially with L for all $\rho < \rho_{abs}^{max}$.

The case $n = 1$ is the CLG model, discussed in Chapter 2. Here the only allowed transitions are $110 \rightarrow 101$ and $011 \rightarrow 101$, both occurring at equal rates. Here $\rho_c = \frac{1}{2}$. The steady-state consists of clusters of 1s separated by single 0s (e.g. $011011110110\dots$). The case $n = 2$ has been studied as Model 3 in [1]. In this case $\rho_c = \frac{1}{3}$, but there exist absorbing states up to density $\rho = 2/5$ e.g. the absorbing state with maximum density, $1001010010\dots$. The phase space for $n = 2$ is illustrated in fig. 5.2, along with some examples of configurations. As shown in the figure, one can arrange the configurations to form a ladder of states. We define the height of a state on this ladder as the number of 'extra' 0s in the configuration, that is, the sum $\sum_{i>n} (i-n)C_i$ where C_i is the number of 0-clusters with length $i > n$ in a given configuration. (This corresponds to the number of 'anti-defects' in the corresponding defect configuration, see section 5.5.) The evolution only keeps the system on the same level or takes it down the ladder. Also present in the configuration space are absorbing states at all heights, for $\rho < 2/5$. The lowest rung on the ladder is the steady-state sector. The structure of the configuration space is similar for all models with $n > 1$.

During evolution, the system might fall into an absorbing state before reaching the lowest rung of the ladder, ie, the steady-state. Simulations of the model with $n = 2$, at density

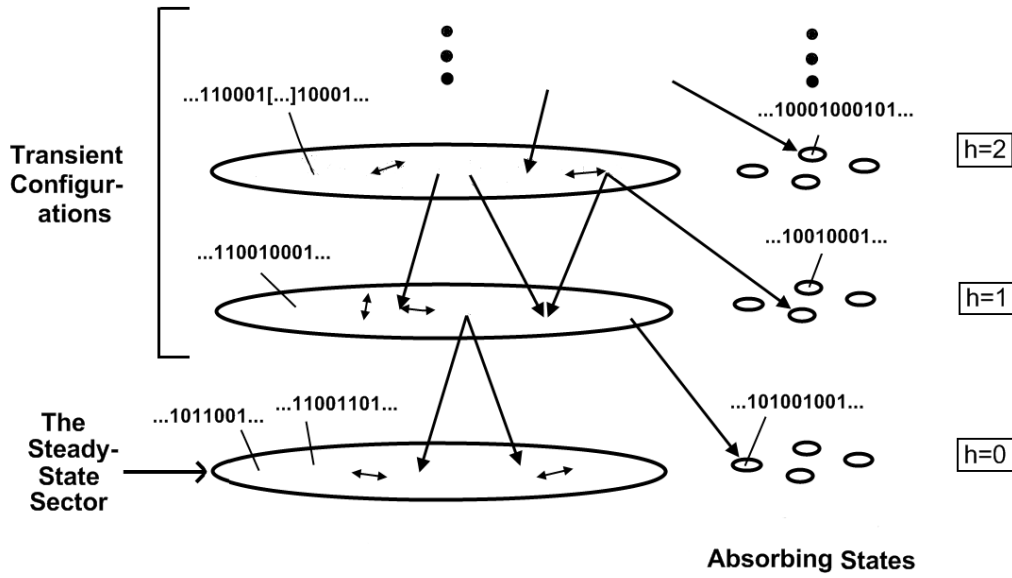


Figure 5.2: The structure of the configuration space for models with $n > 1$, for densities $\frac{1}{n+1} < \rho < \frac{2}{n+3}$. The small ellipses denote individual absorbing states. The height h is defined as $\sum_{i>n} (i-n)C_i$ where C_i is the number of 0-clusters with length $i > n$ in a given configuration (in the language of section 5.5, this is the number of ‘anti-defects’ in the configuration). The transitions within each h sector are reversible, but transitions between h -sectors only go down in h . For $\rho < \frac{1}{n+1}$, there is no steady-state, while for $\rho > \frac{2}{n+3}$, there are no absorbing states. Examples of representative strings which are part of configurations in each sector are shown for the model with $n = 2$.

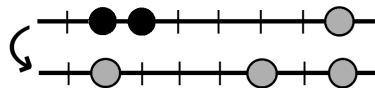


Figure 5.3: An irreversible transition in the $n = 3$ model which decreases the activity, where grey circles denote inactive particles and black circles denote active (movable) particles

$\rho = 0.38$, give the probability of a random initial configuration falling into an absorbing configuration for lattice sizes $L = 50, 100, 150$ and 200 as $6.9 \times 10^{-3}, 1.4 \times 10^{-4}, 1 \times 10^{-5}$ and 2×10^{-7} respectively. This is numerical evidence that, above ρ_c , the probability that a random initial configuration at a given density ends up in an absorbing state goes to zero in the thermodynamic limit.

Now we prove that the steady-state sector is ergodic. Consider a configuration with density ρ , with $\rho_c \leq \rho \leq \rho_{abs}^{max}$, which has at least one mobile particle. As the particle moves, it may give rise to a configuration in which all particles are immobile. In such a case the previous configuration would have had a longer 0-cluster of length $> n$. Such a configuration would be a transient configuration. The other case is when there are no 0-clusters of length $> n$. In such a configuration, for all allowed hoppings, the reverse

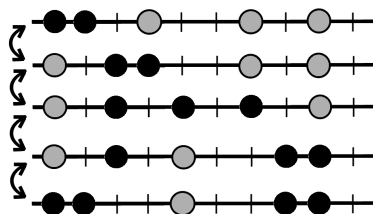


Figure 5.4: A sequence of reversible transitions in the $n = 2$ model which (top to bottom) lead to activation of an inactive particle; grey circles denote inactive particles and black circles denote active (movable) particles

move is also allowed. Also, from any such active configuration C we can go to a standard configuration C_0 , in which the number of 0-clusters is the least possible (i.e. $\lceil (L - N)/n \rceil$), and they occur as far to the right as possible. Then, since in this subset of configurations all moves are reversible, we can go from any configuration to any other, the active steady state is unique. Since all transition rates are unity, all steady-state configurations, given N and L have equal weight in the steady-state.

5.3 Counting steady-state configurations using generating functions

In the steady-state, all configurations with N particles on L sites with no 0-clusters of length $> n$, and having at least one mobile particle, are present with equal probability. Let $C(N, L)$ is the number of such configurations with N particles on an open line of L sites, that start with a 1. We define

$$C_L(x) = \sum_{N=1}^L C(N, L)x^N \quad \text{and} \quad (5.6)$$

$$C(x, y) = \sum_{L=1}^{\infty} C_L(x)y^L \quad (5.7)$$

For the purposes of easy counting, we include in this sum absorbing configurations that however satisfy the steady-state constraint that all 0-clusters are of length $\leq n$. We call these the ‘near-steady-state absorbing configurations’, and appendix I shows that they do not affect the counting in the thermodynamic limit. The counting now follows similar steps as that done for the Conserved Lattice Gas in Chapter 2. Then the set of all configurations we wish to count is generated by the strings 1, 10, 100, ..., 10^n , and hence

$$C(x, y) \approx (1 - (xy + xy^2 + \dots + xy^n))^{-1} - 1 \quad (5.8)$$

$$= \left(1 - xy \frac{1 - y^{n+1}}{1 - y}\right)^{-1} - 1 \quad (5.9)$$

Define $\Lambda = 1/y$. Expanding $C(x, y)$ in partial fractions, and then expanding the various terms in $1/y$ for fixed x , we get $C_L(x) \sim \sum_i c_i \Lambda_i(x)^L$, where the $\Lambda_i(x)$ are the $n + 1$ roots of the equation,

$$\Lambda^{n+1} = x \frac{1 - \Lambda^{n+1}}{1 - \Lambda} \quad (5.10)$$

and the c_i are constants fixed by evaluating C_L for the first few L s. Note that this implies all roots $\Lambda_i = 0$ when $x = 0$.

For large L , $C_L(x) \sim \Lambda_+(x)^L$, where Λ_+ is the largest root. For x tending to 0, the largest root may be evaluated to be

$$\Lambda_+(x) = x^{1/(n+1)} \left(1 + \frac{1}{1+n} x^{1/(n+1)} + \dots \right) \quad (5.11)$$

We expand about $x = 0$ because as $x \rightarrow 0$, $\Lambda_+ \rightarrow 0$, and we shall see below that this implies $\rho \rightarrow 0^+$. Hence this is the right limit to take to get near-critical properties. The limit $x \rightarrow 0$ could also be seen as minimising the fugacity of particles, and giving the steady-state configuration with the least number of particles for a given L , that is, $L/(n + 1)$. Using $\rho = x \frac{d}{dx} \log \Lambda(x)$, we get

$$\frac{1}{\rho} = (n + 1) - \frac{\Lambda}{1 - \Lambda} + \frac{(n + 1)\Lambda^{n+1}}{1 - \Lambda^{n+1}} \quad (5.12)$$

this gives, near $x = 0$,

$$\rho = \frac{1}{n + 1} \left(1 + \frac{1}{1+n} x^{1/(n+1)} + \dots \right) \quad (5.13)$$

We can also determine the second largest root of Eq.(5.10). This gives

$$\Lambda_-(x) = \omega x^{1/(n+1)} \left(1 + \omega \frac{1}{1+n} x^{1/(n+1)} + \dots \right) \quad (5.14)$$

where ω is the $(n + 1)^{th}$ root of unity closest to $z = 1$. To determine the particle-particle correlation length of the system, we need the two largest eigenvalues of the transfer matrix which generates configurations of the system. It can be shown that the roots of equation 5.10 correspond to eigenvalues of this transfer matrix (see Appendix I of chapter 2). Hence, the particle-particle correlation length is given by

$$\begin{aligned} \xi^{-1}(x) &= \log \left| \frac{\Lambda_+(x)}{\Lambda_-(x)} \right| \\ &\sim x^{1/(n+1)} \end{aligned} \quad (5.15)$$

Denoting $\rho - \rho_c$ by ϵ , we see that $\epsilon \sim x^{1/(n+1)} \sim 1/\xi$. The correlation length exponent

ν is defined by the equation $\xi \sim \epsilon^{-\nu}$. This gives us, for all n , $\nu = 1$.

The reason for the appearance of $x^{1/(n+1)}$ in the above equations is not immediately obvious. In section 5.5, we present a mapping to a gas of defects and anti-defects, which makes it so. However, first we introduce the concept of a transience field, which is a field conjugate to the activity, and allows us to determine the one remaining static critical exponent, the exponent for the response to an external field, δ .

The order parameter for the transition is the activity density in the steady-state, that is, the density of movable particles, as a function of ρ . There are two types of movable particles in the steady-state, ones on the boundary of active *clusters*, ie, particle clusters of length > 1 , and the other being *isolated active particles* in between two 0-clusters with total length $\leq n$. Within the generating function formalism, it is easiest to calculate the density of active clusters by adding a weight factor α to all 1-clusters of length > 1 . (The density of isolated active particles is proportional to the density of active clusters, as is shown in appendix II.)

We do this by writing down a generating function of the form

$$C(x, y, h) = \sum_{L, N, a} C(L, N, a) x^N y^L e^{ha} \quad (5.16)$$

where $C(N, L, a)$ counts the number of configurations on a line of L sites with N particles and a active 1-clusters. The activity density in the steady-state is then given by $\rho_a = \frac{d}{dh} C(x, y, h)|_{h=0}$. The fugacity of active clusters e^h can also be thought of as the result of a field h which increases the activity; we shall explore this viewpoint in the next section.

To get the generating function $C(x, y, h)$, we need to write down the appropriate set of generating strings. In the previous set of generating strings, namely $1, 10, \dots, 10^n$, there is no control on the generation of 1-clusters, which is done whenever the string ‘1’ comes before any of the other strings, or itself. To separate the active clusters from the rest, first we generate active clusters using the strings 1 and 10 , giving the generating function $xy^2 + \frac{e^h x^2 y^3}{1-xy}$ - notationally, $10 + 110 + 1110 + \dots$, where the terms from the second on have weight e^h . Now to the 1-cluster-plus-0 generated by this procedure, we attach at most $n-1$ more zeros, to get the set of all generating strings. Thus the set of generating strings for the model with $n=2$, for instance, is $10, 100, 110, 1100, 1110, 11100, \dots$, where the first two come with unit weight and the rest with weight e^h . Hence we can write the generating function as

$$C(x, y, h) = \left(1 - xy^2 \left(\frac{1 - y^{n+1}}{1 - y} \right) \left(1 + \frac{xye^h}{1 - xy} \right) \right)^{-1} - 1 \quad (5.17)$$

Using $\rho_a = \frac{d}{dh}C(x, y, h)|_{h=0}$, we get

$$\rho_a(\Lambda) = \frac{x^2}{\Lambda^{n+2}} \frac{1 - \Lambda^n}{(n+1)(1-\Lambda) + x(n+1) - \Lambda} \quad (5.18)$$

$$= \frac{\Lambda^n}{1 - \Lambda^{n+1}} \frac{(1 - \Lambda^n)(1 - \Lambda)^2}{(n+1)(1-\Lambda) - \Lambda} \quad (5.19)$$

Near $x = 0$, this gives $\rho_a \approx \frac{1}{n+1}\Lambda^n$. Using this and eqn. (5.12),

$$\rho_a \sim (\rho - \rho_c)^n \quad (5.20)$$

giving $\beta = n$.

5.4 Activity and Transience fields

We define as a field a modification of the transition rates that increases the expectation value of a given quantity in the steady-state. We then say that the field couples to the quantity. In this section, we introduce two types of fields, where one which couples to the activity and another which allows evolution back up the transient ladder (it can be said to couple to the density of forbidden 0-clusters). We find that the steady-state with the field can also be determined exactly, and this allows us to determine the field critical exponent δ , defined as $\rho_a|_{\rho=\rho_c} \sim h^{1/\delta}$. Another advantage of having fields with non-trivial effects which can be exactly determined is that this allows one to control the initial conditions precisely in simulations to study the time-dependent relaxation of the system.

We know that the transient states of the model with $\beta = n$ are the ones which have 0-clusters of length $> n$. We have already set $\Gamma_1(i, k) = \Gamma_2(i, k)$ for $k \leq n$, but have so far said nothing about $\Gamma_1(i, k)$ for $k > n$ except that $\Gamma(1, k)$ is non-zero for all k , so that all 0-clusters are susceptible to breaking up. Now we specialise to the case $\Gamma(i, k) = 0$ for all $i \neq 1$, so that when the length of the 0-cluster is $> n$, the only activated hop into the cluster possible is of range 1. Thus, the model we start with in this section is given by the following allowed transitions

$$1^{m+1}0^k \rightarrow 1^m010^{k-1} \text{ for } k > n \text{ and } m \geq 1 \quad (5.21)$$

$$10^i10^{k-i}1 \rightleftharpoons 110^k1 \text{ for } k \leq n \text{ and } i \leq k \quad (5.22)$$

$$10^{k-i}10^i1 \rightleftharpoons 10^k11 \text{ for } k \leq n \text{ and } i \leq k \quad (5.23)$$

where all rates are unity.

5.4.1 Activity field

First we introduce a field which couples to the activity. Let C_1 and C_2 be two configurations within the active steady-state which are reversibly connected by eqns. (5.21-5.23). Then the field h introduces the following additional transitions are connected by the additional transitions (where $A(C)$ is the number of active clusters in configuration C)

$$C_1 \xrightarrow{h} C_2 \text{ if } A(C_1) < A(C_2) \quad (5.24)$$

$$C_1 \xrightleftharpoons[h]{} C_2 \text{ if } A(C_1) = A(C_2) \quad (5.25)$$

This is interpreted as follows. In the active steady-state, the rates of transitions which do not decrease the cluster activity are increased by an amount h . We assume that the weight of a configuration factorises into the weights of its 1-clusters and 0-clusters, $W(C) = \prod_{1\text{-clusters}} W^1(k) \prod_{0\text{-clusters}} W^0(m)$, where $W^1(k)$ is the probability of a cluster of n 1's and similarly for $W^0(m)$, and the product is over all the 1-clusters and 0-clusters present in the configuration C .

The transitions which reduce the cluster activity are ones which look like $01101^m0 \rightarrow 0101^{m+1}0$ with $m > 1$, or like $0110^n \rightarrow 010^i10^{n-i}$. That is, transitions in which a particle hops away from a 1-cluster of the form 11 , into either a cluster of 0s or a cluster of 1s which is already active. Then, assuming $W^1(1) = 1$, $W^0(m) = 1$ for $m \leq n$, and $W^0(m) = 0$ for $m > n$, we find that the remaining weights are given by

$$W^1(k) = (1 + h) \text{ for } k > 1 \quad (5.26)$$

Note that the steady-state *sector* is still the same: only the weights of different configurations in it have changed. Thus, each active cluster gets a weight $(1 + h)$ and the weight of a configuration is $(1 + h)^a$ where a is the number of active clusters in the configuration. These are exactly the weights assumed in the previous section to calculate the cluster activity, except we set $h = 0$ at the end of the calculation. The generating function for the steady-state was already calculated as eqn. (5.17). We now see that $h \neq 0$ also makes sense as the steady-state of a system with the addition field h .

5.4.2 Transience field

Now we introduce another kind of field - one that takes the evolution back up the 'transience ladder' in fig 5.2, so that the steady-state sector when the field is non-zero expands to include all active configurations. Note that with the transition rates (5.21)-(5.23), the evolution down the transient ladder defined in section 4.2 is a single step down the ladder at a time. We now introduce a reverse hop with rate α and modify the eqns. (5.22) and (5.23) into

$$1^{m+1}0^k \xrightleftharpoons[\alpha]{} 1^m010^{k-1} \text{ for } k > n \text{ and } m \geq 1 \quad (5.27)$$

The new steady-state measure also contains configurations that are forbidden in the zero-field steady-state, namely configurations with 0-clusters of length $> n$. The weight of a configuration depends on their distance from the zero-field steady-state sector. We call α a ‘transience field’ because of this property. Now all non-absorbing configurations are present in the steady-state, but all configurations are not equally likely, their weights being dependent on their height on the transience ladder.

We again assume a product ansatz for the weights of configurations: $W(C) = \prod_{1\text{-clusters}} W^1(k) \prod_{0\text{-clusters}} W^0(m)$. Then detailed balance is obeyed when

$$W^1(k) = 1 \text{ for all } k \quad (5.28)$$

$$W^0(m) = 1 \text{ for } m < n \quad (5.29)$$

$$W^0(m) = \alpha^{m-n} \text{ for } m > n \quad (5.30)$$

That is, the weight of a configuration is proportional to α^d where d is its distance from the steady-state up the transient ladder.

The generating function for the model with range n in a transience field α is

$$C_\alpha(x, y) = \left(1 - xy \left(\frac{y - y^{n+1}}{1 - y} + \frac{\alpha y^{n+1}}{1 - y\alpha} \right) \right)^{-1} - 1 \quad (5.31)$$

For the field, ρ can be found from eqn. (5.12) and counting the cluster activity as in the previous section (eqn. (5.19)). For the transience field α , the exponent δ is defined by $\rho_a|_{\rho=\rho_c} \sim \alpha^\delta$. Evaluating the roots of denominator on the right hand side of the above equation, and setting $\rho = \rho_c$ gives the largest eigenvalue $\Lambda_{max} \sim \sqrt{\alpha}$ for all n . One can calculate ρ_a by assigning weights e^h to active clusters, as in the previous section. This gives $\rho_a \sim \Lambda^n$ at $\rho = \rho_c$. Thus we get $\rho_a \sim \alpha^{n/2}$, giving $\delta = \frac{n}{2}$ for the model with $\beta = n$.

There are several possible ways of introducing fields in models of active-absorbing phase transition with conserved particle number. Universality suggests that any field which climbs back up the transient ladder would give rise to the same δ . However, any field, like the activity field, which restricts itself to the steady-state sector would not be a good candidate for an external field, as it does not have any effect on the absorbing side of the transition, and hence at the critical point. In the context of the CLG, Lubeck ([6]) used as a field a random hopping process in which all particles hop at a rate a to one of their available neighbours. In the case of the models defined here, we see that this field can indeed take the evolution back up the transient ladder. This field changes the transition rates in eqn. 5.27 to

$$1^{m+1}0^k \xrightleftharpoons[a]{1+a} 1^m010^{k-1} \text{ for } k > n \text{ and } m \geq 1 \quad (5.32)$$

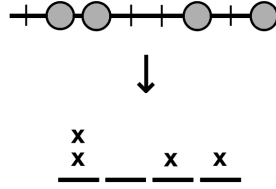


Figure 5.5: A configuration in the $n = 2$ model on a ring of $L = 8$ sites with $N = 4$ particles, and corresponding defect gas configuration with $N_d = 4$ defects on N sites

while all other transitions continue to have equal forward and backward rates. This is equivalent to an effective transience field $\alpha' = \frac{a}{1+a}$. Thus such a field would also give the same critical exponent $\delta = n/2$.

5.5 A Mapping to a Gas of Defects

Consider the model with range n . We consider as reference the inactive and periodic configuration at the transition density, $10^n 10^n 10^n \dots$. All steady-state configurations can be formed from this by adding particles (replacing some of the 0s with 1s) or by changing the lengths of the 0-clusters while maintaining the total number of 0s constant (also maintaining the constraint of not more than n consecutive 0's). A general steady-state configuration can be represented as $10^{s_1} 10^{s_2} 10^{s_3} \dots$ where s_i 's give the lengths of the 0-clusters. We write $r_i = n - s_i$. A 0-cluster of length $n - r_i$ will be said to have r_i defects. Here r_i can be negative, in which case, the cluster is said to have $s_i - n$ anti-defects. A defect is denoted by x , and an anti-defect by \bar{x} . Then a general configuration with N occupied sites can be represented by a gas of defects and anti-defects on N sites with r_i defects at site i . We will denote a configuration, say with $(r_1, r_2, r_3, \dots) = (2, 1, 0, -1, 3, \dots)$ as $1xx1x11\bar{x}1xxx\dots$, where the 1's are now considered as sites and the x 's are particles on the 1 to the left of them. (See Fig. 5.5.)

It is straightforward to translate the transition rules (1)-(4) into the rule for evolution of the corresponding defect configurations: two neighbouring sites can exchange defects at finite (given) rates if they have a total of $>n$ defects. Thus, under time evolution, $\{r_i\}$ evolve by groups of defects together jumping to a neighbouring site to the left or right. However, the r_i 's are always constrained to be $\leq n$. Anti-defects do not move. If a defect and anti-defect meet, they annihilate each other. For densities $\rho < \rho_c$, the final state has no mobile defects. For $\rho > \rho_c$, in any recurrent configuration with non-zero activity, there are no anti-defects left.

For a given N and L , all configurations in the steady-state are equally likely. The static properties in the *active* steady state can thus be calculated by considering the number of configurations $C_d(N_d, N)$ of a gas of nearly free defects, and no anti-defects. The only

constraint is that no site can have more than n defects. Adding one particle is equivalent to adding $(n + 1)$ defects. These defects unbind, and at low densities, form a nearly ideal gas. The fugacity associated with one defect is $x^{1/(n+1)}$, and forms a natural variable to describe properties of this gas.

Since all allowed configurations with a fixed number $N_d = (n+1)N - L$ defects on N sites are equally likely, we can define the generating function $C_d(w, z) = \sum_{N_d=0, N=1} C_d(N_d, N) w^{N_d} z^N$. It can be verified that $C_d(w, z) = C(x = zw^n, y = 1/w)$.

In terms of defects, the activity is the probability that two neighbouring sites have a total of $\geq n$, but strictly less than $2n$ defects. (If two neighbouring sites have $2n$ defects then the original configuration is 111, and hence the middle particle cannot move.) This probability can be calculated to give (using the fact that in the thermodynamic limit $w = 1/y = \Lambda_+$)

$$\rho_a = \rho \Lambda^n \frac{(n+1) - (n+2)\Lambda - \Lambda^n + 2\Lambda^{n+1}}{(1 - \Lambda^{n+1})^2} \quad (5.33)$$

Near the transition, since the gas of defects is nearly ideal, the probability of two neighbouring sites having a total of $\geq n$ defects varies as n -th power of density of defects, hence as ϵ^n . As the exponent β by the variation of the mean activity as a function of $(\rho - \rho_c)$, $\rho \sim (\rho - \rho_c)^\beta$, this immediately gives us that $\beta = n$.

5.6 Non-equilibrium exponents of the Conserved Lattice Gas

In this section we take the first step towards a description of the non-equilibrium dynamics of the models defined by equations (5.1)-(5.4), by analysing the evolution of the conserved lattice gas (our model with $n = 1$) starting from various initial conditions and deriving the non-equilibrium exponents θ and z defined in Chapter 2. The dynamics of the CLG has been studied earlier, and the analysis is non-trivial and the dynamical exponents seem to be initial-condition dependent. The non-equilibrium evolution of the CLG starting from random initial conditions was studied numerically by Lee and Lee in [7] and [8] through a finite-size-scaling analysis, and the study of the evolution from certain initial conditions closer to the steady-state was done by Bondyopadhyay [9], who found a different set of exponents. We explain this discrepancy by showing the existence of two scaling regimes, based on the initial conditions, with different consistent sets of exponents.

5.6.1 Steady-state exponents

Active-absorbing transitions, as mentioned in Chapter 2, are characterized by four steady-state exponents, defined by the scaling of the following quantities near the critical point, in

the steady-state:

$$\rho_a \sim (\rho - \rho_c)^\beta \quad (5.34)$$

$$\rho_a|_{\rho=\rho_c} \sim h^\delta \quad (5.35)$$

$$C(r, \rho) \sim f(r^{1/\nu_\perp}(\rho - \rho_c)) \quad (5.36)$$

$$C(t, \rho) \sim f(t^{-\nu_\parallel}(\rho - \rho_c)) \quad (5.37)$$

where $C(r, \rho)$ is the equal-time density-density correlation function, and $C(t, \rho)$ is the auto-correlation function for the density. We have already derived that for the CLG, $\beta = \nu_\perp = 1$ and $\delta = 1/2$. We now determine the behaviour of the autocorrelation function of the density.

We work close to the critical point $\rho = 1/2$, in the low-activity limit. Denote the density indicator variable at the site i by ν_i . The mapping to defects defined in the previous section maps the CLG to a symmetric exclusion process on N sites. Here we provide a slightly different mapping to an exclusion process on L sites, on the dual lattice. Denoting the occupation variable on the dual lattice site between sites i and $i + 1$ on the original lattice by $b_{i+\frac{1}{2}}$, the mapping is given by $b_{i+\frac{1}{2}} = \nu_i \nu_{i+1}$. We shall denote dual sites with $b = 0$ by an empty circle, \circ , and those with $b = 1$ by a filled circle, \bullet . The CLG configuration 101101011101 on the set of sites $0, 1, 2, \dots, 10, 11$ then corresponds to the dual lattice configuration $\circ \circ \bullet \circ \circ \circ \bullet \bullet \circ \circ$ on the sites $\frac{1}{2}, 1\frac{1}{2}, \dots, 9\frac{1}{2}, 10\frac{1}{2}$. Note that any two \bullet s are separated by an even number of \circ s. The transition $1101 \rightarrow 1011$ translates to a two-site hop $\bullet \circ \circ \rightarrow \circ \circ \bullet$.

We want to consider the density autocorrelation function $\langle \nu_i(0) \nu_i(t) \rangle$. This is equal to the probability $P(\nu_i(t) = 1 | \nu_i(0) = 1) \times P(\nu_i(0) = 1)$. Consider the transition (after two hops) $101011 \rightarrow 110101$, or in dual language, $\circ \circ \circ \circ \bullet \bullet \rightarrow \bullet \circ \circ \circ \circ$. Note that the parity of the sites 2 to 5 flipped from 0 to 1 or vice versa in this transition. The parity of site i thus stays the same after a time t if there have been an even number of hops $i - \frac{1}{2}$ to $i + \frac{1}{2}$ in that time (hops the other way are counted as negative). $P(\nu_i(t) = 1 | \nu_i(0) = 1)$ is simply equal to the probability that there have been an even number of flips from 1 to 0 or back, and is equal to the probability that there have been even number of hops across the bond on the dual lattice which corresponds to this site, in time t . The process on the dual lattice is an undirected exclusion process with a finite-range of hopping. It is known that, for a symmetric exclusion process with finite-range hops, the probability that there are a total of m hoppings across a given bond, in time t , is given for large times by [10]

$$P(m, t) \approx N \exp\left(-\frac{m^2}{A(\rho_d)\sqrt{t}}\right) \quad (5.38)$$

where $A(\rho_d)$ is a function of the density of the particles and N denotes the normalization constant. For low densities $\rho_d \ll 1$, $A(\rho_d) \approx C\rho_d$ where C is a constant that depends on the model. This can be seen by taking the continuum limit for low density, where we imagine

the particles to be point particles in a continuum. Then the particles perform independent random walks with a diffusion constant which depends on the model, with the exclusion interaction corresponding only to an exchange of particle labels when two random walkers cross. The number of walkers on the right of the origin which end up on the left after time t can then be shown to be a Poisson random variable with parameter $\lambda = \rho\sqrt{Dt/\pi}$ [11], and the same for the walkers on the left of the origin which end up on the right. The difference between these Poisson distributions then gives eqn. (5.38) with $A(\rho_d) \approx 2\rho\sqrt{D/\pi}$ for small ρ .

The sum over all m can be expressed in terms of Jacobi theta functions as $N \vartheta(0; i a(\rho_d, t))$, where $a(\rho_d, t) = 1/A(\rho_d)\sqrt{t}$. Setting this sum to 1 gives $N = (\vartheta(0; i a(\rho_d, t)))^{-1}$. The difference between the even and odd sums is $\vartheta(\frac{1}{2}; i a(\rho_d, t))$. Expanding these in MathematicaTM for small $a(\rho_d, t)$ (large times), we get the final answer

$$P(\nu_i(t) = 1 | \nu_i(0) = 1) \approx \frac{1}{2} + \exp(-A(\rho_d)\sqrt{t}) \quad (5.39)$$

Thus the connected part of the correlation function, for large times, has a stretched exponential form $\exp(-\sqrt{t/\tau})$ where $\tau \sim \rho_d^{-2} \sim (\rho - \rho_c)^{-2}$. Hence the exponent $\nu_{||}$ defined according to eqn. (5.37) is 2.

However, in this case the density autocorrelation function is a special observable - it depends only on the particles hopping across a bond on the dual lattice. A more general observable, for example the activity autocorrelation function, depends also on the autocorrelation of the density in the dual lattice exclusion process. (The activity, for low ρ , is simply the number of 11s, which is the number of particles on the dual lattice.) For large times, since the density diffuses, this goes as $1/\sqrt{t}$. Thus the activity autocorrelation function for the CLG has a $1/\sqrt{t}$ that dominates the stretched exponential contribution. A stretched exponential behaviour of the autocorrelation function, which also occurs through a mapping to an exclusion process, has earlier been observed, in some sectors of the phase space, in a model with infinitely many conservation laws [12].

The behaviour of the activity autocorrelation for short times ($1 \ll t \ll \rho^{-2}$) also goes as $t^{-1/2}$, since this is proportional to the probability that a particle on the dual lattice comes back to its initial position. (For $t \ll \rho^{-2}$, the particles do not interact.) This behaviour was observed in simulations in [9].

5.6.2 Random initial conditions

We consider starting from a high-activity set of initial conditions at a given density, on a finite ring of size L . One can then assume the following finite-size scaling ansatz for the

long-time decay of the activity with time, near ρ_c :

$$\rho_a = t^{-\hat{\theta}} f(t^{1/\hat{\nu}_{\parallel}}(\rho - \rho_c), tL^{-\hat{z}}) \quad (5.40)$$

where we have put hats on the exponents to denote that these exponents might be initial-condition dependent, and might not be equal to their steady-state counterparts. The equation above can be taken as the definition of $\hat{\theta}$, \hat{z} and $\hat{\nu}_{\parallel}$. We assume that the scaling function obeys the limits $f(z, 0) \sim z^{\hat{\nu}_{\parallel}\hat{\theta}}$ for $z \gg 1$ and $f(0, y) \sim y^{\hat{\theta}}$ for $y \gg 1$. This gives that for large times, the activity saturates at

$$\rho_a|_{\rho=\rho_c} \sim L^{-z\hat{\theta}} \quad \text{and} \quad (5.41)$$

$$\rho_a \sim (\rho - \rho_c)^{\hat{\nu}_{\parallel}\hat{\theta}} \quad \text{for } L \rightarrow \infty \quad (5.42)$$

If we assume that the system reaches the steady-state at the end of this scaling regime, we get the scaling relation $\hat{\nu}_{\parallel}\hat{\theta} = \beta$. Lee and Lee also make the observation that, if one stays a finite number of particles about the critical density $L/2$, then for large L , in the steady-state only a finite number of active sites survives. That is, $\rho_a|_{t \rightarrow \infty} = 2/L$ in the steady-state. From eqn. (5.41), this leads to the scaling relation $\hat{z}\hat{\theta} = 1$. Note that the violation of these scaling relations would signal that the system does not reach the steady-state at the end of the scaling regime for eqn. (5.40).

Violation of the second scaling relation was precisely what Lee and Lee ([7, 8]) observed, when starting with random initial conditions (a Bernoulli process on each site with parameter ρ , and constrained so that the total number of particles is ρL). They found, by fitting the data to the scaling eqn. (5.40)

$$\hat{\theta} = 1/4, \hat{\nu}_{\parallel} = 4 \text{ and } \hat{z} = 2 \quad (5.43)$$

It is seen that $\hat{z}\hat{\theta} = 1/2$. Also, $\hat{z} = z$ but is not equal to $\hat{\nu}_{\parallel}/\nu_{\perp}$, which is another signal that the steady-state exponents do not matter in this regime of decay. In [8], Lee and Lee re-examined the data for the saturation values of the activity density, and found that at the end of the scaling regime, $\rho_a|_{sat} \sim L^{-1/2}$. Thus, the data seem to indicate the existence of a consistent scaling regime with the above exponents, but the system does not reach the steady-state at the end of this regime.

The CLG starting from random initial condition can, in the defect picture, be mapped to an A-B annihilation process. Recall that for the CLG on a line of length L with N particles, the corresponding defect configuration is on a line of N sites. Each 1 becomes a site on the line, and if it is followed by a 0-cluster of length n , the corresponding site has $1 - n$ defects on it ($-m$ defects = m anti-defects). There can be at most one defect on a site, but any number of anti-defects. In the defect configuration, defects can diffuse around,

anti-defects are stationary, and defects and anti-defects annihilate each other. The steady-state contains no anti-defects, and the dynamics in the steady-state thus maps exactly to a symmetric exclusion process. Starting from random initial conditions, however, would map on to an A-B annihilation process with B stationary [13]. The activity is equal to twice the number of particle clusters in the defect configuration.

The A-B annihilation process in one dimension is known to separate, after a short transient, into domains consisting only of particles of a single type. The exponents for the dynamical evolution of the A-B annihilation process have been derived in the thermodynamic limit by Bramson and Lebowitz [14]. We use the simpler domain picture, originally due to Leyvraz and Redner [13], to explain the exponents observed by Lee and Lee and explain the existence of a scaling regime. Since the A defects are mobile and diffuse around, if they meet any anti-defects they annihilate. Consider starting with equal densities of defects and anti-defects, which corresponds to starting with random initial conditions in the CLG at $\rho = 1/2$. In a time t , the A-defects have almost surely visited every site within a length \sqrt{Dt} . The domain picture of A-B annihilation says that in $d \leq 2$ dimensions, the system separates into domains of excess A or excess B particles. Since the initial conditions were created by a poisson process, the number of excess defects or anti-defects in a length $\sim t^{1/2}$ is $\sim t^{1/4}$. Thus the number of defects surviving up to time t in a system of length L is $\sim t^{1/4} \times L/t^{1/2} = t^{-1/4}L$. Since each domain of length $t^{1/2}$ contains only $t^{1/4}$ particles, the particles are well-separated and there would be almost no defect clusters of length > 1 . Hence the activity would be proportional to the number of defects, and hence $\rho_a \sim t^{-1/4}$ for $t \ll L^2$.

Once t is of $O(L^2)$, the diffusing defects have explored large parts of the system, and hence there would be very few anti-defects left. The number of surviving defects at this time-scale is simply $\sim t^{1/4} \times t^{1/2}/t^{1/2} = t^{1/4} \sim L^{1/2}$, and hence $\rho_a \sim L^{-1/2}$ at the end of the scaling regime.

Now consider starting with a density slightly above the critical density. In this case, the number of excess defects in a length l is $\sim l(\rho - \rho_c)$. The A-B annihilation regime stops only when the domain length becomes large enough so that most domains have an excess of defects over anti-defects. This happens when $l(\rho - \rho_c) \sim l^{1/2}$, and hence the scaling regime is valid till a time $t \sim l^2 \sim (\rho - \rho_c)^{-4}$. Thus the scaling form of A-B annihilation should be

$$\rho_a = t^{-1/4} f(tL^{-2}, t(\rho - \rho_c)^4) \quad \text{with} \quad (5.44)$$

$$\rho_a^{sat}|_{\rho=\rho_c} \sim L^{-1/2} \quad (5.45)$$

which is consistent with Lee and Lee's results.

Note that, however, at the end of this regime the activity, although proportional to $(\rho - \rho_c)$, is still higher than its equilibrium value, because although some regions have equilibrated, regions at the edges of domains have not equilibrated with regions near their centre, and hence there are more isolated particles and less defect-clusters of larger length. There follows another regime of equilibration, only after which the system reaches the steady-state. This regime of equilibration can be viewed as coarsening in the dual lattice exclusion process. There is no clear separation of scales between the two regimes, however, and if one starts with a state sufficiently close to the steady-state sector, one might not see the $t^{-1/4}$ decay. Bondyopadhyay [9] studied the evolution starting from this kind of initial condition. If one assumes the existence of a single regime starting from this initial condition, after which the system is in the steady-state, the exponents found will obey the scaling relations $\nu_{\parallel}\theta = \beta$ and $z\nu_{\perp} = \nu_{\parallel}$ where the exponents β , ν_{\perp} and ν_{\parallel} are the steady-state exponents determined in this chapter. Bondyopadhyay's values are indeed consistent with these scaling relations.

5.7 Summary and Concluding Remarks

In summary, we have studied a class of non-equilibrium models of assisted hoppings in one dimension, characterized by a range parameter n , for all positive integer values of n , generalizing the model studied by da Silva and de Oliveira [1]. We determined the steady-state measure exactly and showed that the critical exponents have the values $\beta = n$ and $\nu = 1$ for these models. For $n \geq 3$, these define previously unknown universality classes of active-absorbing phase transitions.

It is straightforward to extend our discussion to models with asymmetrical hoppings, where particles can hop only to the right (say), on a ring. For concreteness we set all non-zero rates to 1. Then, one can check that in the active state, all recurrent configurations occur with equal probability. There is a net mean current in the active steady state, which is proportional to mean activity, and thus also varies as $|\rho - \rho_c|^{\beta}$, with $\beta = n$. Thus we see that adding a directionality to these models does not change the critical exponent β .

If one considers the decay of activity with time starting from a randomly prepared state outside the steady-state sector, then this process can be expressed as the annihilation dynamics of defects and anti-defects, where the anti-defects do not move, but are eventually annihilated by invading defects. Thus the activity at the critical density, where one starts with an equal number of defects and anti-defects, would decay as $t^{-\frac{1}{2z}}$ where z is the dynamical exponent in the steady-state. This has been observed in the CLG (which is the model with range 1) [7] where it has also been explained in terms of a mapping to a two-species annihilation process [16].

The exponent of the initial power-law relaxation of the activity at the critical density has, in a number of models, been observed to be different for relaxation from a random initial condition and for relaxation within the steady-state sector [7]. In the class of models defined here, one can characterize the structure of transient and steady state configurations in some detail, which might be useful in elucidating the origin of this dependence on the initial conditions. We plan to explore this in the future.

Appendix I: Counting the Absorbing Configurations

The most interesting absorbing configurations above ρ_c are ones which obey the steady-state condition of having no 0-clusters of length $>n$, and these are the ones which are included in the generating function for the active steady-state. They can be converted into steady-state configurations by adding a single active particle. We now wish to show that they don't affect the counting in the thermodynamic limit.

Thus, here we show how to count the number of such 'near-steady-state' (NSS) absorbing configurations. The structure of these configurations is closely related to the structure of the configurations in the active steady-state, and also sheds light on the origin of the exponent $\beta = n$.

The condition that a configuration is absorbing is that it must consist of isolated 1s such that if the neighbouring 0-clusters to the left and right of a particle have length n_r and n_l respectively, then $n_r + n_l > n$. Consider the model with range 2: this means that the "near-steady-state" absorbing configurations consist of 1s with the neighbourhoods '0100', '0010' and '00100'. All such configurations are generated by the strings '100' and '10100', and thus

$$A(x, y) = \frac{1}{1 - xy^3 - x^2y^5} - 1 \quad (5.46)$$

where the term xy^3 corresponds to the string 100 and the term x^2y^5 to the string 10100.

The number of NSS absorbing configurations grows as $\lambda_a(x)^L$ at fugacity x , where λ_a is the largest solution of $\lambda_a^5 = x^2 + x\lambda_a^2$. Here we will confine ourselves to studying the behaviour near ρ_c and show that the number of NSS absorbing states is negligible in the thermodynamic limit near ρ_c .

Near $x = 0$, $\lambda_a(x) = x^{1/3}(1 + \frac{1}{3}x^{1/3} - \frac{7}{9}x^{2/3} + \dots)$. Now let $\lambda_+(x)$ be the exponential of the entropy per site for the active steady-state. Near $x = 0$, $\lambda_+ = x^{1/3}(1 + \frac{1}{3}x^{1/3} + \frac{1}{3}x^{2/3} + \dots)$.

Thus, $\lambda_+ - \lambda_a \approx \frac{4}{9}\lambda_+^3$.

First we show that near the critical point, the average length between active particles

can be found from eqn. (5.46). For the model with $n = 2$, the background is not static - active particles can become inactive until they are activated by a passing active particle (fig. 4.4). Active particles are separated by inactive strings, where most of the extra $N - L/3$ potentially active particles in the system reside as part of inactive strings, making the activity $\sim (\rho - \rho_c)^2$. The inactive strings between the active particles are generated by the elementary strings '100' and '10100', and hence their generating function is also given by eqn. (5.46).

Asymptotically, the generating function of inactive configurations between two active particles in the system is given by $A(x, y) \approx \frac{C}{1 - \lambda_a(x)y}$, where C is a constant. The average length between two active particles is hence given by the average length of an inactive configuration is

$$\langle L \rangle = \frac{y}{A(x, y)} \frac{d}{dy} A(x, y) \quad (5.47)$$

$$\approx \frac{\lambda_a y}{1 - \lambda_a y} \quad (5.48)$$

Since we want to find the average length between two active particles in the infinite system, we put $y = 1/\lambda_+$, and using that $\lambda_+ - \lambda_a \approx \frac{4}{9}\lambda_+^3$, we get that near ρ_c ,

$$\langle L \rangle \approx \lambda_+^2 = \frac{1}{(\rho - \rho_c)^2} \quad (5.49)$$

which is to be expected since the density of active particles for the model with range 2 goes like $(\rho - \rho_c)^2$. For general n , since $\rho_a \sim (\rho - \rho_c)^n$, we expect that

$$\langle L \rangle \sim \frac{1}{(\rho - \rho_c)^n} \approx \frac{\lambda_a y}{1 - \lambda_a y} \quad (5.50)$$

Assume $\lambda_+ - \lambda_a \sim \lambda_+^a$. We can then carry out the above reasoning in reverse and obtain that for the model with range n , $a = n + 1$. That is,

$$\lambda_+ - \lambda_a \sim \lambda_+^{n+1} \quad (5.51)$$

The total number of active configurations in a system of length L at a certain fugacity of particles is given by λ_+^L and the number of near-steady-state absorbing configurations by λ_a^L . Thus, near the critical point, the number of active configurations is exponentially larger than the number of near-steady-state absorbing configurations for given N and L . Notice that this result depends solely on the dependence of the activity on $(\rho - \rho_c)$.

Appendix II: Counting the isolated active 1s

In this appendix we prove that the activity of isolated 1s in the model with range n scales near the critical point in the same way as the cluster activity, namely as $(\rho - \rho_c)^n$.

We consider the model with range n on a ring with L sites and N particles. The partition function $Z(N, L) = C_r(N, L)$ where $C_r(N, L)$ is the number of configurations on the ring with no clusters of more than n zeroes. (We leave out the subscript n for simplicity in notation.) We also denote the number of configurations on the ring with a particle present at a particular site (say site 0) as $C_r^1(N, L)$.

Because of translation invariance, $C_r^1(N, L) = \frac{N}{L}C_r(N, L) = \rho C_r(N, L)$. Also, on either side of the particle at site zero there can be either a 1 or a 0. That means $C_r^1(N, L) = C(N-1, L-1)$, where $C(N, L)$ is the number of configurations of N particles on a line of length L with free boundary conditions. $C(N, L)$ is given implicitly in terms of the generating function in eqn (5.9).

For the calculation of the number of active isolated 1s, we restrict to the model with range 2 for concreteness, but the same calculations can easily be carried out for higher n as well. What we want to calculate is the probability that a particular site contains an active isolated 1, that is,

$$\rho_{10101} = \frac{C_r^{10101}(N, L)}{C_r(N, L)} \quad (5.52)$$

where $C_r^{10101}(N, L)$ is the number of configurations containing the string 10101 at sites [1,5]. (In Model 3 for instance we will need to calculate $C_r^{101001}(N, L)$.) It is seen that $C_r^{10101}(N, L) = C(N-3, L-5)$. We need to calculate $\rho_{10101} = \frac{C(N-3, L-5)}{\rho C(N-1, L-1)}$.

We first find an expression for $C(N, L)$ from eqn. (5.9). The notation $[y^n]C(y)$ denotes the coefficient of the n^{th} term in the series expansion of $C(y)$ about $y = 0$. What we need to find is

$$C(N, L) = [y^L][x^N] \frac{1}{1 - (y + y^2) \left(\frac{xy}{1-xy} \right)} \quad (5.53)$$

$$= [y^L](y + y^2 + y^3)^N \quad (5.54)$$

$$= [y^{L-3N}](1 + y^{-1} + y^{-2})^N \quad (5.55)$$

$$= [z^{3N-L}](1 + z + z^2)^N \quad (5.56)$$

$$= [z^a](1 + z + z^2)^N \quad (5.57)$$

$$= \frac{1}{2\pi i} \oint z^{-(a+1)} (1 + z + z^2)^N \quad (5.58)$$

$$= \frac{1}{2\pi i} \oint e^{-NS(z)} \quad (5.59)$$

where we have defined $a = 3N - L$, which obeys $a = (\rho - \rho_c)L$. $S(z) \equiv \frac{a+1}{N} \log z - N \log(1 + z + z^2)$. The contour in the integral is the unit circle.

Evaluating the integral by the saddle point method, assuming $1 \ll a \ll N$ would give us the correct powers of a and N , multiplied by constants which might have a weaker dependence on a and N . Since we want the leading dependence of ρ on a/L , the saddle point method is sufficient for our purposes. The equation to be solved for the saddle-point is

$$\frac{d}{dz} S(z) = 0 \quad (5.60)$$

$$\text{where } S(z) = -\frac{a+1}{N} \log z + \log(1 + z + z^2) \quad (5.61)$$

The saddle point which gives the dominant contribution is at $z = a/N - a^2/N^2 +$ higher order terms. Then asymptotically

$$C(N, L) = A \left(\frac{a}{N}\right)^{-a} \left(1 + 8\frac{a}{N}\right)^N (1 + \dots) \quad (5.62)$$

where A is only weakly dependent on a/N .

Since ρ_{10101} is given by $\frac{C(N-3, L-5)}{\rho C(N-1, L-1)}$, where we see that $a = 3N - L - 2$ in the denominator and $a = 3N - L - 4$ in the numerator. Hence, remembering that $N = L/3 + a/3$, to first order in a/L we get

$$\rho_{10101} \sim (a/L)^2 \quad (5.63)$$

$$\sim (\rho - \rho_c)^2 \quad (5.64)$$

Thus confirming that $\beta = 2$ for the model with range 2.

Similar saddle-point evaluations can be done for the longer-range models too. The equation for the saddle-point of the n -range model is $\frac{a+1}{N}(1 + z + \dots + z^n) = z$ (where $a = N - (n+1)L$). This has one solution which goes as $a/L + \dots$, while all the other solutions are of the form constant $+O(a/L)$. Thus the former solution dominates for $a/L \ll 1$, and $C(N, L) \sim (a/L)^a$. Then $\rho_{10\dots010\dots01}$ where the number of 0s on both sides of the central 1 sum to n is given by $(a/L)^n$, giving $\beta = n$.

For the model with range 2, there is a closed-form evaluation for $C(N, L)$ in eqn. (5.57),

given by the Gegenbauer polynomials defined by [17]

$$(1 - 2xt + t^2)^{-\alpha} = \sum_{n=0}^{\infty} C_n^{(\alpha)}(x)t^n \quad (5.65)$$

$$\text{where } C_n^{(\alpha)}(x) = \frac{\Gamma(2\alpha)}{\Gamma(2\alpha - n)n!} {}_2F_1\left(-n, 2\alpha + n; \alpha + \frac{1}{2}; \frac{1-x}{2}\right) \quad (5.66)$$

evaluated at $x = -\frac{1}{2}$.

The cluster activities can also be evaluated by this method. For example, in the 2-range model, $\rho_{clus} = C_r^{110}/C_r^1 = C^{1011}/C_r^1 + C^{10011}/C_r^1$, where in the numerator is second 1 is taken to be at site zero. The dominant contribution comes from the C_r^{10011} term, which goes as $(\rho - \rho_c)^2$, while the first term goes as $(\rho - \rho_c)^3$.

Bibliography

- [1] E. F. da Silva and M. J. de Oliveira, J. Phys. A: Math. Gen. **41**, 385004 (2008).
- [2] D. Stauffer and A Aharony, *Introduction to percolation theory*, CRC press (1994).
- [3] B. Derrida, D. Stauffer, H. J. Hermann, and J. J. Vannimenus. Phys.(Paris) Lett. 1983 **44** L913 (1984)
- [4] S. Feng and P. N. Sen, Phys. Rev. Lett. **52**, 216 (1984).
- [5] M. P. A. Fisher, P. B. Weichman, G. Grinstein and D. S. Fisher, Phys. Rev. B **40** 546 (1989)
- [6] S. Lubeck and A .Hucht, J. Phys. A: Math. Gen. **35** 4853 (2002).
- [7] S. B. Lee and S.-G. Lee, Phys. Rev. E. **78**, 040103(R) (2008).
- [8] S.-G. Lee and S. B. Lee, Complex, Part I, LNICST **4**, 841 (2009).
- [9] S. Bondyopadhyay, Phys. Rev. E. **88**, 062125 (2013).
- [10] S.N. Majumdar and M. Barma, Physica (Amsterdam) **177A**, 366 (1991)
- [11] P. L. Krapivsky, S. Redner, and E. Ben-Naim, *A kinetic view of statistical physics*, Cambridge University Press, 2010.
- [12] M. Barma and D. Dhar, Phys. Rev. Lett. **73**, 2135 (1993)
- [13] F. Leyvraz and S. Redner, Phys. Rev. Lett., **66**, 2168 (1991)
- [14] M. Bramson and J. L. Lebowitz, J. Stat. Phys. **65**, 941 (1991)
- [15] F. Leyvraz and S. Redner, Phys. Rev. A **46**, 3132 (1992)
- [16] K. Jain, Phys. Rev. E **72**, 017105 (2005).
- [17] E. W. Weisstein, “Gegenbauer Polynomial”, MathWorld – A Wolfram Web Resource. <http://mathworld.wolfram.com/GegenbauerPolynomial.html>

Chapter 6

Summary and Concluding Remarks

In this thesis, we studied the patterns formed by rotor-router walkers on periodic and random backgrounds, and defined and solved for the steady-state properties of a new class of active-absorbing phase transitions.

First, we studied the growing patterns formed by depositing rotor-router walkers on the origin of a finite two-dimensional lattice, starting with periodic background configurations of arrows. We find that the patterns show rich internal structure which scales proportionately with the size of the pattern. We characterized this structure by mapping it to a resistor network and solving the Kirchoff equations on the network. We make some reasonable assumptions that the regularities seen in the observed patterns continue to hold for larger N , and this allows us determine the exact asymptotic scaling limit of the visit function $\phi(\xi, \eta)$. We find that the function $\phi(\xi, \eta)$ is a piece-wise linear function of its arguments, with integer slopes. We presented numerical evidence that the magnitude of deviation of the pattern size from the linear growth estimate remains less than 1, and is a quasiperiodic function of the number of walkers.

It would be interesting to explore other patterns where the basic tiles are not squares, for which there is no equivalent of the Brooks-Smith-Stone-Tutte theorem. Also, the quasiperiodicity of the deviations in the diameters of patches from linear dependence on N in these rotor-router patterns and the reason these deviations are as small as possible (the deviation never exceeds 1 in magnitude) remains to be understood. It would certainly be desirable to have a more rigorous derivation of the presumably exact results presented in this thesis.

Then, in chapter 4 we studied the growth of patterns formed by rotor-router walkers on two noisy backgrounds. We showed that in one case the visit function of the pattern can be mapped to the height function in a model of Bernoulli Matchings, which shows KPZ fluctuations and where the exact distribution of the fluctuations follows a Tracy-Widom law. In the second case we argued that part of the boundary of the pattern shows not KPZ

but EW fluctuations.

The class of models which map to growing discrete PNG interfaces has been studied quite a lot in recent years, as was discussed in chapter 1. Among these models are the Totally Asymmetric Exclusion Process, Directed Polymers at zero temperature with uncorrelated noise, etc. These models are special cases of more general models, namely the Partially Asymmetric Exclusion Process and Directed Polymers at zero Temperature with short-range correlated noise, etc. In these general cases, although the mapping cannot be carried out exactly, the general property of KPZ fluctuations and also that of their distribution being Tracy-Widom is expected to hold. This is based on the fact that the coarse-grained equation for these models is the KPZ equation (see chapter 1) and this has recently been exactly solved and found to give a Tracy-Widom distribution for the height fluctuations.

In the same manner, we expect that the Tracy-Widom distribution is a generic feature of rotor-router patterns growing on noisy backgrounds - earlier studies have found that the fluctuations on a totally random background grow as KPZ, although the distribution of fluctuations has not been measured. However, further studies need to be done to confirm the conjecture of Tracy-Widom universality in cases other than the ones studied here. EW fluctuations also seem to play a part in some cases - the class of patterns where one observes EW scaling, and the crossover between KPZ and EW within the pattern in such cases, are interesting questions we plan to explore in the future

In chapter 5, we studied a class of non-equilibrium models of assisted hoppings in one dimension, characterized by a range parameter n , for all positive integer values of n , generalizing the model studied by da Silva and de Oliveira. We determined the steady-state measure exactly and showed that the critical exponents have the values $\beta = n$ and $\nu = 1$ for these models. For $n \geq 3$, these define previously unknown universality classes of active-absorbing phase transitions.

It is straightforward to extend our discussion to models with asymmetrical hoppings, where particles can hop only to the right (say), on a ring. For concreteness we set all non-zero rates to 1. Then, one can check that in the active state, all recurrent configurations occur with equal probability. There is a net mean current in the active steady state, which is proportional to mean activity, and thus also varies as $|\rho - \rho_c|^\beta$, with $\beta = n$. Thus we see that adding a directionality to these models does not change the critical exponent β .

If one considers the decay of activity with time starting from a randomly prepared state outside the steady-state sector, then this process can be expressed as the annihilation dynamics of defects and anti-defects, where the anti-defects do not move, but are eventually

annihilated by invading defects. Thus the activity at the critical density, where one starts with an equal number of defects and anti-defects, would decay as $t^{-\frac{1}{2z}}$ where z is the dynamical exponent in the steady-state. This has been observed in the CLG (which is the model with range 1) where it has also been explained in terms of a mapping to a two-species annihilation process.

The exponent of the initial power-law relaxation of the activity at the critical density has, in a number of models, been observed to be different for relaxation from a random initial condition and for relaxation within the steady-state sector. In the class of models defined here, one can characterize the structure of transient and steady state configurations in some detail, which might be useful in elucidating the origin of this dependence on the initial conditions. We plan to explore this further in future.